UC Irvine
UC Irvine Electronic Theses and Dissertations

Title
HDEHP Activity Coefficients by Vapor Pressure Osmometry

Permalink
https://escholarship.org/uc/item/7mg0z8tz

Author
Gray, Michael Francis

Publication Date
2015

Peer reviewed|Thesis/dissertation

eScholarship.org Powered by the California Digital Library
University of California

UNIVERSITY OF CALIFORNIA,
IRVINE

HDEHP Activity Coefficients by Vapor Pressure Osmometry

DISSERTATION

submitted in partial satisfaction of the requirements
for the degree of

DOCTOR OF PHILOSOPHY

in Chemical and Biochemical Engineering

by

Michael Francis Gray

Dissertation Committee:
Professor Mikael Nilsson, Chair
Professor Hung Nguyen
Professor Frank Shi

2015

© 2015 Michael Francis Gray

Table of Contents

List of Figures iii

List of Tables iv

Acknowledgements v

Curriculum Vitae vi

Dissertation Abstract vii

1 Introduction 1
- *1.1 Study motivation 1*
- *1.2 HDEHP overview 4*
- *1.3 HDEHP in the literature 7*
- *1.4 Chemical activity measurements 15*
- *1.5 Overview of the study 18*

2 Vapor Pressure Osmometry 20
- *2.1 Measuring a sample using VPO 21*
- *2.2 Validation experiments 24*
- *2.3 VPO equation derivation 31*
- *2.4 VPO equation assumption part 1 35*
- *2.5 VPO equation assumptions part 2 39*
- *2.6 Chapter conclusions 51*

3 Chemical Activity of HDEHP 52
- *3.1 Experiment overview 53*
- *3.2 Data analysis overview 57*
- *3.3 Chemical property source 57*
- *3.4 VPO Standard Selection 58*
- *3.5 Calculating the diluent activity for the standard solutions 60*
- *3.6 Machine constant evaluations 68*
- *3.7 Experimental HDEHP activity 71*
- *3.8 Comparison with slope analysis and isopiestic results 78*
- *3.9 Solubility parameter results. 81*
- *3.10 RST+FH based standard corrections and solubility parameter 86*
- *3.11 Chapter conclusions 89*

4 VPO on ternary systems and activity coefficients by slope analysis 89
- *4.1 VPO on HDEHP metal complexes 90*
- *4.2 Complex behavior at high metal loading 91*
- *4.3 Metal complex 92*
- *4.4 VPO solution preparation 96*
- *4.5 VPO results and analysis 98*
- *4.6 Activity coefficients of HDEHP by slope analysis 103*

5 Conclusions 110

6 References 112

Appendix A. List of Symbols and Abbreviations 119

Appendix B. Osmometer Quality Control 122

List of Figures

Fig. 1.1: HDEHP Structure 5
Fig. 1.2: Example extraction 5
Fig. 2.1: Diagram of the VPO cell. 20
Fig. 2.2: Example VPO sample measurement 22
Fig. 2.3: A complete VPO experiment 24
Fig. 2.4: Steady state VPO data 26
Fig. 2.5: $CaCl_2$ validation data 28
Fig. 2.6 KNO_3 validation data 28
Fig. 2.7: Na_2SO_4 validation data 29
Fig. 2.8: Sucrose validation data 29
Fig. 2.9: Sample thermistor resistance values 43
Fig. 2.10: Reference thermistor resistance values 43
Fig. 2.11: Thermistor resistance curve over a wide range of temperature 44
Fig. 2.12 Steady state temperature differences in the VPO cell. 47
Fig. 2.13: VPO signal fall off over time 49
Fig. 3.1: Structures of potential VPO standards 61
Fig. 3.2: Evaluation of thermodynamic models. 66
Fig. 3.3: Evaluation of thermodynamic models. 66
Fig. 3.4: Evaluation of thermodynamic models. 67
Fig. 3.5: Evaluation of thermodynamic models. 67
Fig. 3.6: Activity coefficient of the diluent when HDEHP is treated as a monomer 72
Fig. 3.7: Activity coefficient of the diluent when HDEHP is treated as a dimer 72
Fig. 3.8: Fit to the diluent activity data. 74
Fig. 3.9: Calculated HDEHP dimer activity for three alkane data sets. 75
Fig. 3.10: Calculated HDEHP dimer activity for three aromatic data sets. 76
Fig. 3.11: Calculated HDEHP dimer molar activity for three alkane data sets. 76
Fig. 3.12: Temperature dependence of β 77
Fig. 3.13: Comparison of the activity coefficient from VPO and from Danesi et al.[34] 79
Fig. 3.14: Comparison of the activity coefficient from VPO and from Baes.[33] 80
Fig. 3.15: RST-pFV solubility parameter fit to the diluent activity data. 82
Fig. 3.16: RST-pFV solubility parameter comparison 83
Fig. 3.17: Temperature trend of the fitted HDEHP dimer solubility parameters. 83
Fig. 3.18: HDEHP dimer solubility parameter versus diluent solubility parameter. 85
Fig. 3.19: HDEHP dimer solubility parameter minus the diluent solubility parameter. 86
Fig. 3.20 Comparison of RST-FH (light gray) and pFV based analysis (dark gray) 87
Fig. 3.21: Comparison of RST-FH (light gray) and pFV based analysis (dark gray) 88
Fig. 4.1: Ternary plot for the mole fractions 97
Fig. 4.2: Ternary plot for the mole fractions 97
Fig. 4.3: Average VPO signals for in heptane at 21°C 99
Fig. 4.4: Diluent activity assuming exclusively 6:1 complex 100
Fig. 4.5: Diluent activity assuming exclusively 6:2 complex 101
Fig. 4.6: *n*-Octane activity assuming exclusively 6:1 complex 102
Fig. 4.7: Extraction results for europium-152 tracer by HDEHP 105
Fig. 4.8: Comparison of the activity coefficient of HDEHP dimer 108

List of Tables

Table 2.1: Aqueous solutions for validation. 25
Table 2.2: Ratios of experimental water activity to the theoretical activity. 30
Table 2.3: Concentration and temperature results. 45
Table 2.4: Variation of the constant β_1 47
Table 2.5: VPO signal for hexadecane in heptane 48
Table 2.6: Values used for evaluating inequality 2.33 51
Table 3.1: Summary of the experimental conditions for VPO on HDEHP 56
Table 3.2: VPO machine constant based on four different standards in octane. 59
Table 3.3: Summary of the VPO machine constant 70
Table 3.4: β parameter for each system for Eq. 3.11 74
Table 3.5: HDEHP dimer solubility parameters fit for each system 84
Table 3.6: Parameter results using of RST-FH 88
Table 4.1: Concentrations of the three components as prepared. 96

Acknowledgements

I would like to express my sincere gratitude and thanks to everyone who has supported my journey at UC Irvine.

The opportunity, support and guidance provided by my advisor Professor Mikael Nilsson.

Professor Mikael Nilsson and Dr. Peter Zalupski for providing the opportunity to tackle a challenging and important research topic.

The DOE for funding my project under subcontract 107827 with the Idaho National Laboratory, Fuel Cycle Research and Development program (FCR&D), U.S. DOE, Office of Nuclear Energy.

Dr. Giuseppe Modolo, everyone at IEK-6, and the DAAD.

The members or my doctoral thesis committee, Professor Mikael Nilsson, Professor Frank Shi and Professor Hung Nguyen, along with my qualifying committee members Professor Ali Mohraz, Professor A.J. Shaka, and Dr. Peter Zalupski. And Dr. George Miller, Professor Martha MecCartney, and the rest of the faculty at UCI.

The nuclear group at UCI.

ChEMS graduate students and staff.

All the scientists who attended my conference presentations.

My family, friends, and girlfriend.

Curriculum Vitae

Michael Francis Gray

2009	B.S. in Chemical Engineering, University of California, Davis
2010 – 2015	Graduate Student Research Assistant, Department of Chemical Engineering, University of California, Irvine
2011 – 2013	Teaching Assistant, Department of Chemical Engineering, University of California, Irvine
2012	M.S. in Chemical and Biochemical Engineering, University of California, Irvine
2015	Ph.D. in Chemical and Biochemical Engineering, University of California, Irvine

FIELD OF STUDY

Solvent Extraction and Ion Exchange

Dissertation Abstract

HDEHP Activity Coefficients by Vapor Pressure Osmometry

By

Michael Francis Gray

Doctor of Philosophy in Chemical and Biochemical Engineering

University of California, Irvine, 2015

Professor Mikael Nilsson, Chair

Components of used nuclear fuel remain more radiotoxic than natural uranium ore for over one hundred thousand years, but advanced fuel recycling could reduce that time to a thousand years. Yet several engineering challenges need to be addressed, including the scale up of certain solvent extraction based separations. To do so, an improved thermodynamic understanding of the chemistry is required since data for many of the chemical components is unreliable. The topic of my work, di(2-ethylhexyl) phosphoric acid (HDEHP), is one such example: past studies on HDEHP yield inconsistent thermodynamic data.

The technique of vapor pressure osmometry was used to address that problem, and extensive validation was carried out. The equation relating the vapor pressure osmometry signal to the solution activity was examined in detail, and its accuracy was demonstrated on aqueous solutions. Analysis of VPO data using the

Gibbs-Duhem equation yielded activity coefficients for HDEHP in seven different hydrocarbon diluents. The values for HDEHP at 21°C matched two results from past literature, building a consensus. A second analysis was performed using regular solution theory with entropic corrections. That second result provides qualitative values of the activity coefficient in systems where no experimental data is available. The final section of the report analyzes osmometry data collected for HDEHP metal complex and the activity coefficient of HDEHP obtained with slope analysis. The slope analysis data points to two main reasons for discrepancies between the current VPO activity coefficient results and slope analysis data in the literature. Further analysis of the metal complex data may help resolve that discrepancy.

The data on HDEHP presented in this dissertation will improve the accuracy of extraction models, assisting the scale up of advanced separation processes for used nuclear fuel.

1 Introduction

1.1 Study motivation

The primary motivation of this work is to improve the understanding of separation processes for used nuclear fuel, but the benefits will not be limited this area. The subject of this study is the chemical di(2-ethylhexyl) phosphoric acid (HDEHP, also denoted DEHPA, D2EHPA elsewhere), which can be used to separate a wide array of elements including zinc, cobalt, cadmium, nickel, and rare earth metals.[1–5] Beyond the initial mining and purification of materials, HDEHP has applications ranging from battery recycling[6] to trace metal extraction in environmental assays.[7–9] The relation to nuclear fuel processing, however, is emphasized as this research was comissioned by the Idaho National Laboratory as part of a larger effort to improve the undersanding of actinide/lanthanide partitioning for used nuclear fuel treatment.[10,11]

Nuclear reactors provide a significant amount of energy with low carbon emissions and minimal air pollution, both important features in the effort to minimize the effects of anthropogenic climate change and diminish the environmental impact of energy generation.[12,13] Yet the radioactive used nuclear fuel (UNF) must be treated in a socially acceptable and economically efficient manner since portions of it remain hazardous on a timescale of over a hundred thousand years.[12,14,15] To answer this problem, specialized, secure geological waste repositories are required, similar to the well known but temporarily cancelled Yucca Mountain high-level waste repository.[14] Not only are the repositories costly, but

approximately 96% of the UNF is reusable material. Although basic recycling may not reduce the total volume of waste, it improves waste management by concentrating the longest lived radioisotopes,[14] and greatly reduces the quantity of uranium required compared to a non-recycle reference case. Recycle enhances the sustainability of the fuel cycle and provides significant front-end waste reduction, i.e. from mining processing, and enrichment.

While current industrial scale UNF recycling only permits the reuse of uranium and plutonium for further power generation, separation of the minor actinides (americium and curium) and neptunium is being developed. That separation will permit fission of the long-lived neptunium and minor actinides (MA), into shorter-lived products using fast neutron reactors, a process termed transmutation. Not only will this step reduce ingestion toxicity down to the level of natural uranium ore on the order of a thousand years rather than hundreds of thousands, it can reduce the heat load to the final repository.[14,15] However, separation schemes for these elements remain the subject of much ongoing research due to the difficulty of partitioning the MA from the lanthanides. The chemical separation step must overcome the similar solution behavior of these f-elements, which both form trivalent ions of similar ionic radii as the most stable oxidation state under typical solvent extraction conditions.[16,17]

The primary separation method for recycling and treating UNF, solvent extraction, selectively partitions the different elements in UNF between an organic and aqueous phase. This separation occurs based on the relative affinities of each element to lipophilic complexing agents in the organic phase compared to the

aqueous phase, which can also contain metal binding compounds to selectively hold back elements. Recycling of uranium and plutonium from UNF has been done on a commercial scale using solvent extraction for several decades,[18] but no process to separate the MA from the lanthanides has been developed on a similar scale.

Nonetheless, separation methods for the MA via solvent extraction have been designed[16,19–23] and demonstrated on small scale using genuine used fuel.[21,22] In the United States these schemes frequently involve the extractant HDEHP.[19,23] One such process is TALSPEAK (Trivalent Actinide-Lanthanide Separations by Phosphorous reagent Extraction from Aqueous Komplexes) that has been demonstrated on a kilogram scale.[22] However, TALSPEAK has not been further scaled up since DOE policy shifted to focus on increasing the understanding and characterization of the separation processes at a thermodynamic and solution chemistry level prior to making a commitment.[11]

HDEHP and similar compounds continue to feature in proposed extraction systems for this type of separation. Thus, accurate characterizations of the solution behavior of HDEHP will directly benefit the design and implementation of solvent extraction schemes for the minor actinides. The methods developed will be equally applicable to investigations on the solution behavior of other extractants, where similar knowledge gaps exist. In the class of extractants similar to HDEHP, di-alkyl organophosphoric acids, the literature data remains unreliable on basic solution properties such as association constants, acid dissociation constants, and water/organic phase partition coefficients.[24]

1.2 HDEHP overview

Extractants such as HDEHP display complex solution behavior, showing significant non-ideality due to association phenomena and non-specific chemical effects. Characterization of that non-ideality is important for design and implementation of extraction systems in a controllable fashion regardless of application, yet especially so in nuclear separations.

HDEHP based metal ion extraction from a mildly acidic aqueous phase to a low-polarity organic diluent can be represented by the ion exchange reaction given in Eq. 1.1 for a generic metal ion, M^{x+} of charge $+x$ under low metal loading conditions. Eq. 1.2 illustrates the extraction process for a trivalent metal ion, denoted M^{3+}, characteristic of a MA or lanthanide.[10]

$$M_{Aq}^{x+} + \left(\frac{x+n}{2}\right)(HDEHP)_{2,Org} \leftrightarrow (M(DEHP)_x(HDEHP)_n)_{Org} + xH_{Aq}^{+} \quad 1.1$$

$$M_{Aq}^{3+} + 3(HDEHP)_{2,Org} \leftrightarrow (M(DEHP)_3(HDEHP)_3)_{Org} + 3H_{Aq}^{+} \quad 1.2$$

DEHP signifies the deprotonated form of HDEHP, and $(HDEHP)_2$ indicates a dimer of HDEHP as depicted below in Fig. 1.1. n is an integer that varies depending on the exact extraction system and metal loading, among other things. Here the subscripts *Aq* indicate the aqueous phase and the subscripts *Org* indicate the organic phase.

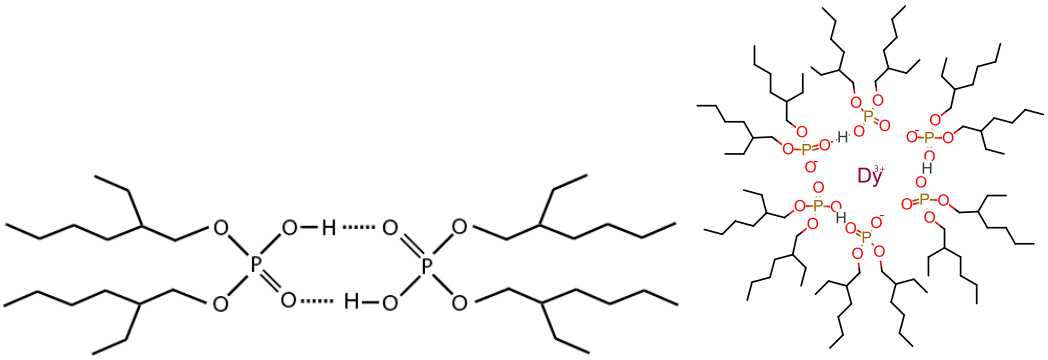

Fig. 1.1: HDEHP Structure
Structure of a dimer of HDEHP (left) and a metal complex with three HDEHP dimers

A solvent extraction system is illustrated in Fig. 1.2 for a trivalent ion. For the case of the trivalent ions, three HDEHP molecules deprotonate, forming a strong metal complex in conjunction with three more HDEHP molecules. DEHP and HDEHP form a strong hydrogen bond in the complex, reported to be symmetric for at least one metal ion based on IR spectroscopy.[21] In this complex the trivalent ion holds a coordinate number of six, whereas the typical coordination of a trivalent MA or lanthanide in aqueous media is 8-9.[25] Varying the pH of the system shifts the equilibrium of the metal ion to either favor the organic phase or the aqueous phase. As different groups of metals tend to exhibit differing equilibrium constants for the extractions depicted in Eq 1.1 and Eq. 1.2, the selective partitioning of metal ions can be accomplished by selecting an appropriate pH. Other influences on the metal partitioning include

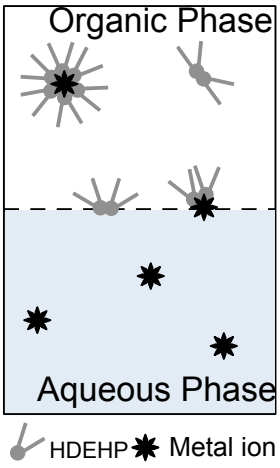

Fig. 1.2: Example extraction
A simplified extraction of a metal ion by three HDEHP dimers

the choice of organic diluent or choice of the anion in the aqueous phase. The equilibrium metal distribution tends to be higher when the diluents is an alkane, e.g. dodecane, versus an aromatic e.g. toluene.[19,26]

Due to their similar solution characteristics, HDEHP alone cannot efficiently separate the MA from the lanthanides. However, HDEHP preferentially complexes lanthanides to a small degree, and the separation can be made when an aqueous phase ligand with a small preference toward the MA is included, as for example the chelating agent diethylenetriaminepentaacetic acid does in TALSPEAK.[16,27]

The phase transfer reactions, Eq.1.1 and Eq. 1.2, yield the equilibrium expressions given by Eq. 1.3 and Eq. 1.4.

$$K = \frac{\{M^{x+}(DEHP)_x(HDEHP)_n\}\{H^+\}^x}{\{M^{x+}\}\{(HDEHP)_2\}^{\frac{x+n}{2}}} \qquad 1.3$$

These expressions are used to model the partitioning of each metal ion between the organic and aqueous phases, i.e. the ratio of the metal concentration present in each phase, and determine the relative separations between individual elements or groups of elements. The braces '{ }' denote chemical activities in Eq. 1.3,. Generally the equilibrium is not expressed as given in Eq. 1.3, but with concentrations and activity coefficients as given in Eq. 1.4, illustrating a typical trivalent metal extraction. The subscripts *HA* and A are abbreviations for HDEHP and DEHP, respectively. γ denotes activity coefficients and the brackets '[ ]' denoted chemical concentrations.

$$K = \frac{[M^{3+}(DEHP)_3(HDEHP)_3][H^+]^3}{[M^{3+}][(HDEHP)_2]^3} \bullet \frac{\gamma_{MA_3HA_3}\gamma_H^3}{\gamma_M\gamma_{(HA)_2}^3} \quad 1.4$$

Frequently, the activity coefficients are neglected, particularly in the organic phase,[28,29] introducing inaccuracy as concentrations, temperature or diluent changes. Thus one important step in characterizing the extraction of metal is to determine the activity coefficient of each component, including the activity coefficient for HDEHP dimer, which is the subject of this work.

Due to the importance of establishing the solution behavior of HDEHP, a number of authors have published works on the activity coefficient of HDEHP. Others attempt to characterize the solution behavior of HDEHP based on aggregation. These past works are reviewed below along with a brief historical introduction of HDEHP and its solution behavior.

1.3 HDEHP in the literature

In the 1950's, HDEHP became of interest after it was found to be more stable towards hydrolysis and posses lower aqueous solubility than to dibutyl phosphate. Dibutyl phosphate, in turn, was being investigated after favorable distribution ratios for thorium-lanthanide separations were found.[3] Investigations suggested HDEHP behaved primarily as a dimer in diluents of low polarity to at least temperatures of 80.2°C, the melting point of naphthalene which was used in the freezing point depression experiments.[30,31] Slope analysis showed HDEHP extracted UO_2^{2+} as a dimer according to the proposed equilibrium given by Eq. 1.1 with *n* equal to 2 under low metal loadings.[30] Thus, HDEHP was proposed to form a cyclic dimer

similar but stronger than analogous carboxylic acids. Similar to carboxylic acids, the cyclic dimers are less polar than the monomeric form of HDEHP. Dialkyl organophosphates in general tend to form cyclic dimers in low polar diluents,[24] yet form monomer in highly polar diluents such as acetic acid or alcohols.[32]

Since those early studies, there has been much work involving HDEHP and Scifinder® lists over 7000 references for the compound. A significant portion of these studies deal with the use of HDEHP in metal extractions: characterizing the complexes, kinetics, microstructure, phase equilibria and thermodynamics of these processes at different conditions. However, work directed towards the solution behavior of non-metal complexed HDEHP and the concentration effects of HDEHP in the organic phase is not conclusive, particularly in terms of the activity coefficient of the dimer and association phenomena of the HDEHP molecule in the bulk diluent. A variety of techniques have been employed and a variety of conclusions have been formed,[33–40] but areas for improvement exists, as a consensus is not present.

A caveat that must be considered with any model may be found in the words of Scatchard, "The best advice which comes from years of study of liquid mixtures is to use any model in so far as it helps, but not to believe that any moderately simple model corresponds very closely to any real mixture", as quoted by Apelblat in his review of models for associating solutions.[41] Determining accurate chemical activities and true chemical species is a challenge, and the subject of many textbooks.[42,43] Two main approaches were taken in early theories of activity coefficients. On one extreme, a chemical theory of solutions has been considered where non-ideality arises due to the formation of distinct associates, i.e. new

chemical species, while neglecting non-specific interactions. Then, on the other extreme, chemical associations are not considered and the non-specific interactions or physical interactions give rise to the solution behavior. These physical interactions include structural effects, electrostatics, induction forces and dispersion forces. Identifying the predominating factor and treating the solution in terms of functions derived based on it can provide the most straightforward mathematics, with minimal fitting parameters, to describe the solution chemistry. There are systems that are well described by assuming either the view that chemical forces dominate or that the non-specific forces dominate the non-ideality and the other contributions may be neglected. However, even for these cases, it is not a perfect description of the true state of the solution. In real solutions, particularly involving amphiphilic molecules, the behavior is due to a combination of the factors in both conceptual models. Fully incorporating the parameters associated with both the chemical species and nonspecific interactions for a practical application is challenging due to the number of parameters required and often limited data. Indeed, the effects of each parameter are difficult or impossible to isolate, and multiple parameters must be simultaneously determined. These challenges explain the reason behind the variety of tactics used to model the solution behavior of HDEHP.

In one of the earlier studies, Baes[33] investigated the effect of HDEHP concentration using both isopiestic techniques and slope analysis techniques. HDEHP was assumed to be fully dimerized, with negligible monomer contribution. The isopiestic data collected at 25°C in octane was compared to slope analysis

results on Fe^{3+} extractions. In this case, the isopiestic standard, triphenyl methane, exhibited significant non-ideality, adding a substantial uncorrected error to the results. The two methods yielded activity coefficients differing by approximately 25% at the tested concentrations. The challenge to distinguish specific associates (e.g. trimerization) versus nonspecific effects leading to the non-ideality, as was the case for the standard, was also highlighted in the paper.

In later extraction experiments, Danesi et al.[34] studied dependence of the distribution ratio of Eu^{3+}, Tm^{3+}, and Ca^{2+} in *n*-dodecane on HDEHP concentrations ranging from 0.001 to 1 formal concentration. HDEHP was considered fully dimerized, and the deviation of the metal ion distribution from third power dependence on HDEHP concentration was modeled based on the activity coefficient rather than specific associations, e.g. using Eq. 1.3 and 1.4. While Eu^{3+}, and Tm^{3+} follow Eq. 1.4, the extraction of Ca^{2+} forms a complex with three dimers which exchange two protons in forming the complex, i.e. *n* equals 4 in Eq. 1.3. Despite using different acid concentrations and ionic strengths in the aqueous phase for each metal ion, the three data sets yield activity coefficients in agreement according to the model. The results show approximate agreement with data found by other groups, and is on the same order of magnitude as the isopiestic results by Baes. On the other hand, the data of Baes shows a different slope. While the data presented by Danesi et al. does not show scatter, an assessment of error was not presented. Not only is the method highly affected by even minor phase entrainment and contamination, but the analysis also makes the problematic assumption that the activity coefficient of the HDEHP metal complex is constant with respect to HDEHP

concentration.

In a study by Marcus et al., the heat of mixing of HDEHP with the diluent dodecane or 1,3-diethylbenzene was examined, in addition to corresponding data for dibutylphosphate .[35] In the analysis they assume no excess volume of mixing, which had not been investigated at the time of this study, but has been reported in later literature on HDEHP in another *n*-alkane.[44] Dilution of HDEHP was an endothermic processes in the n-alkane dodecane, but exothermic in diethylbenzene. The HDEHP-alkane system was modeled by treating HDEHP as a dimer with Mecke-Kempter type series association[41] occurring for associates of higher order than dimer, and also by assuming only dimer and trimer formed. For the diethylbenzene system, considering the possibility of HDEHP-diluent adduct was deemed necessary, which increased the number of parameters present and made a meaningful fit non-feasible. The continuous association model provided a better fit to HDEHP compared to the dimer-trimer model.

Li et al. made use of gas chromatographic headspace analysis to examine the diluent vapor pressure in binary systems of HDEHP at 7-8 points spanning the mole fraction range from pure diluent to pure HDEHP.[36] The lowest concentration of HDEHP tested in each diluent was a mole fraction of approximately 0.1. Using the calculated diluent activities, the activity coefficients of HDEHP are obtained via the Gibbs-Duhem equation for a variety of hydrocarbon diluents. They estimated a Hildebrand solubility parameter for HDEHP using the Hansen-Beerbower group contribution theory, obtaining 16.97 $(MPa)^{1/2}$. Their estimation does agree with a later publication.[45] Based on this estimated solubility parameter, a new interaction

parameter is proposed and fit to the experimental data to account for deviations from the predicted behavior. It is unclear why they proposed a new parameter rather than using established extensions to the Scatchard-Hildebrand regular solution equation.[46] In the article by Li et al. is unclear if the results treat HDEHP as a dimer or are only in reference to the formal concentration. The physical constants used are also neither listed nor cited.

The work of Li et al. is one example among many of authors who have used the regular solution theory of Scatchard and Hildebrand to model non-ideality in solvent extract for the organic phase.[45,47,48] In fact, software developed by the Oak Ridge National Laboratory for modeling and predicting equilibrium values in solvent extraction makes uses of this type of model; the current version is called SXFIT.[49] However, even when regular solution theory is applied, lack of the solubility parameter for HDEHP dimer has led researchers to take other approximations even less accurate than estimations by the Hansen-Beerbower group contribution method, such as assuming the solubility parameter of HDEHP is equal to that of the diluent.[48]

Miyake et al.[37] measured vapor pressure depression on binary systems of HDEHP and diluent. They used this data to calculate the diluent activity, which was then analyzed with an ideal associating solution model. Based on these results they determined the amount of HDEHP monomer and dimer present, yielding $\log_{10}$ dimerization constant ($log_{10}K_2$) of 7.5 in heptane and 7.0 in benzene at 40°C, several orders of magnitude larger than typically reported. Although the analysis ignored the non-ideality of the standard, benzil,[50,51] it is doubtful those corrections account

for the substantial discrepancy. It is unclear what exact assumptions were made since the description was limited. Likely for these reasons, the dimerization constants found by Miyake et al. are listed as unreliable in the review by Kolarik.[24]

Jenináková-Křížová et al. collected VPO data on the diluent activity for binary systems of HDEHP in benzene and cyclohexane.[38] In this study benzil was used as a standard without correcting for the reported non-ideality.[50,51] Both an empirically modified Margules two suffix equation with a total of two fitting parameters, and an ideal association model taking the form of monomer-dimer equilibrium was used to fit the data on HDEHP. $log_{10}K_2$ found based on the association model was 4.1 in cyclohexane and 5.26 in benzene. For comparison, values in benzene were reported as 3.25 and 7.34 by two other groups.[24] Jenináková-Křížová et al. did not report whether a model with specific higher order associates or a continuous association type model was evaluated for the HDEHP data. The author also fit activity coefficients to HDEHP, but did not make the assumption that it was dimerized for those calculations.

Citing the disparity in experimentally determined dimerization constants in toluene, Miralles et al. used vapor pressure osmometry data to determine the association of HDEHP in toluene at three temperatures with benzil as the reference standard. [39] Again ideal behavior of the standard, benzil, was assumed. The system was analyzed based on an ideal associating solution (IAS) model,[29] along the data analysis methods presented by Rossotti and Rossotti.[52] In the IAS model, solution behavior is explained by the formation of associates, i.e. monomer, dimer, trimer equilibrium, where each species interacts ideally. The analysis by Miralles et al.

requires extrapolation of the data to determining the concentration of HDEHP at which the formal concentration equals the free monomer concentration, a step that tends to introduce error when sufficiently low concentrations to provide an accurate extrapolation are not measured. The IAS model of monomer-dimer equilibrium does yield a good fit to their data of HDEHP in toluene, but the $log_{10}K_2$ determined in toluene of 3.68 at 25°C is lower than 4.38 and 5.10 as reported elsewhere,[24] suggesting that either their analysis or the VPO data is unreliable.

Buch et al. collected VPO data for modeling the behavior of HDEHP in pentane with trioctylamine as the standard.[40] Again, non-ideality of the standard[53,54] was not accounted for. Similar to the work of Miralles et al., an IAS model was used to analyze the data based on the methods of Rossotti and Rossotti. The reported dimerization constant, K_2, was equal to 115.2±0.5 and the trimerization constant, K_3, was equal to 3286±3. Concentrations of up to approximately 1.4 molal HDEHP are measured, quite high for VPO.[55]

The results summarized here demonstrate that despite groups having studied the solution behavior of HDEHP, the variety of methods and limited agreement between results have not created a definitive description of the solution behavior of HDEHP. Neither the characterization of the system via activity coefficients of the dimer, nor the various association models show a clearly superior result. While there is approximate agreement among studies on the dimerization constant for HDEHP in certain solvents (dodecane for example), this is not true for others such as benzene and toluene as illustrated earlier. Some issues in the past studies were the assumption of ideal standards, ideal association assuming only

dimerization, and in general a minimal discussion of methods, error and assumption. These past drawbacks are taken as lessons of areas to be improved upon over the course of the present project. Furthermore, obtaining an accurate Hildebrand solubility parameter for HDEHP is of clear value, as illustrated by its use in the SXFIT program and the attempts at estimating it by other researchers. The solubility parameter does not appear to be experimentally established, as highlighted by the use of group contribution estimations,[36,45] and is not listed in relevant databases.[46,56,57]

1.4 Chemical activity measurements

There are several methods that could be used to collect data on the chemical activity of HDEHP in order to determine activity coefficients and a solubility parameter for the dimer. Accurate vapor liquid equilibrium and chemical activity measurements are vital for optimum process design and operation, and many methods were developed for these measurements over the past century. The common methods for VLE data and activity include recirculating stills, termed 'dynamic methods', and vapor equilibrium cells, termed 'static methods' for measurements with significant concentration of each component.[43] If characterizing the vapor is not important, methods such as the isopiestic technique[58] or vapor pressure osmometry[55] can be used for chemical activity measurements.

Each method is optimal for different systems, and all require careful design and operation in order to prevent significant errors. Many of the early dynamic methods, for example, suffered from design flaws that led to measurement being made away from equilibrium.[43] Data produced on the earlier apparatus designs

were generally not reproducible on new ones. Overall measuring reliable equilibrium data is challenging and costly. In 1987 it was estimated to cost an estimated at $3800[43] (inflation adjusted to 2015 dollars) for each paired vapor and liquid point.

Recirculating stills are a common VLE and are cited to comprise a significant fraction of the VLE data sets available in literature.[43] The basic operating principle is liquid and vapor are equilibrated in using a Cottrell pump,[59] then vapor and liquid phases are separated, sampled, and recirculated. The typical set up provides isobaric equilibrium data on both the vapor and liquid compositions, allowing a thermodynamic consistency check using the Gibbs-Duhem equation. Careful apparatus design is required to prevent problems inherent to the recirculating still design. Condensation, liquid entrainment in the vapor phase, and many other problems can easily lead to sampling of non-equilibrium conditions.[43] However, this method is only suited for miscible liquids with close relative volatilities,[43] so it is unsuitable for HDEHP in typical alkane diluents.

Unlike recirculating stills, vapor liquid equilibrium cells are capable of measuring VLE for components with large differences in relative volatilities.[43] In this technique, the mixture is held under isothermal conditions in a closed cell where equilibrium between liquid and vapor is established. Measuring the vapor phase composition without disturbing the equilibrium is a challenge, but this value can be calculated from the measured liquid composition and total vapor pressure. However, the vapor inside the cell must consist only of the components being

measured in order to use the total pressure for those calculations. Thus the system must be degassed and without vacuum leaks, which is a major difficulty.

The isopiestic technique is suitable for systems where one component is essentially non-volatile. A small amount of the liquid sample is allowed to equilibrate with a second liquid solution containing a non-volatile standard and the same volatile component. The volatile component transfers between the two liquid samples until the activity of the volatile component is equal, which can take weeks.[60] The composition of each liquid sample is determined and the activity of the non-volatile component can be calculated using the Gibbs-Duhem equation. The activity of the volatile component must be well characterized in solutions of the standard, but this can be a challenge with components of greatly differing volatilities. This constrain is also present for vapor pressure osmometry.

Like the isopiestic method, vapor pressure osmometry is only practical for systems with one volatile component and requires a reference solution. Vapor pressure osmometry offers several advantages over the other three techniques just mentioned, but is limited to relatively dilute systems. Each of the other techniques can be used at significant concentrations of either component, but vapor pressure osmometry can only be used up to 3-5%[55] mole fraction of the non-volatile component. On the other hand, the technique does not require degassing and is more rapid than the isopiestic technique. The activity of the volatile component is determined by comparing the temperature difference between a drop of solution and a pure drop of the volatile component in a chamber saturated with the volatile components vapor. These temperature differences are related to the volatile

components activity by comparison to measurements made using a non-volatile standard under the same conditions.

The past work on HDEHP summarized in this chapter shows that VPO, isopiestic, and static vapor-liquid equilibrium cells are all viable methods for characterizing the solution behavior of HDEHP. The current study selected VPO due to the potential for rapid data collection and the availability of commercial instruments. The isopiestic technique and the vapor-liquid equilibrium cell method typically require custom manufacture of the devices.

1.5 Overview of the study

The first step in the process to characterize the solution behavior of HDEHP does not actually involve HDEHP. Instead, the first task to validate the VPO instrument purchased for the project. Thus chapter 2 is devoted to a detailed discussion and validation of the data from the UIC model 833 vapor pressure osmometer. The osmometer is shown to accurately yield chemical activity measurements using several aqueous salt systems and the equation used to relate the VPO signal to the chemical activity of the diluent is analyzed in detail.

Based on the favorable results in chapter 2, chapter 3 moves on to describe the collection and analysis of HDEHP in seven different hydrocarbon diluents at range of different temperatures. Here, the activity coefficient of HDEHP is presented based on an empirical application of the Gibbs-Duhem equation and a solubility parameter based method. Although both of these methods yield HDEHP dimer activity coefficients following trends published in literature, the empirical

application of the Gibbs-Duhem is found to be more reliable and in better agreement with the works of Baes,[33] and Danesi et al.[34]

Chapter 4 builds on the results of chapter 3 by developing two areas where the work can be continued. In the first part, VPO is used to characterize HDEHP metal complexes by VPO. However, this data could only be collected on solution of three components, making the analysis more challenging and less definitive due to an increased number of assumptions required. Additional analysis and potentially more data is needed before that work gives substantive conclusions. The second part of chapter 4 represents a different direction in which the work could be progressed. An alternative technique to calculate the activity coefficient of HDEHP dimer, slope analysis, is revisited to resolve the remaining discrepancy between those results and the results of VPO. It is shown that the technique of slope analysis is easily prone to underestimate activity coefficient, which would potentially explain the difference between the VPO results and the activity results of Danesi et al. A method to prevent one of the main errors leading to the underestimated activity coefficient is proposed.

Chapter 5 then concludes the work by briefly summarizing the main conclusions, including a summary of the areas where the work could be extended.

2 Vapor Pressure Osmometry

The experimental technique of vapor pressure osmometry (VPO) relies on measuring the temperature difference between two samples of solution in order to determine the diluent activity. One sample consists of pure diluent and the other sample is a mixture of the diluent with a non-volatile solute. Droplets of these two samples are held on highly temperature sensitive thermistors in a chamber saturated with the diluent vapor, as illustrated in Fig. 2.1. In the sample containing solute, the diluent activity is lower than that of the pure diluent, causing condensation on this sample. The condensation increases the temperature of the drop as the enthalpy of vaporization is released. A pseudo-steady state occurs when the rate of heat input to the drop of solution due to condensation of the vapor equals the rate of heat loss back to the cell surroundings. At the pseudo-steady state, the voltage signal of the osmometer can be related to the diluent activity in the solution, as shown in Eq. 2.1.

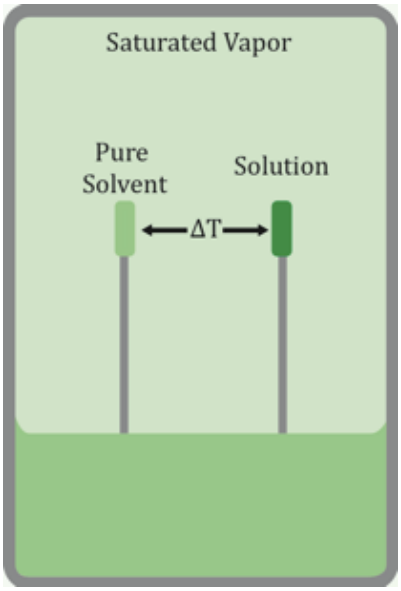

Fig. 2.1: Diagram of the VPO cell. ΔT is temperature difference between the two thermistors.

$$\Delta V = k(1 - a) \qquad 2.1$$

ΔV (μV) is the voltage readout of the osmometer, a is the activity of the diluent, and k is the machine constant. The machine constant is determined by fitting to data on a standard. This equation is commonly used to analyze VPO data[61], often with the assumption that the solution behaves as an ideal associating solution if the diluent

is an alkane[40,62] or simple aromatic, such as toluene[63]. The equation is based on heat and mass transfer relations,[64] to be shown later.

The equation provides a straightforward path to calculate the diluent activity in binary solutions, and is validated for our system using aqueous salt solutions in this chapter.

2.1 Measuring a sample using VPO

A VPO experiments requires measuring at least at least two series of solutions. One concentration series must be a standard such that the activity of the diluent is known in order to calculate the machine constant. Using this calibration, a second series or more than one series of solutions can be measured and analyzed.

The lower bound for the concentrations is determined by the noise and variance in triplicate measurements. The lowest concentrations for the organic solutions investigated in this work are between 0.0025 to 0.005 molal. Triplicate measurements typically present a standard of deviations of less than 5% for these concentrations. Above this limit the standard of deviation is usually between 0.5% and 3% for the triplicate measurement, with an occasional value between 5-6%. The high limit occurs as the assumptions behind the equation begin to break down, so solute mole fractions of over 4% are not reliable.

The VPO signal baseline must be measured prior to taking a sample. Although the thermistors equilibrate to the same temperature when diluent is injected on each of them, the voltage readout at this baseline is not zero. Since the resistances of the two thermistors are only matched to within 1% of their total resistance, that remaining difference leads to a significant natural voltage imbalance

in the circuit. In order to account for this inherent imbalance, a baseline is measured and subtracted from the measured sample signals. The baseline is determined by reading the VPO signal with pure diluent on both thermistors.

An example of the raw VPO data collected for a single sample concentration is given in Fig. 2.2.

The first step of the data collection is to measure the baseline with diluent on both thermistors, shown by gray markers (•). Next, a solution is injected on the

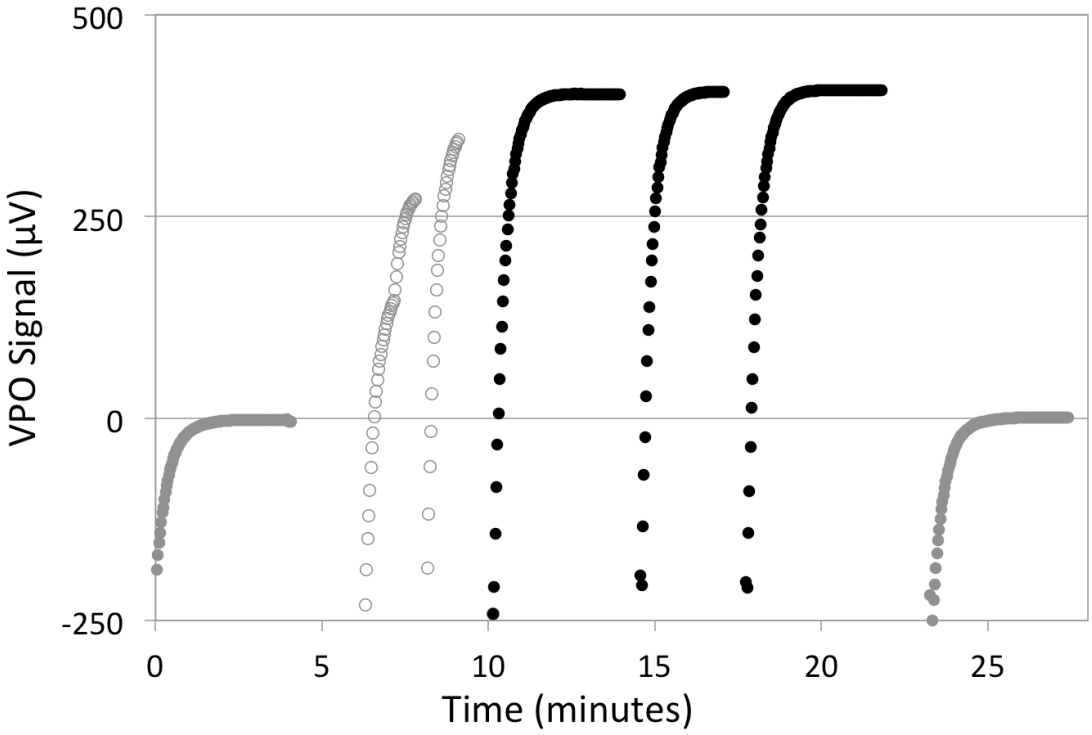

Fig. 2.2: Example VPO sample measurement
The solid gray points mark the baseline reading with water on both thermistors, the open marks show the readings while the measuring thermistor is being conditioned with the sample solution to wash of pure diluent, and the black solid marks show the VPO signal for 0.1 molal calcium chloride in water. The signal jumps by several millivolts immediately after each injection, and exponentially approaches the steady state value, but only the signal nearing steady state is shown here. The reading is taken when the signal reaches the clearly visible plateau, indicating the steady state.

sample thermistor several times without taking a reading in order to condition the thermistor with the new solution, shown by the open markers (o). After

conditioning, the sample is injected and measured three times, or up to five times if the readings show variation over 2-3%. This data is shown by the black markers (•). The VPO signal for each measurement is taken to be the voltage output at steady state, where the signal plateaus. After the solution measurements are finished, the sample thermistor is rinsed with diluent, and the baseline re-checked. The process repeats until all solutions are tested. The initial baseline check of the day is always done in triplicate, and subsequent ones are done once to check for any change.

By convention, the thermistor that gives a positive voltage change with increasing temperature is used as the sample thermistor. That selection is arbitrary, and selecting the other thermistor would reverse the sign of both the signal and machine constant without affecting the end result.

The total data collected for a complete VPO experiment is graphed in Fig. 2.3, where the data has been concatenated to give a continuous plot. The overall timescale shows that the measurements alone, without considering sample preparation, require a week of constant, repetitive work. The data plotted here corresponds to measurements on five different series of binary aqueous solutions, and is the data used to validate the VPO equation, Eq. 2.1. The steady state voltage signals were used to calculate the diluent activity for comparison against published data. The next section presents the details of this experiment.

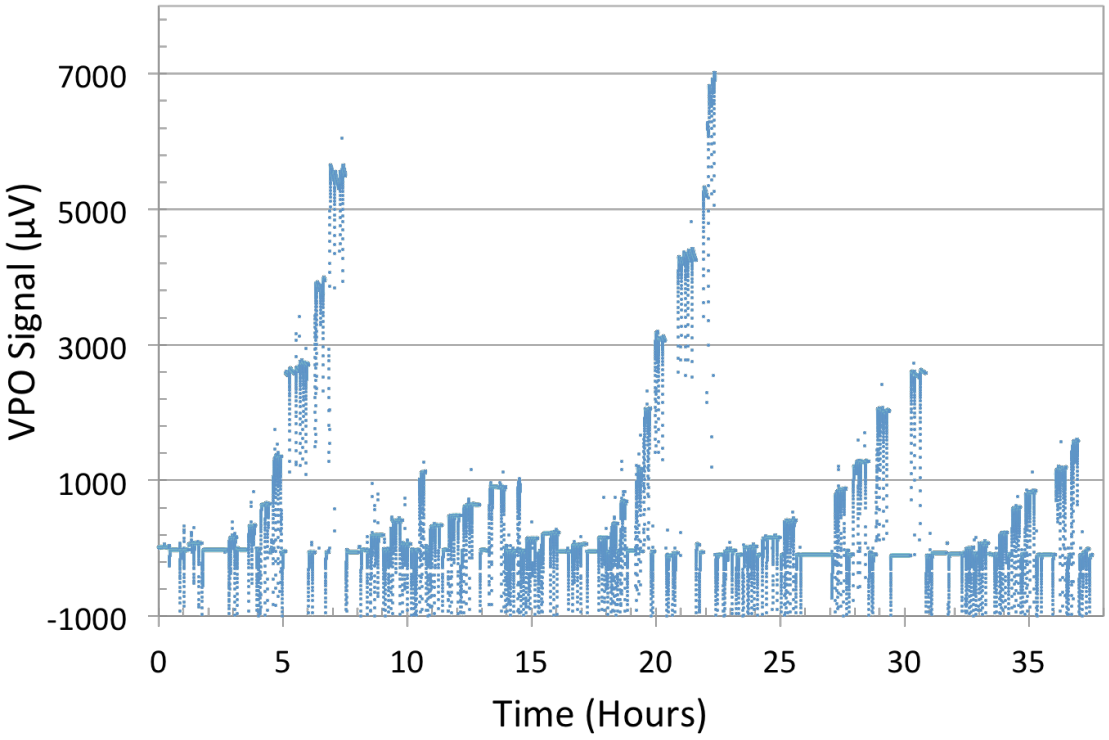

Fig. 2.3: A complete VPO experiment
Raw data from measurements of each series of concentrations of five different binary aqueous systems is shown here. Only the points near steady state are shown for clarity.

2.2 Validation experiments

The VPO signal was measured for well-characterized aqueous solutions in order to verify the VPO equation. The salts potassium nitrate, sodium chloride, sodium sulfate, and calcium chloride were tested along with sucrose. Experimental literature data on the water activity for the salt solutions was obtained from the *Handbook of Electrolyte Solutions*[65], and water activity in sucrose solutions was calculated using an empirical correlation from the work of Starzak[66]. The water activities of the salt solutions was also calculated using the Pitzer method with the coefficients given in the thermodynamic textbook by Prausnitz et al.[42] Comparing the water activity calculated from the VPO results and the literature values showed

excellent agreement for all four substances tested. The calcium chloride, sodium sulfate, potassium nitrate, and sucrose solutions matched literature data closely. The sodium chloride data was used as the reference standard in order to fit for the machine constant. The water activities calculated for sodium chloride solutions using the Pitzer method were used for that fit.

All solutions were prepared gravimetrically. Initial stock solutions were prepared by dissolving weighed amounts of each crystalline powder. The sucrose, and potassium nitrate were sourced from Fisher Chemical; the sodium chloride and calcium chloride dihydrate were sourced from Macron Fine Chemicals; and the sodium sulfate originated from Ricca Chemical Company. These materials were all ACS reagent grade. The water used for all solutions and the VPO diluent was facility deionized water further purified by a NANOpure™ 18.2 MΩ unit followed by bubbling with nitrogen to remove dissolved CO_2. The initial stock solutions were used to prepare the samples for VPO gravimetrically via dilution. The final concentrations of each substance are given in Table 2.1.

Table 2.1: Aqueous solutions for validation.
Mole fractions are nominal mole fractions calculated based on the formal moles of substance added rather than moles of dissociated ions.

Sodium Chloride NaCl		Calcium Chloride $CaCl_2$		Sodium Sulfate Na_2SO_4		Potassium Nitrate KNO_3		Sucrose $C_{12}H_{22}O_{11}$	
Molality	Mole Fraction	Molality	Mole Fraction	Molality	Mole Fraction	Molality	Mole Fraction	Molality	Mole Fraction
2.152	0.0373	1.484	0.0260	0.385	0.0069	1.399	0.0246	1.069	0.0189
1.571	0.0275	1.032	0.0183	0.307	0.0055	1.037	0.0183	0.855	0.0152
1.087	0.0192	0.797	0.0142	0.211	0.0038	0.619	0.0110	0.646	0.0115
0.556	0.0099	0.551	0.0098	0.157	0.0028	0.410	0.0073	0.479	0.0085
0.273	0.0049	0.331	0.0059	0.107	0.0019	0.208	0.0037	0.224	0.0040
0.133	0.0029	0.213	0.0038	0.081	0.0015	0.102	0.0018	0.111	0.0020
0.164	0.0024	0.112	0.0020	0.052	0.0004	0.043	0.0008	0.060	0.0011
0.078	0.0014	0.056	0.0010	0.022	0.0009	0.023	0.0004		
0.068	0.0012	0.027	0.0005						

The VPO cell was cleaned and loaded with a new inner wick, as standard, and equilibrated overnight at 25.3°C. The raw data, shown earlier in Fig. 2.3, was collected over five days, and Fig. 2.2, presented the data collection for the 0.112 molal $CaCl_2$ solution of this data set. At that relatively low concentration, the plateaus are flat and dilution was not significant. Sample dilution, however, was measureable for the higher concentrations as will be discussed later.

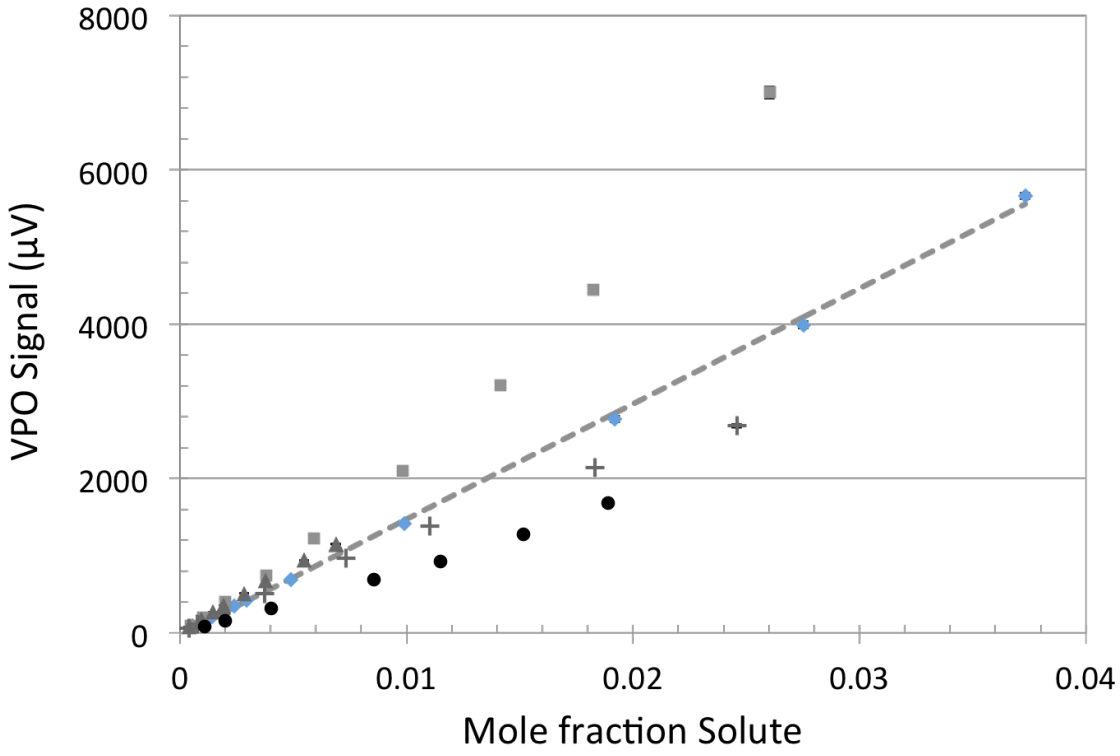

Fig. 2.4: Steady state VPO data
The dashed line (--) gives the fit for the machine constant using the NaCl data (◆). $CaCl_2$ data (■) KNO_3 data (+), Sucrose data (•), Na_2SO_4data (▲) The standard of deviation of the triplicate points fall within the markers.

The average steady state values for each of the solutions are shown in Fig. 2.4. The concentration series for each solute gives a smooth trend, and one standard of deviation calculated from the triplicate measurements falls within the marker of each point, except for the highest concentration point of $CaCl_2$ where it is barely visible. The data for NaCl was used to fit for the constant in Eq. 2.1, which

yielded the value $7.82 \bullet 10^4 \pm 800$. The dashed line along the NaCl experimental points gives this fit. If the highest concentration point, 2.15 molar NaCl, is neglected, the value fit decreases by 0.01%, and the effect on the activities calculated using it is small. For example, the highest change for the water activity in the $CaCl_2$ solutions is from 0.9105 to 0.9104 when the highest NaCl point is left out of the machine constant fit. The signal for the most concentrated value of NaCl appears to fall slightly above the trend, but not significantly enough to greatly effect the calculated water activity for the other solutions, as was just discussed.

Using the machine constant obtained from fitting the NaCl data, the activity of water in each solution of the four other solutes was calculated by applying Eq. 2.1 to the data shown in Fig. 2.4. The result for each system is shown in Fig. 2.5 to Fig. 2.8 along with the literature data. Each of the calculated water activity series matches the literature data well, thereby validating the VPO equation for calculating diluent activity.

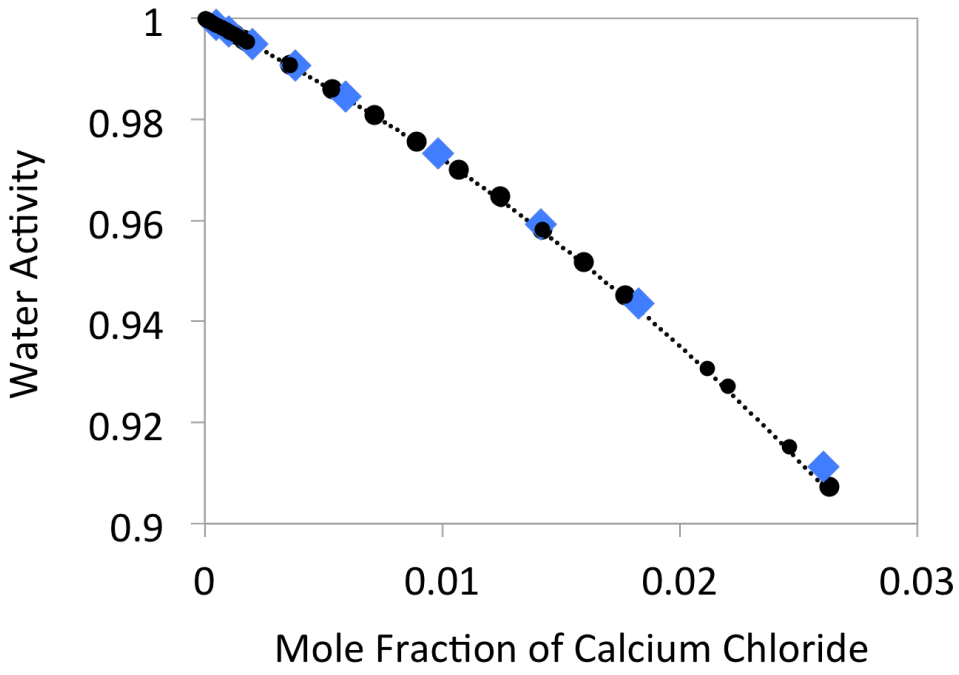

Fig. 2.5: $CaCl_2$ validation data
Based on VPO data (◆) Reference Data (•)[65] Pitzer Model(---)[42]

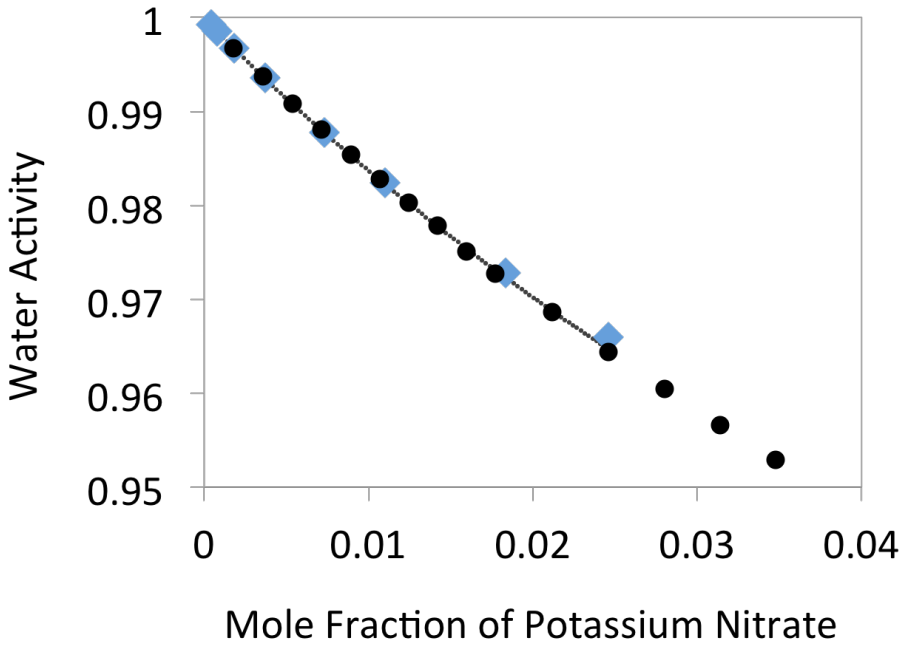

Fig. 2.6 KNO_3 validation data
Based on VPO data (◆) Reference Data (•)[65] Pitzer Model(---)[42]

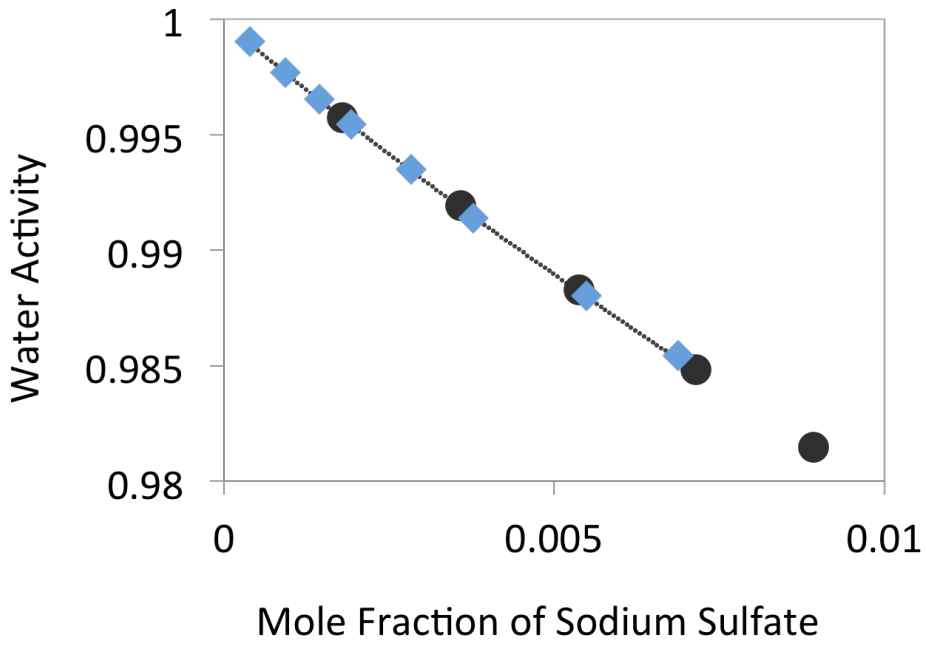

Fig. 2.7: Na_2SO_4 validation data
Based on VPO data (◆) Reference Data (•)[65] Pitzer Model(---)[42]

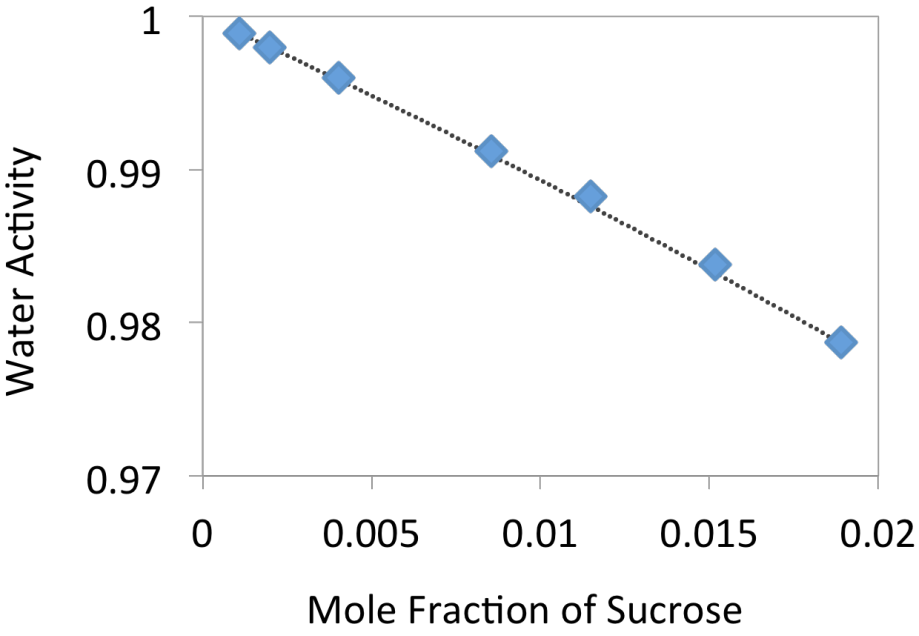

Fig. 2.8: Sucrose validation data
Based on VPO data (◆) Calculated from reference correlation (•)[66]

Based on the aqueous experiments shown in Fig. 2.5 through Fig. 2.8, the accuracy of the VPO equation, Eq. 2.1, is verified by the close match between experimental and literature values. Table 2.2 shows this agreement using the ratio of the water activity calculated from the experimental VPO data to the activity calculated from correlations. These ratios are unity to at least three decimal places in all but three of the 33 samples.

Table 2.2: Ratios of experimental water activity to the theoretical activity.
The theoretical water activity for the salt solutions was calculated using the Pitzer method,[42] and the theoretical water activity for the sucrose solutions was calculated using the equation given by Starzack.[66]

Calcium chloride		Potassium nitrate		Sodium sulfate		Sucrose	
Mole fraction	Ratio	Mole fraction	Ratio	Mole fraction	Ratio	Mole fraction	Ratio
0.0005	1.00003	0.0004	1.00001	0.0004	1.00003	0.0011	0.99999
0.0010	1.00005	0.0008	0.99994	0.0009	1.00000	0.0020	1.00000
0.0020	1.00003	0.0018	1.00005	0.0015	1.00004	0.0040	1.00011
0.0038	1.00049	0.0037	1.00010	0.0019	0.99999	0.0085	1.00020
0.0059	1.00017	0.0073	0.99991	0.0028	1.00001	0.0115	1.00059
0.0098	1.00052	0.0110	1.00004	0.0038	0.99988	0.0152	1.00042
0.0142	1.001	0.0183	1.00027	0.0055	0.99996	0.0189	0.99986
0.0183	1.00081	0.0246	1.00101	0.0069	1.00005		
0.0260	1.00339			0.0069	1.00004		

The highest concentrations, as in $CaCl_2$ at 0.026 mole fraction, show only a small deviation from the literature trends at a water activity of 0.9105. At these concentrations the dilution rate is apparent over the time scale of measurement, but is equally present in the standard data and thus the effects cancel out. Thus, as the current results show, the effect of dilution only introduces a very minor deviation. This result gives confidence to the later experiments on HDEHP dimer even at the highest concentrations tested, around diluent activities of 0.96, much less extreme than the most concentrated $CaCl_2$ solution. Since the diluent activity is much closer to one in the most concentrated HDEHP samples, the driving force for condensation is lower and there the dilution effects are likewise lower. In terms of diluent activity,

the most concentrated HDEHP samples tested are comparable with the 0.0098 mole fraction $CaCl_2$ sample and 0.0246 mole fraction KNO_3 sample shown in Table 2.2.

This empirical validation of the VPO equation would be enough to move on to analyzing the HDEHP solutions with confidence, but several aspects of the VPO system are worth investigation. These include the derivation of the equation, and also of the actual temperature change realized between the thermistors in the VPO cell.

2.3 VPO equation derivation

The VPO equation is based on a heat and mass transfer balance, and a clear presentation was published by the author Kamide[64]. Over several papers this author investigated many aspects of vapor pressure osmometry.[64,67–69] That derivation is adapted here.

Assume the VPO cell (Fig. 2.1) is saturated with diluent vapor at temperature T_0. Let the reference thermistor have a drop of pure diluent and also have a temperature of T_0. It is in equilibrium with the diluent vapor in the cell. The sample thermistor is coated in a drop of solution but is not at equilibrium when at T_0, since the diluent activity is lower in the drop than the vapor pressure of the cell. Diluent vapor condenses, raising the temperature of the solution drop, thereby increasing the diluent activity. However, as the condensation raises the temperature, heat conducts away from the solution drop into the thermistor and into the surrounding vapor. These three major heat flows decide the temperature change of the solution drop and are given mathematically in Eqs. 2.2, 2.3 and 2.5

Heat increase, Q_1, in the drop due to condensation

$$\frac{dQ_1}{dt} = \Delta H \frac{dn_s}{dt} \quad (2.2)$$

t is time, ΔH is the enthalpy of vaporization, n_s is the moles of diluent in the drop.

Heat loss via conduction, Q_2, from the drop to the surrounding vapor

$$\frac{dQ_2}{dt} = -k_1 A_1 \Delta T \quad (2.3)$$

k_1 is the heat transfer coefficient from the drop to the vapor due to conduction and natural convection, A_1 is the surface area of the drop, and ΔT is the temperature difference between the drop and the VPO cell.

$$\Delta T = (T_s - T_0) \quad (2.4)$$

T_s is the temperature of the solutions drop, and T_0 is the temperature of the VPO cell.

Heat loss via conduction from the drop to the thermistor

$$\frac{dQ_3}{dt} = -k_2 A_2 \Delta T \quad (2.5)$$

k_2 is the heat transfer coefficient from the drop to the vapor due to conduction and natural convection, A_2 is the surface area contact between drop and thermistor.

Other lesser heat inputs and outputs are neglected in the derivation by Kamide.[64] These include the energy required to heat the diluent condensing at temperature T_0 up to the temperature T_s; the heat of mixing between condensed diluent and the solution; the thermistor self-heating, and the radiative heat transfer. Thus the total heat flux into the drop is

$$\frac{dQ}{dt} = \frac{dQ_1}{dt} + \frac{dQ_2}{dt} + \frac{dQ_3}{dt} \quad (2.6)$$

And the temperature change of the drop is

$$\frac{dQ}{dt} = mC_p \frac{dT}{dt} \qquad 2.7$$

m is the mass of the drop, and C_p is the constant pressure heat capacity.

The rate of diluent increase in the drop is given by the mass transfer rate

$$\frac{dn_s}{dt} = k_3 A_1 \left(P_0(T_0) - P(T)\right) \qquad 2.8$$

$P_0(T_0)$ is the saturation pressure of diluent at temperature T_0 . $P(T)$ is the partial pressure of the diluent in the drop at temperature T and is given by

$$P(T) = a\, P_0(T) \qquad 2.9$$

Where a is the activity of the diluent.

Since the temperature change is small, a first order Taylor expansion for the saturation pressure, P_0 centered at T_0 introduces little error.

$$P_0(T) = P_0(T_0) + \left[\frac{dP_0}{dT}\right]_{T=T_0} \Delta T \qquad 2.10$$

From the Clausius-Clapeyron equation

$$\left[\frac{dP_0}{dT}\right]_{T=T_0} = \frac{\Delta H}{RT_0^2} P_0(T_0) \qquad 2.11$$

Inserting this into Eq. 2.11 gives

$$P_0(T) = P_0(T_0) + \frac{\Delta H}{RT_0^2} P_0(T_0)\Delta T \qquad 2.12$$

Substituting this expression into Eq. 2.9, and that result into Eq. 2.8 gives

$$\frac{dn_1}{dt} = k_3 A_1 \left(P_0(T_0) - a\left(P_0(T_0) + \frac{\Delta H}{RT_0^2} P_0(T_0)\Delta T \right) \right) \qquad 2.13$$

This equation combined with Eqs. 2.3, 2.5 and 2.6 gives the temperature change over time as

$$mC_p \frac{dT}{dt} = \Delta H k_3 A_1 \left(P_0(T_0) - a \left(P_0(T_0) + \frac{\Delta H}{RT_0^2} P_0(T_0) \Delta T \right) \right) - (k_1 A_1 + k_2 A_2) \Delta T \qquad 2.14$$

Assuming a steady state is attainable

$$\frac{dT}{dt} = 0 \qquad 2.15$$

In practice the decreasing signal over time indicates that this term is not exactly zero, although an order of magnitude analysis, discussed later, demonstrates that this approximation introduces negligible error.

$$\Delta H k_3 A_1 \left(P_0(T_0) - a \left(P_0(T_0) + \frac{\Delta H}{RT_0^2} P_0(T_0) \Delta T \right) \right) - (k_1 A_1 + k_2 A_2) \Delta T = 0 \qquad 2.16$$

Rearranging gives

$$\Delta T = \frac{(1 - a)}{\frac{k_1 A_1 + k_2 A_2}{k_3 A_1} \frac{1}{P \Delta H} + a \bullet \frac{\Delta H}{RT^2}} \qquad 2.17$$

In order to go from this equation to the VPO equation, the mass transfer and heat transfer coefficients are assumed to be constant. The pressure is a constant and the enthalpy of vaporization is approximately constant for the small temperature changes. Neglecting the change in activity (the effects of this approximation are discussed later) the denominator is equal to a constant, β_1.

$$\Delta T = \frac{(1 - a)}{\beta_1} \qquad 2.18$$

The circuit is designed such that the voltage signal is proportional to the temperature difference.

$$\Delta V = \beta_2 \Delta T \qquad 2.19$$

Substituting this into Eq. 2.18 and combing the constants gives the commonly used VPO equation.

$$\Delta V = k(1 - a) \qquad 2.1$$

This equation has been shown to accurately give the diluent activity by Kamide,[67] and was validated with the four aqueous data sets shown earlier in this work. However, the derivation is for an idealized system. Several of the assumptions are not strictly valid and will be discussed.

2.4 VPO equation assumption part 1

The derivation of equation 2.1 assumes the diluent vapor is in equilibrium with pure diluent at the cell temperature. In practice this is not true. The vapor is in equilibrium with the diluent at a changing concentration as samples are injected. The equation derivation assumes the temperature difference between the thermistors reaches a steady state. Experimentally the temperature difference goes through a maximum and declines. The equation derivation pushes the activity term in the denominator of Eq. 2.17 into a constant with respect to concentration, yet the entire point of the experiment is to measure the dependence of the activity on concentration.

While aqueous data demonstrates that Eq. 2.1 is empirically accurate, the three major faulty assumptions in the derivation raise the question of how that is possible. The implication of relaxing each assumption will be discussed starting with the unsaturated vapor in the VPO cell.

Initially, when the VPO has been cleaned and set up, the vapor pressure is saturated for the first measurement. But more sample solution is injected into the cell for each subsequent measurement, mixing in with the pure diluent that started out in the chamber. Now the vapor is in equilibrium with this solution that grows more concentrated as samples are measured. The vapor pressure is no longer the saturation vapor pressure of pure diluent, as the original derivation assumes. The driving force for condensation on the solution drop is now smaller than that given in Eq. 2.8.

In compensation of this smaller driving force, however, is the vapor pressure of the pure diluent on the reference thermistor. Pure diluent is injected on this thermistor at every measurement. Here the vapor pressure is higher than the partial pressure in the cell, and diluent evaporates from the thermistor. This evaporation decreases the temperature of the reference thermistor by the same amount as the sample thermistor, offsetting the error. If the dependence of the resistance on temperature is closely matched for the two thermistors, then the voltage read out remains as if the cell was saturated.

That compensating effect can be shown mathematically. In order to evaluate this effect, each thermistor is considered separately. While the derivation of Eq. 2.1 considered only the temperature change between the sample thermistor and the cell, a new derivation will consider the temperature change between each thermistor and the cell.

Each thermistor can be treated independently using the same derivation with a slight modification,[64,67] and then the results combined to give the overall

temperature change. This modification is done by using different expressions for the driving force of the condensation/evaporation for each thermistor. The other parameters, such as the areas, the mass transfer and heat transfer coefficients are approximately equal since the thermistors are nearly identical.

The vapor pressure of diluent in the cell is not the saturation vapor pressure for pure diluent, but may be corrected by using Eq. 2.20

$$P_c(T_0) = a_c\, P_0(T_0) \tag{2.20}$$

Where P_c is the vapor pressure of the diluent vapor in the cell, being in equilibrium with the diluent solution at the cell temperature. The subscript 'c' indicates a value refers to the VPO cell. With this change the driving force in Eq. 2.8 is modified to Eq. 2.21 for the sample thermistor, and Eq. 2.22 for the diluent thermistor. The subscript '*r*' indicates a value for the reference thermistor.

$$\frac{dn_s}{dt} = k_3 A_1 \left(a_c\, P_0(T_0) - P(T_s)\right) \tag{2.21}$$

$$\frac{dn_r}{dt} = k_{3r} A_{1r} \left(a_c\, P_0(T_0) - P_0(T_r)\right) \tag{2.22}$$

Aside from this alteration, the derivation for the temperature change between each thermistor and the cell follows the earlier path. The two results for the thermistors are given in Eqs. 2.23 and 2.24.

For the sample thermistor

$$\Delta T = (T_s - T_0) = \frac{(a_c - a_s)}{\frac{k_1 A_1 + k_2 A_2}{k_3 A_1}\frac{1}{P\Delta H} + a_s \bullet \frac{\Delta H}{RT^2}} \tag{2.23}$$

For the reference thermistor

$$\Delta T_r = (T_0 - T_r) = \frac{(a_c - 1)}{\frac{k_{1r}A_{1r} + k_{2r}A_{2r}}{k_{3r}A_{1r}} \frac{1}{P\Delta H} + \frac{\Delta H}{RT^2}} \quad 2.24$$

Since these are both differences with respect to the cell temp, subtracting them gives the overall temperature difference between the two thermistors.[67]

$$\Delta T = (T_s - T_r) = \frac{(a_c - a_s)}{\frac{k_1A_1 + k_2A_2}{k_3A_1} \frac{1}{P\Delta H} + a_s \bullet \frac{\Delta H}{RT^2}} - \frac{(a_c - 1)}{\frac{k_{1r}A_{1r} + k_{2r}A_{2r}}{k_{3r}A_{1r}} \frac{1}{P\Delta H} + \frac{\Delta H}{RT^2}} \quad 2.25$$

If the solution in the cell is pure diluent, then a_c is 1, and the equation reduces to the original derived equation, Eq. 2.1. In practice, however, the solution in the cell is not pure diluent after the initial sample is measured. However, the surface area terms, along with the mass and heat transfer coefficients are approximately equal for each thermistor, so the denominators are, to a good approximation, equal. In this case the equation again reduces to the original equation. There are two ways this reasoning would not be valid. First, it would fault if the thermistors were greatly different in any aspect, including the surface area or slope of the resistance as a function of temperature. The other way for this approximation to break down is if the activity of the solution on the sample thermistor is greatly different than 1 since the denominator for the reference thermistor does not match that dependence (evaluated later in this chapter for hexadecane-heptane solutions). In this system the thermistor geometry is the same and their resistance is matched to within 1% for the VPO operating temperatures. Thus even without the assumption that the cell is saturated at the pure diluent

vapor pressure, the VPO equation remains accurate, as was clearly shown by the success of the validation experiment.

2.5 VPO equation assumptions part 2

With the concerns over first assumption addressed, now the approximation that a steady state is reached will be examined. In practice the signal does not plateau into a steady state voltage signal, but forms a down ward sloped plateau. The change is not appreciable for low concentration signals, such as the one plotted in Fig. 2.2, but the voltage change over time is obvious for the higher concentrations. Kamide briefly examined dilution effects, but not the effects on Eq. 2.1. Despite the assumption made to derive Eq. 2.1, the temperature change over time is not zero.

$$\frac{dT}{dt} \neq 0$$

In this case, Eq. 2.14 cannot be simplified but may be rearranged to give a new expression for the voltage signal.

$$\frac{\Delta V}{\beta_1} = \frac{(1-a)}{\frac{k_1A_1 + k_2A_2}{k_3A_1}\frac{1}{P\Delta H} + a \bullet \frac{\Delta H}{RT^2}} + \frac{\left(mC_p\frac{dT}{dt}\right)/(k_3A_1P\Delta H)}{\frac{k_1A_1 + k_2A_2}{k_3A_1}\frac{1}{P\Delta H} + a \bullet \frac{\Delta H}{RT^2}} \qquad 2.26$$

The two denominators are identical, so the original VPO equation remains valid only if relation 2.27 is true.

$$(1-a) \gg \left(mC_p\frac{dT}{dt}\right)/(k_3A_1P\Delta H) \qquad 2.27$$

Precise values for the mass transfer coefficient and surface area are not easily obtained. Instead, these terms can be identified to an order of magnitude, and the rate of temperature change can be determined experimentally.

Although the temperature change can be measured, it requires several steps. The VPO instrument is designed to output the voltage drop in the circuit, and provides no direct information on the absolute temperature difference between the thermistors. The proportionality constant between voltage signal and temperature difference is a function of the cell temperature and is not given. Neither does the instrument output the individual resistance of each thermistor, which could be used to calculate the temperature difference.

Experimentally, however, the resistances can be measured with a sensitive multi-meter. Temperature response of the thermistors can likewise be mapped, and then the temperature difference between the thermistors can be calculated. That data can be used to analyze Eq. 2.17 , and those results subsequently allow the rate of change of the temperature to be determined based on the voltage signal of the VPO.

An initial attempt to the measure the resistance of each thermistor was made using the multi-meter provided with the VPO. The primary function of this multi-meter is to interface between the VPO instrument and the computer logging software for the voltage signal. The μV signal is amped 1000x to the mV level inside the VPO electronics before being fed to the multi-meter, so the provided multi-meter is not high precision. At the cell temperature investigated, the resistance changes at steady state were on the order of a few hundred 100 ohms at most, whereas the total resistance was ~37K Ohm. The multi-meter provided only measures three significant digits so it was inadequate for the task. Measurements with this meter only showed that the temperature change between the thermistors was

approximately 0.2°C for the highest concentration of solute tested in the diluent octane. The rate of change could not be measured.

Accurately measuring the resistance required a more sensitive multi-meter. A Fluke 8808A 5-1/2 digit multi-meter was located and used in experiments to determine both the temperature change across the thermistors and an upper bound of the dilution rate.

There were two main parts for the temperature change experiment. In the first part the temperature responses of the thermistors were mapped by adjusting the VPO cell temperature set point. In the second part, the resistance of each thermistor was measured for a series of concentrations of hexadecane in the diluent heptane at 21°C. Using the temperature response of the thermistors from the first part, this data gave the temperature differences between the thermistors and the rate of temperature change.

To measure the resistances at a known temperature, the VPO was used without injecting samples. Instead, the temperature set point of the thermostat was modified to give a series of known temperatures. After the chamber equilibrated at each temperature set point the resistance of each thermistor was measured. Initially the chamber was equilibrated overnight, and subsequent equilibrations went until the resistance response of the thermistors leveled off, indicating a stable temperature. The resistances were measured by disconnecting the cable leading from the thermistors to the VPO unit, and disassembling the end cap on the plug to gain access to the leads. Here, wires leading directly too and from each thermistors were exposed. With this cable unplugged, no other components were in the circuit

along the loop to each thermistor. By attaching multi-meter to these wires, the only quantity being measures is the thermistor resistance and the neglible wire resitance. Alligator clips from the Fluke multi-meter were attached to the wires exposed under the end cap. The readings were recorded using the Fluke software, and then exported to csv files for analysis and plotting.

The resistance and temperature data is shown in Fig. 2.9, Fig. 2.10, and Fig. 2.11. Over a narrow range of temperature, such as those shown in Fig. 2.9 and Fig. 2.10, the temperature response may be considered linear, representing a tangent to the wider curve shown in figure Fig. 2.11. The linear range shown here encompasses several degrees Celsius, a range much greater than the max temperature difference between the thermistors and the cell of about 0.2°C for alkane diluents. Due to the design of the VPO, the instrument only displays the cell temperature to one decimal place. This limit creates a ±0.05°C uncertainty in the cell temperatures tested in this calibration, which is approximately the width of the point markers in Fig. 2.9 and Fig. 2.10.

A linear fit to the sample thermistor data gives a slope of-5.49 ±0.08kOhm/°C for the range indicated by the line in Fig. 2.9. The fit for the reference thermistor data over the same range gives a slope of -5.52±0.09 kOhm/°C, shown in Fig. 2.10. As discussed earlier, a close match between these values is required for reliable VPO data on unsaturated systems, and experimentally the two values agree well. They are within 0.55% of each other, a value smaller than the measurement error of 1.5% and 1.6% for the sample and reference thermistors, respectively.

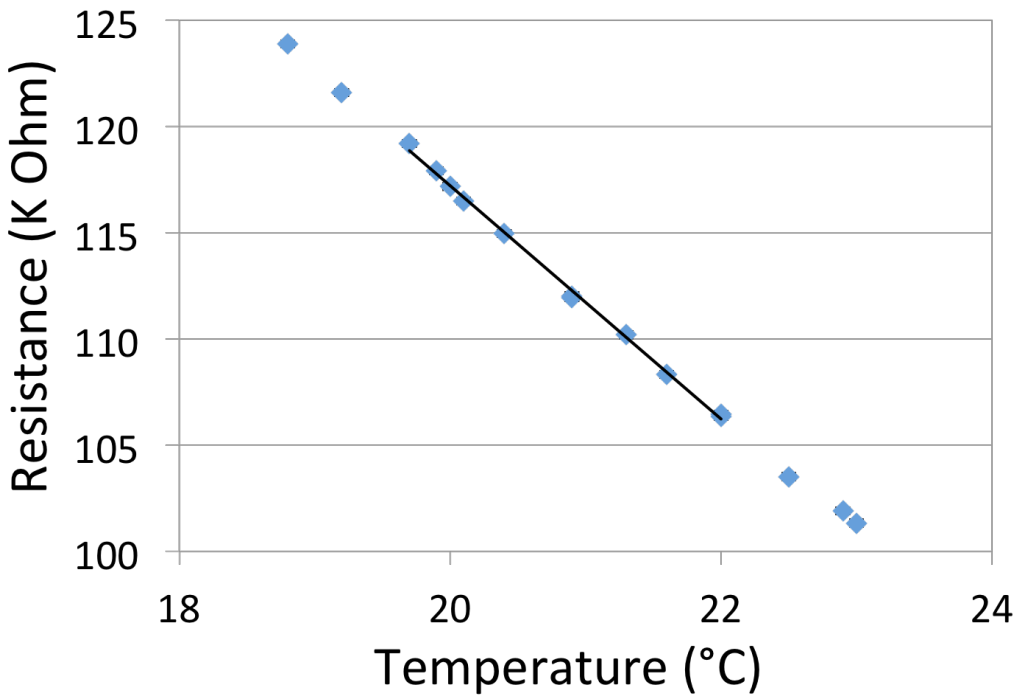

Fig. 2.9: Sample thermistor resistance values
Sample Thermistor (◆) The fit has a slope of -5.49 KOhm/°C

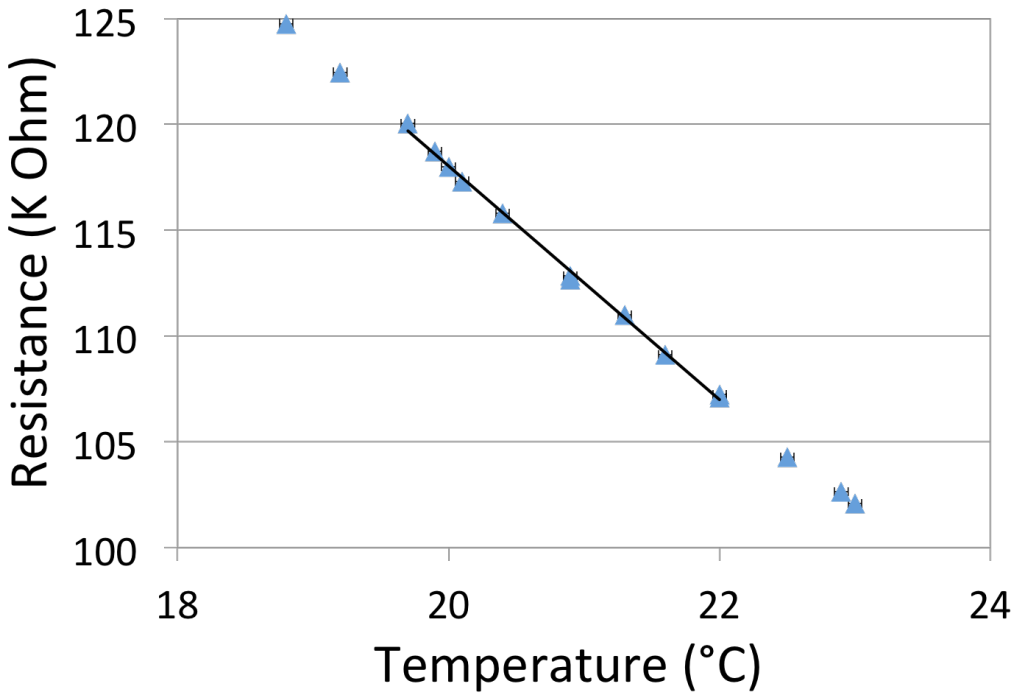

Fig. 2.10: Reference thermistor resistance values
Reference Thermistor (▲) The fit has a slope of -5.52KOhm/°C

The thermistor resistance yields an exponentially decreasing function over broader temperature ranges, as seen in Fig. 2.11. On this graph, the point at 21°C was taken during this experiment and the higher temperature points were collected previously using the less accurate multi-meter. In order to show the overall response, three significant figures are sufficient.

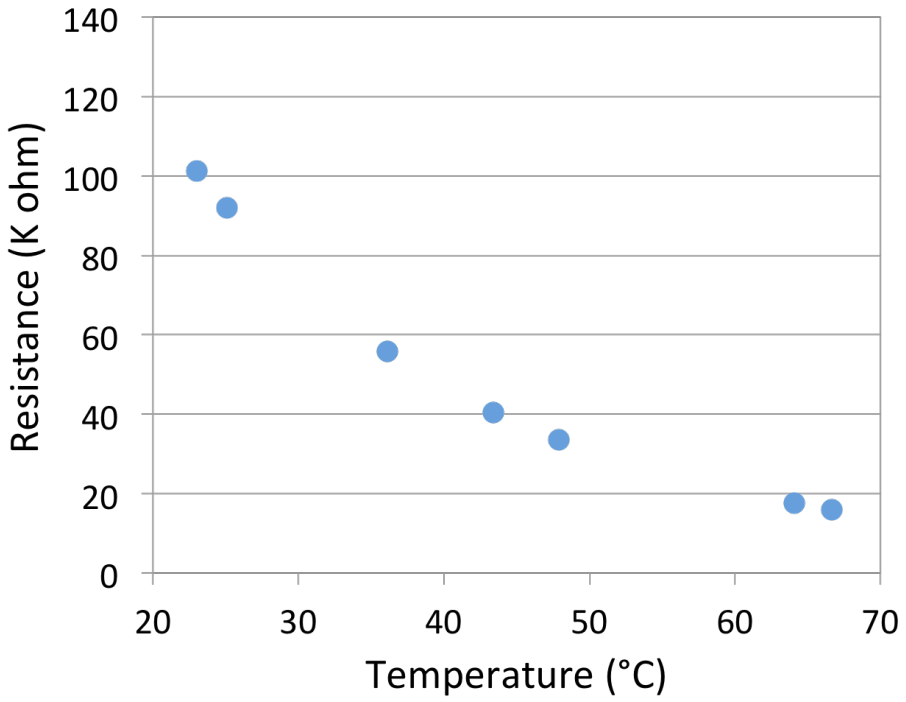

Fig. 2.11: Thermistor resistance curve over a wide range of temperature

The linear fits allowed calculation of the thermistor temperatures, and the difference between them. With these results, the next portion of the experiment determined the temperature difference between the thermistors during VPO measurement

The VPO cell was equilibrated to 20.9°C with heptane as the diluent, and a series of binary solutions of hexadecane in heptane were prepared gravimetrically.

Table 2.3: Concentration and temperature results. This table gives the average temperature difference between the two thermistors at the steady state for each concentration

Concentration of hexadecane in heptane		Temperature difference	
Molality (m)	Mole Fraction (x)	Average (°C)	Standard of deviation
0.086	0.0085	0.053	0.001
0.099	0.0098	0.063	0.005
0.126	0.0125	0.079	0.004
0.152	0.0150	0.094	0.006
0.172	0.0169	0.113	0.002
0.191	0.0188	0.125	0.002
0.222	0.0218	0.150	n/a

The sample injection and measurement procedure for this experiment differed from the procedure described for the aqeuous system. The VPO voltage signal was only used to verify the qualitative behavior for this experiment. Instead, the resistances were measured by disconnecting the cable leading from the thermistors to the VPO unit, as described earlier. The samples were measured in triplicated with baseline checks in between for the concentrations below 0.17 molal. The 0.17 molal and 0.19 molal solutions were measured in duplicate rather than triplicate, and the final point was a single measurement. Averages were used for plotting and analysis. These values are given in Table 2.3 along with the temperature change between the thermistors for each concentration at steady state.

The temperature resolution was 0.0002°C based on the thermistor temperature calibration curve and the Fluke multi-meter resistance resolution for the 100kOhm range. But due to noise in the last digit, the reliable temperature

resolution is closer to 0.002°C. This value corresponds to a change of 10 Ohm against the overall thermistor resitance of ~112kOhm.

The temperature data given in Table 2.3 can be used to fit a new constant in Eq. 2.17 , repeated below.

$$\Delta T = \frac{(1-a)}{\frac{k_1A_1 + k_2A_2}{k_3A_1}\frac{1}{P\Delta H} + a \bullet \frac{\Delta H}{RT^2}} \qquad 2.17$$

The denomiator to Eq. 2.17 was treated as a constant earlier refered to as β_1.

$$\beta_1 = \frac{k_1A_1 + k_2A_2}{k_3A_1}\frac{1}{P\Delta H} + a \bullet \frac{\Delta H}{RT^2} \qquad 2.28$$

However, the cell temperature is known, and the enthalpy of vaporization and vapor pressure can be calculated.[56] So a new constant is defined, β_4.

$$\beta_3 = \frac{k_1A_1 + k_2A_2}{k_3A_1} \qquad 2.29$$

With this definition, 2.17 becomes Eq. 2.30

$$\Delta T = \frac{(1-a)}{\beta_3\frac{1}{P\Delta H} + a \bullet \frac{\Delta H}{RT^2}} \qquad 2.30$$

Assuming that the activity of heptane is equal to the mole fraction for these dilute solution of hexadecane, and fitting with the temperature data using Matlab yielded a value of 18,300±400 J•mol•K^{-1}•kPa^{-1}. The line shown in Fig. 2.12 represents this fit. Using this parameter value, the variation of the denominator can be calculated in order to evaluate the effect of neglecting the change in the activity term in the denominator when using the VPO equation. Table 2.4 presents this result. The enthalpy of vaporization, ΔH, is 3.69kJmol^{-1} and the vapor pressure, P, is 4.927kPa for heptane at 20.9°C. Going from pure diluent to the highest concentration studied

changes the denominator, β_1, from 0.1523 K^{-1} to 0.1512 K^{-1}, a change of only 0.74%. In other words, assuming the denominator is constant introduces little error at least up to concentrations up to 0.22 molal.

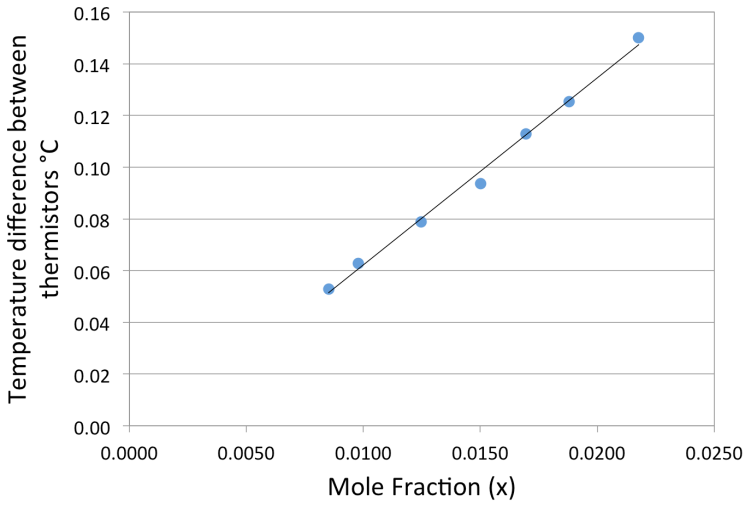

Fig. 2.12 Steady state temperature differences in the VPO cell. The points show the steady state temperature difference between the thermistors calculated based on the resistance of each thermistor. The line was fit to determine the constant β_3.

Table 2.4: Variation of the constant β_1

Hexadecane mole fraction	Denominator value
0	0.1523
0.0085	0.1518
0.0098	0.1518
0.0125	0.1516
0.0150	0.1515
0.0169	0.1514
0.0188	0.1513
0.0218	0.1512

The last of the experiment is determining the rate of temperature change at the pseudo steady state. For this task, a series of hexadecane in heptane solutions were measured in the VPO for the voltage signal without measuring resistance . These

Table 2.5: VPO signal for hexadecane in heptane

Concentration of hexadecane in heptane Mole Fraction (x)	VPO signal ΔV (μV)	One standard of deviation of ΔV (μV)
0.0029	171.2	1.3
0.0049	264.7	1.7
0.0079	419	4
0.0097	507	2
0.0116	616	6
0.0136	714	2
0.0168	885	5
0.0192	998	6
0.0228	1171	7

measurements were carried out as detailed for the aqeuous VPO experiments, but used hexadecane in heptane at 20.9°C in place of the aqueous solutions. The solutions were prepared gravimetrically, yielding the concentrations listed in Table 2.5, and the average pseudo steady state voltage signals indicated.

The voltage recording time for the highest concentration samples was extended in order to calculate the rate of the voltage drop.

The new data can be used to determine the proportionally constant, β_2, between the voltage signal and the temperature difference between the thermistors since the temperature is given by both Eq. 2.30 and Eq. 2.31.

$$\Delta V = \beta_2 \Delta T \tag{2.31}$$

The fit yields a β_2 of 7860 ± 50 μV/°C. Using this value, the voltage signal over time recorded for the highest concentrations can be converted into temperature difference over time. Fig. 2.13 shows the product of this conversion. The data for

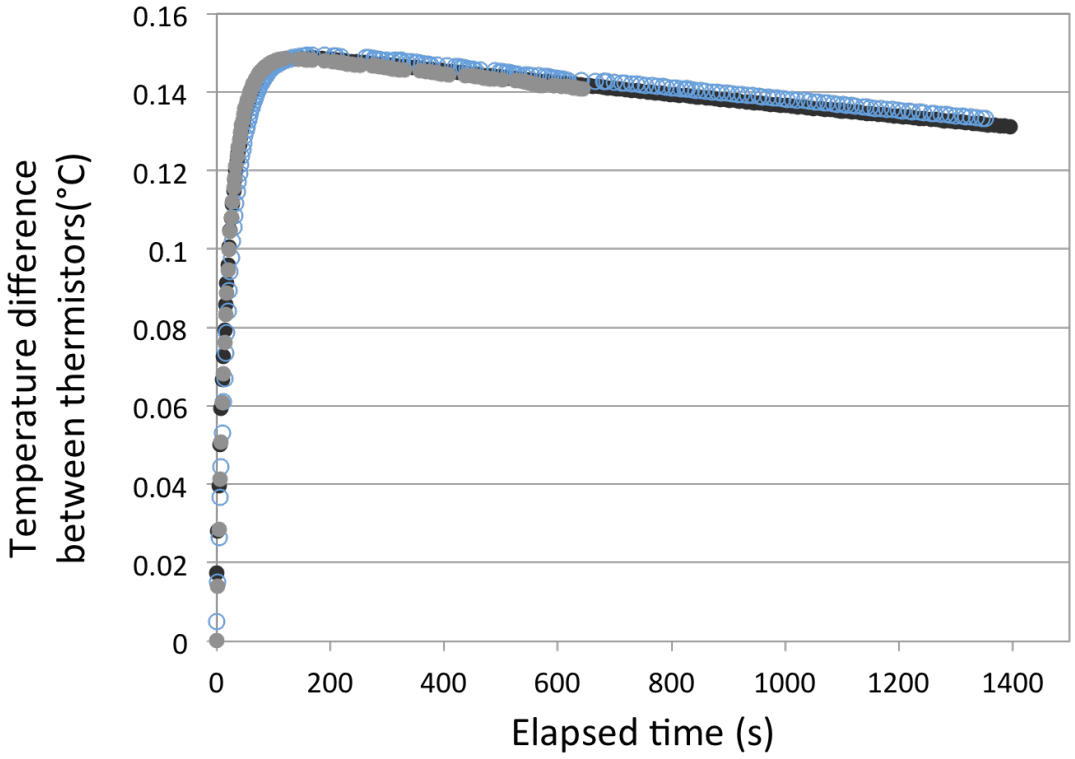

Fig. 2.13: VPO signal fall off over time
Temperature change across the thermistors as a function of time elapsed after sample injection for three samples of 0.0228 mole fraction hexadecane in heptane

the three individual time series show visually identical trends. Each decreases with the same linear slope, within error. The linear decrease is $-(8.8\pm0.5)\bullet10^{-4}$ °C/min.

Using this data, the impact of the non-zero time derivative can be assessed. In order to do so, relation 2.27 needs evaluated.

$$(1-a) \gg \left(mC_p \frac{dT}{dt}\right)/(k_3 A_1 P \Delta H) \qquad 2.27$$

All the terms here are now known or may be estimated.

From the definition of the constant β_3 the heat transfer coefficients can be used instead of the mass transfer coefficient

$$k_3 A_1 = \frac{(k_1 A_1 + k_2 A_2)}{\beta_3} \qquad 2.32$$

Inserting Eq. 2.32 into the inequality gives

$$(1 - a) \gg \frac{mC_p \frac{dT}{dt} \beta_3}{(k_1 A_1 + k_2 A_2) P \Delta H} \qquad 2.33$$

The mass, *m*, was taken to be the diluent hold up on the thermistor cap. A spare clean, dry stainless steel mesh end cap was placed on a thermistor bead identical to the VPO thermistors. The combination was then weighed before and after wetting the cap with hexadecane similarly to what happens to the thermistors in the VPO. Hexadecane was used instead of heptane in order to prevent evaporation during the measurements, and will provide a slight over estimate since the density is greater than that of heptane.

The heat capacity, vapor pressure and enthalpy of vaporization were calculated using correlations in the DIPPR database[56].

For the purposes of evaluating the inequality, only the heat transfer coefficient from the diluent drop to the vapor was estimated. Omitting the conduction term, decreases the denominator and makes the estimate more conservative. The mesh cap on the thermistor keeps the shape of the diluent drop in the form of a cylinder on the end of the thermistor, so the heat transfer coefficient was calculated for a vertical cylinder in air using the correlations for natural convection on a vertical cylinder.[70] The atmosphere remains 95% air, with only 5% heptane vapor based on the calculated vapor pressure, so this is only a minor

approximation. The correlation for the heat transfer coefficient is based on the Nusselt number and typically give values within 30% of the true number.[70]

All of the parameter values used to evaluate the inequality are summarized in Table 2.6, along with the values for each side of the inequality.

Table 2.6: Values used for evaluating inequality 2.33

Mass Hexadecane (g)	Molar Mass heptane (g/mol)	Heat capacity of heptane (J/mol)	dT/dt (K/s)	Diameter of thermistor cap (mm)	Length of thermistor cap (cm)	Nusselt number
0.0087	100.21	222.9	0.000015	2	0.5	10.6
Heptane vapor pressure (kPa)	Enthalpy of vaporization (J/mol)	Gas constant ($J\ mol^{-1}\ K^{-1}$)	Thermal conductivity of air at 20°C($J\ m^{-1}\ sec^{-1}\ K^{-1}$)	Temperature difference (K)	β_3 ($J\ mol\ K^{-1}\ kPa^{-1}$)	Prandtl number
4.927	3.69E+04	8.314	0.025	0.15	18300	0.71
Grashof number	Estimated heat transfer coefficient ($J\ m^{-2}\ s^{-1}\ K^{-1}$)	LHS of the inequality	RHS of the inequation	Ratio RHS to LHS	Estimated heat transfer to the vapor (J/s)	
102000	53	0.0228	1.57E-05	6.87E-04	2.75E-04	

The right side of the inequality evaluated to less than 0.01% of the term (1- a), and is likely an overestimate since the heat transfer coefficient due to conduction along the thermistor was ignored. Importantly, these values show that the rate of temperature change term accounts for an insignificant portion of the VPO signal. Thus, as with the other two incorrect two assumptions, the VPO equations is not effected.

2.6 Chapter conclusions

Vapor pressure osmometry provides an accurate method to calculate diluent activities in binary systems with one volatile component and one non-volatile

component. The expression relating the voltage output is straightforward and easy to derive, as was shown in the first half of the chapter. It remains robust when three assumptions are relaxed in order to more accurately match the true experimental conditions, as was demonstrated in the second half of the chapter. Data sets from four different binary aqueous solutions provided a clear validation of the VPO method. These overall results provide unequivocal support for the experimental data in the following chapters.

3 Chemical Activity of HDEHP

The validation of the VPO instrument in chapter 2 sets the foundation for the experiments presented in this chapter, demonstrating that the results are reliable. Activity coefficients for HDEHP dimer are calculated based on data collected using the VPO, and compared with three outside sources. These values are calculated by integration of the Gibbs-Duhem equation using the diluent activity obtained from the VPO results. The activity coefficient for HDEHP dimer in heptane at 21°C is compared with the data presented by Danesi et al,[34] and Baes.[33] The temperature dependence of the activity coefficient matches the trend predicted using the enthalpy of mixing data by Kolarik.[35] The data for HDEHP in heptane, however, does not seem to follow this temperature trend, but that could potentially be explained by diluent dependence of the activity coefficient. A detailed discussion is given on the selection of the standards for the VPO and accounting for non-ideality in the standard solutions. That evaluation suggests a modified free volume entropic correction proposed by Kontogeorgis[71] et al. for the combinatorial-free volume

component of the activity gives accurate results for the alkane-alkane binary systems. An additional regular solution correction for the residual component of the activity coefficient is needed for the alkane-aromatic systems. Analyzing the HDEHP data with this same theory yields a solubility parameter for HDEHP dimer, which can be used to calculate the activity coefficients of HDEHP dimer. However, the first method involving the integration of the Gibbs-Duhem equation gives more accurate results. The regular solution residual correction is at most qualitatively applicable to systems with polar and hydrogen bonding.[46] Solubility parameters and Gibbs-Duhem based results are also reported for the computations repeated using regular solution theory with the classic Flory-Huggins[42] entropic corrections instead of the corrections proposed by Kontogeorgis. That data overestimates the excess entropy of the standard solutions and HDEHP solutions. Despite being less accurate, this reanalyzed result is still of practical value since it is directly applicable to the modeling program SXFIT,[49] which uses the same theory.

3.1 Experiment overview

A total of 24 sets of VPO data on HDEHP were collected in a temperature range from 21°C and 110°C. Over these 24 experiments, seven different diluents were investigated under the conditions summarized in Table 3.1. The table lists the number of points used for the standard, and for HDEHP, along with the concentration ranges for each experiment. Another data set, outside the 24 already mentioned, was collected to compare four different chemicals for use as VPO standards. But this set is not listed in Table 3.1 since it did include HDEHP. The

heptane experiment listed in Table 3.1 also included data on HDEHP complexed with dysprosium, which is the subject of the next chapter. The five data sets, marked with asterisks in Table 3.1, are the results of preliminary work, and are only of qualitative value. The nineteen best sets were used for the analysis in this chapter along with the data sets on the standards.

Four of the preliminary sets, marked with a single asterisk in the table, were the earliest data collected, and potentially suffer from three sources of uncertainties that were fixed prior to measuring the later sets. For at least two of those four sets, and potentially all four of them, the VPO cell leaked such that the solution in the cell entered the thermistors. This contamination potentially shifted the VPO measurements by altering the resistance in the circuit. The thermistors either developed a stress fracture or were installed improperly, both likely events based on the poor track record of the supplier and manufacturing method of the thermistors. Second, the experimental baseline was only checked at the begging of the day and the end of the day of measurements, but not between samples. This is in accordance the provided manual,[72] but was not sufficient. Possibly due to the leak, the baseline was observed to shift slightly from the initial reading to the final readings. These two issues make the value of these initial data sets only qualitative.

The experiment marked with double asterisks was one of the first experiments using the less sensitive thermistors. When the instrument was sent in for thermistor replacement, the company installed thermistors that they claimed would operate better at higher temperatures and sent it back before notifying of that change. These thermistors, combined with the lower temperature for the

experiment, gave a low signal to noise ratio. The standard of deviations on all points in this set were excessive, making the analysis meaningless. The results and analysis for this data set will not be reported further. A 26th data set was attempted using 1-butanol as the diluent, but the experiment was discontinued due to effects in the transient VPO signal suggesting moisture was being absorbed from the air during sample preparation and measurements. The remainder of the chapter deals with the results and analysis of the 19 higher quality data sets that suffered none of these issues.

Table 3.1: Summary of the experimental conditions for VPO on HDEHP
The standard code 'H' refers to *n*-hexadecane, and the code 'T' refers to *n*-tetracosane

Experiment Code	Diluent	VPO Cell Temperature °C	Standard Code	No. data points for standard	Standard concentration (molal)		No. data points for HDEHP	HDEHP concentration (molal)	
					Maximum	Minimum		Maximum	Minimum
1	Heptane	21	H	14	0.233	0.050	10	0.518	0.092
2	Octane	35	H	7	0.229	0.059	6	0.355	0.061
3	Octane	45	T	11	0.246	0.048	11	0.437	0.120
4	Octane	45	T	7	0.221	0.052	14	0.638	0.011
5	Octane	65	T	8	0.242	0.007	12	0.509	0.008
6	Decane	80	T	9	0.198	0.025	13	0.601	0.021
7*	Dodecane	80	T	14	0.300	0.003	15	0.571	0.024
8*	Dodecane	90	T	7	0.249	0.031	24	0.480	0.008
9	Dodecane	90	T	7	0.177	0.044	12	0.628	0.066
10	Dodecane	93	T	6	0.255	0.108	11	0.511	0.053
11	Dodecane	95	T	8	0.208	0.011	11	0.538	0.018
12	Dodecane	95	T	8	0.143	0.051	7	0.249	0.013
13	Dodecane	100	T	6	0.238	0.049	8	0.638	0.054
14*	Dodecane	100	T	6	0.084	0.007	14	0.253	0.005
15	Dodecane	110	T	11	0.305	0.055	14	0.663	0.054
16	Dodecane	110	T	5	0.231	0.049	10	0.592	0.052
17*	Toluene	30	T	19	0.240	0.032	25	0.429	0.011
18**	Toluene	40	T	7	0.347	0.105	6	0.524	0.206
19	Toluene	45	T	10	0.280	0.061	17	0.533	0.042
20	Toluene	45	T	13	0.300	0.106	15	0.567	0.049
21	Toluene	65	T	8	0.225	0.028	5	0.303	0.041
22	Xylene	45	H	8	0.232	0.024	8	0.453	0.055
23	Cyclooctane	66	T	7	0.261	0.055	13	0.597	0.051

3.2 Data analysis overview

The first step in analyzing each of the VPO data sets is to fit the constant, *k,* in Eq. 2.1 to the data for the standard. This equation was validated using aqueous solution data and discussed in detail in the previous chapter.

$$\Delta V = k(1 - a) \qquad 2.1$$

Where ΔV is the VPO signal (μV), k is the VPO machine constant, and a is the diluent activity. The activity of the standard solutions can be calculated with an appropriate thermodynamic model, and then the machine constant in Eq. 2.1 is obtained by fitting to the experimental VPO signal. Once this value is obtained, the VPO data on the HDEHP solutions can be used to calculate the diluent activity in the HDEHP solutions. Next, a smoothing function can be fit to the diluent activity data, and substituted into the Gibbs-Duhem equation for integration to obtain the activity coefficient of HDEHP. That value is the objective of these experiments. Alternatively, a model, such as the regular solution theory (RST) of Scatchard and Hildebrand, can be fit to the diluent data, and then be used to calculate the HDEHP activity.

3.3 Chemical property source

The physical parameters for each system were obtained primarily from the DIPPR database.[56] The data on molar volume was calculated from the temperature dependent bulk density correlation given in the DIPPR, and solubility parameters were calculated based on the enthalpy of vaporization.[46] HDEHP is not listed in DIPPR, so the molar volume was interpolated from the temperature dependence of the molar volume of pure HDEHP.[73] HDEHP dimer molar volume was approximated as twice the molar volume of pure HDEHP. The Van Der Waal molecular volumes

were calculated using MarvinSketch[74] chemical drawing and modeling software. These values were cross-checked against the value of the classic Bondi[75] method, which are tabulated in DIPPR, and were within 1%. The only source for the HDEHP value was the software calculation. The value for dimer was taken to be twice that of HDEHP monomer, adjusted by an extra bond, approximating the strong hydrogen bonds in the cyclic dimer, using the bond value given by Zhao et al.[76]

3.4 VPO Standard Selection

The VPO standards to determine the machine constant were *n*-tetracosane and *n*-hexadecane. The standards were selected based on three main criteria.

1. The standard had to be available at over 99% pure
2. Have negligible vapor pressure compared to the diluent.
3. Yield calculable diluent activities, preferably with a low degree of non-ideality.

For solutions of alkanes, the straightforward choice to meet these requirements is a longer chain *n*-alkane with a vapor pressure less than 0.1% of the least volatile diluent. In other words, the alkane standard had to have an insignificant vapor pressure compared to *n*-dodecane, the least volatile diluent under the current study. The standard selected was *n*-tetracosane, a 24 carbon *n*-alkane. The vapor pressure of tetracosane is approximately 0.03% of the vapor pressure of *n*-dodecane at 110°C, the highest temperature investigated.

Standards used by other groups for VPO have included benzil,[38,39,77] trioctylamine,[61,77,78] 1-bromotetradecane,[78] for alkane and aromatic diluents. However, the non-ideality of these chemicals would be more challenging to

accurately characterize compared to n-tetracosane. The authors do not account for the non-ideality of the standard in their systems. In the case of 1-bromotetradecane, excessive vapor pressure excludes it from being a VPO standard for dodecane.

Initially our VPO experiments focused on *n*-dodecane, but higher vapor pressure diluents were investigated later, so several further standards were tested. *n*-Tetracosane, *n*-hexadecane, squalane, and tridecylbenzene were all compared in octane at 45.1°C using VPO. The structure of each of these chemicals is shown in Fig. 3.1 (page 61). Although not conducted, an experiment comparing these four standards, along with biphenyl as fifth, in toluene or another aromatic diluent would improve the interpretation of the VPO data. Results of the standard comparison experiment in octane show that the standards *n*-hexadecane and *n*-tetracosane and the two other potential standards, squalane and tridecylbenzene, give consistent machine constant values. These results are shown in Table 3.1. Non-ideality was taken into account during that calculation using the methods outlined in the next sections.

Table 3.2: VPO machine constant based on four different standards in octane.
VPO data was collected on *n*-tetracosane, squalane, *n*-hexadecane, and tridecyl benzene for comparison of the standards. Two experiments discussed in the next chapter used *n*-tetracosane as the standard under the same conditions and are also reported. Non-ideality was corrected using the best method described in the next section.

Standard	Cell Temp. (°C)	Machine constant K/1000 ± uncert.	Change without non-ideality correction
n-Tetracosane	45.2	54.6 ± 0.4	0.3
n-Tetracosane	45.1	54.0 ± 0.2	0.3
n-Tetracosane	45.1	54.4 ± 0.3	0.3
n-Hexadecane	45.1	55.3 ± 0.6	0.0
Squalane	45.1	54.8 ± 0.4	0.5
Tridecylbenzene	45.1	55.1 ± 0.3	-0.4

3.5 Calculating the diluent activity for the standard solutions

Initially, the activity coefficients for the standard solution were calculated based on regular solution theory (RST) with Flory-Huggins(FH) excess entropy terms[79]. Although this model is consistent with SXFIT,[49] there are many improved models that provide better matches to experimental results. Several of these models were evaluated, and it was found that the choice of model did not significantly effect the HDEHP dimer activity coefficient results for heptane, or the other *n*-alkanes. However, for cyclooctane and the aromatic solvents, the choice of the model for the standard does affect the calculated HDEHP activity. The most suitable model was a modification of the free volume theory referred to as 'pFV' that was proposed by Kontogeorgis[71] et al., and modified with an additional RST correction for the alkane-aromatic solutions.

Unless I become famous or run for office I'll be extremely surprised if anyone thoroughly skims, let alone reads, this thesis. Short of that, it will join the countless other theses published at UCI that will not be read.

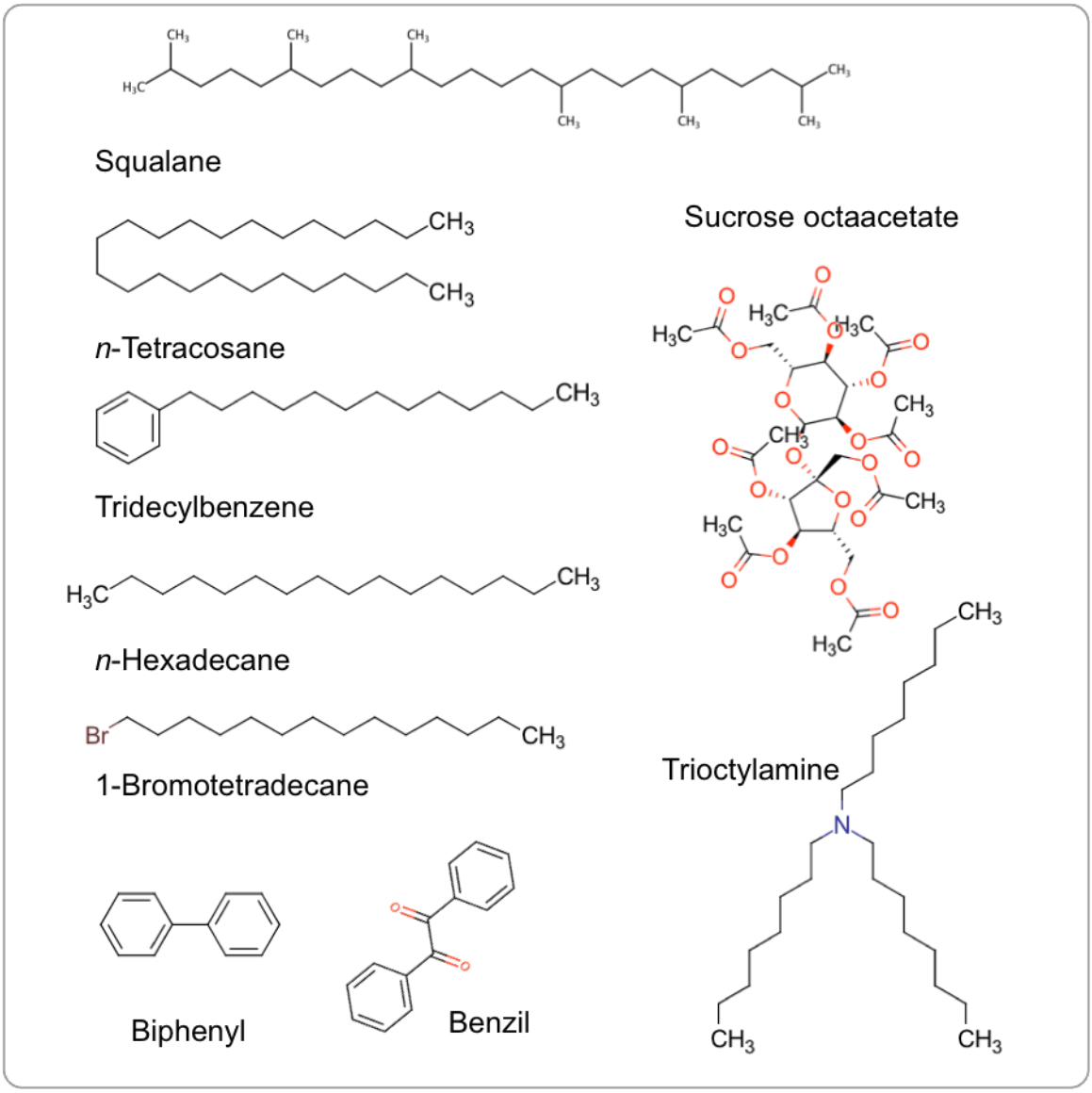

Fig. 3.1: Structures of potential VPO standards

Eight models were evaluated for calculating the activity of the standard solutions based on the mole fraction concentrations, and were evaluated against four test data sets. The overall activity coefficient was treated with the common assumption that it may be evaluated as a function of two separate parts, a residual term and an entropic term.[42,71,80,81] This treatment is expressed mathematically in Eq. 3.1.

$$ln(\gamma_i) = ln(\gamma_i^{res}) + ln\left(\gamma_i^{Comb,FV}\right) \quad 3.1$$

The residual part accounts for energetic or enthalpic interactions between molecules, and the combinatorial, free volume term represents the entropic effects due to the different sizes and volumes of the molecules.

In the treatment of the VPO standard, the residual term will be modeled either using regular solution theory (RST),[46] Eq. 3.2, or by setting the residual term to zero, Eq. 3.4

$$ln(\gamma_i^{res}) = \frac{V_i}{RT}(\delta_i - \bar{\delta})^2 \quad 3.2$$

$$\bar{\delta} = \sum \phi_{V,i}\delta_i \quad 3.3$$

V_i is the molar volume of component *i*; δ_i is the solubility parameter of component *i*; and $\bar{\delta}$ is the volume average solubility parameter; and $\phi_{V,i}$ is the volume fraction of component *i*.

Binary solutions of alkanes are considered to be approximately athermal, and the residual term is frequently considered insignificant and not included in the analysis[71,81] and set to zero, Eq. 3.4.

$$ln(\gamma_i^{res}) = 0 \quad 3.4$$

For alkanes in aromatics, however, the residual term cannot be neglected, as will be demonstrated shortly.

The entropic term will be treated using the four methods presented in Eq. 3.5 to Eq. 3.10.

The simplest case is to assume the system has zero excess entropy. Although not an accurate characterization due to the large size difference between diluent and standard, it is useful as a reference case when comparing the other samples.

i. Assuming zero excess entropy

$$ln\left(\gamma_i^{Comb,FV}\right) = 0 \quad 3.5$$

At the other extreme, an over estimate of the excess entropy is given by the classic Flory-Huggins expression, Eq. 3.6. It is included in the analysis in order to remain consistent with SXFIT, where the final results on HDEHP will be directly applicable.

ii. Flory-Huggins expression (FH)[42]

$$ln\left(\gamma_i^{Comb,FV}\right) = ln\frac{\phi_i}{x_i} + 1 - \frac{\phi_i}{x_i} \quad 3.6$$

$$\phi_i = \frac{x_i V_i}{\sum x_j V_j} \quad 3.7$$

Φ_i is the volume fraction of component *i* as given by Eq 3.7. This equation overestimates the excess entropy, predicting activity coefficients much lower than are observed experimentally. In fact, the FH can overcorrect so far that the estimate is more off than assuming ideality.[81] However, modifications of FH can provide close matches to experimental data simply by changing the Φ_i term.

iii. Flory Free Volume model (FV1.1)[71] by altering Eq 3.7

$$\phi_i = \frac{x_i S_i}{\sum x_i S_i}; \quad 3.8$$

$$S_i = \left(V_i^{1/3} - V_{W,i}^{1/3}\right)^{3c}; c = 1.1 \quad 3.9$$

$V_{w,i}$ refers to the Van der Waals volume of the molecule 'i'. While the FH expression used molar volumes, this is a restatement based on free volumes of the molecules. The term S_i is does not directly translate into the free volume of each component, it is an empirical modification of theory where $V_{w,i}$ is directly subtracted from V_i, which would be analogous to free volume. Setting the factor '*c*' to 1.1 is an empirical choice based on the best fit to the widest range of data.[71] This equation yields good fits for n-alkanes, but underestimates the activity coefficient for cycloalkanes,[71] and aromatics as the tests set show later.

iv. A free volume based expression proposed by Kontogeorgis et al.[71] and referred to as *pFV* where Eq. 3.9 is changed:

$$S_i = (V_i - V_W)^p;\ p = 1 - V_{W,small}/V_{W,large} \quad 3.10$$

$V_{W,small}$ is the Van Der Waals volume of the smaller component, and $V_{W,large}$ is the Van Der Waals volume of the larger component. According to Kontogeorgis, the exponent accounts for the asymmetry of the system components. Although the equation given here is in binary form, it is possible to extend to multicomponent mixtures.[71]

Other treatments are available, but model comparison show that the pFV and the FV1.1 are among the most accurate, and are as good as more complex theories.[71,80,81] These comparisons also demonstrate that no single theory yields the best result across all classes of compounds.

These model comparison papers look at model performance in relation to infinite dilution activity coefficients or solid liquid equilibria, and comparison to activity data at intermediate concentrations is more limited.[71,80,81] In the paper by Kontogeorgis et al.[71] five intermediate data sets were used in addition to extensive limiting activity coefficient data sets, but all theories tested gave poor fits to the intermediate data, including the pFV and FV1.1. Oddly, that mismatch was not discussed.

In light of that discrepancy, several activity coefficient data sets on data relevant to the current study were evaluated to verify the accuracy of the selected models. Binary activity data for *n*-hexadecane + *n*-octane,[82] *n*-hexane + benzene,[83] *n*-octane + benzene,[84] and *n*-hexane + *n*-dodecane,[85] were modeled using the two treatments of the residual term in combination with each of the four entropic correction theories. Activity coefficients for each data sets were calculated using each of the models and compared against the literature data. Fig. 1.2 to Fig. 1.5 show the performance of each model based on those calculations, and it is visually clear as to which model performs best in each solution.

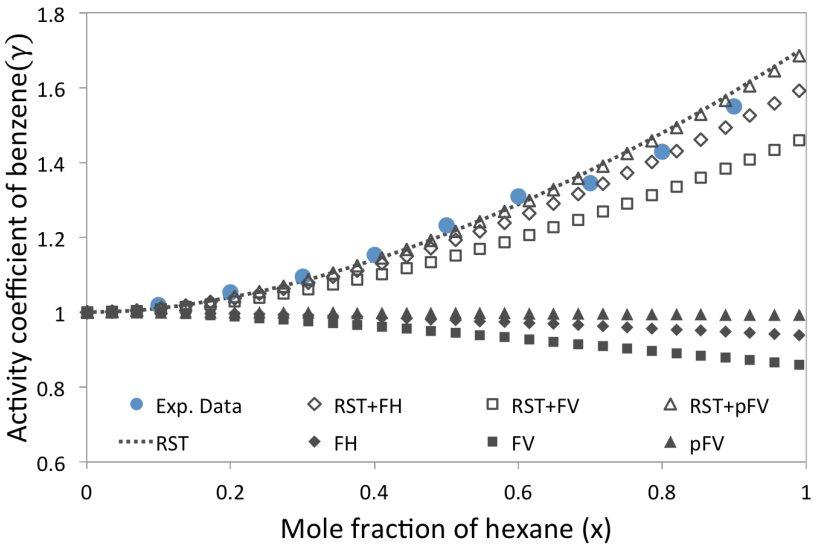

Fig. 3.2: Evaluation of thermodynamic models.
Activity coefficient data[84] for benzene + *n*-hexane at 298.15K compared to calculations made using each theory outlined in this section. Unlike the alkane-alkane mixtures, the RST term is required for an acceptable fit. RST+pFV gives the best fit, but RST and RST+FV1.1 both give acceptable fits since the size difference between molecules is small.

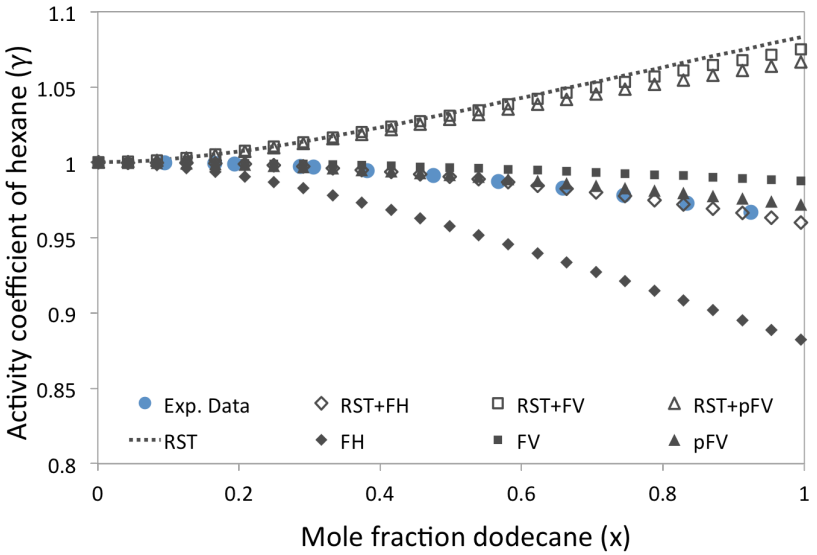

Fig. 3.3: Evaluation of thermodynamic models
Activity coefficient data[85] for *n*-hexane + *n*-dodecane at 308.15K compared to calculations made using each theory outline in this section. The pFV and RST+FH theories give the best fit, but for RST+FH this is due to coincidental cancelling of errors.

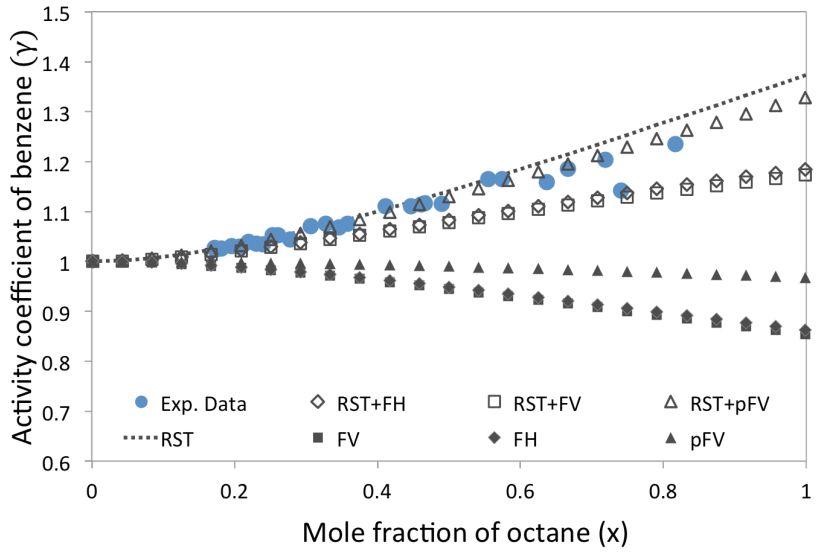

Fig. 3.4: Evaluation of thermodynamic models
Activity coefficient data[84] for benzene + *n*-octane at 328.15K compared calculations made using each theory outlined in this section. Unlike the alkane-alkane mixtures, the RST term is required for an acceptable fit. RST+pFV gives the best fit, but RST is also acceptable since the size difference between the molecules is small.

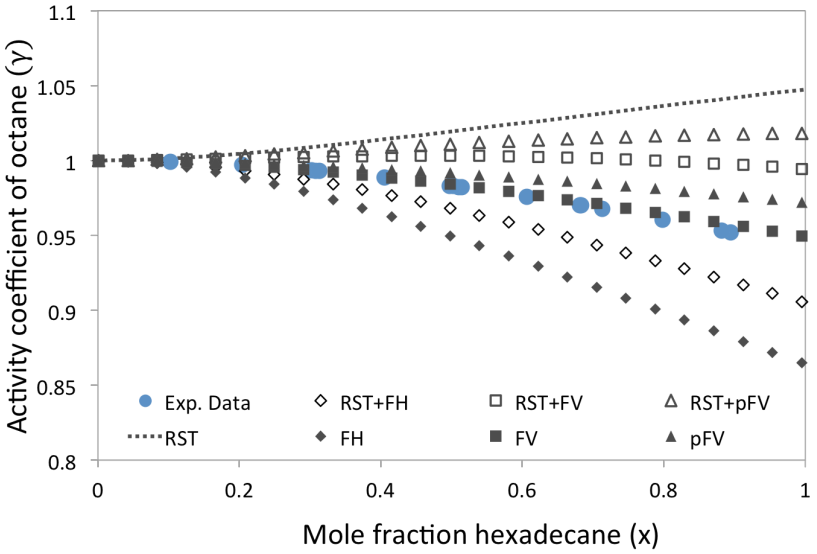

Fig. 3.5: Evaluation of thermodynamic models
Activity coefficient data[82] for *n*-octane + *n*-hexadecane at 298.15K compared to calculations made using each theory outlined in this section. The best fit uses FV1.1, but pFV also gives an approximate fit. FH severely underestimates the activity coefficient.

In agreement with literature, the calculations done performed here show no single theory provides the best to the experimental data fit in all cases. For alkane-alkane mixtures, the inclusion of the RST term is incorrect, but for aromatic-alkane mixtures it yields a good fit, particularly when combined with pFV. From the two alkane-alkane mixtures of larger size difference, it is apparent that both FV1.1 and pFV give reasonable fits, but which gives the best fit depends on the system. The FH expression without RST correction gives poor fits in all cases, and only provides an acceptable fit with RST when the effects of overestimating the excess entropy cancel with the effects of overestimating the excess enthalpy.

Based on the agreement of the test systems with literature assessment, the non-ideality of the standard will be compensated using the pFV theory for the alkane-alkane systems, and the RST+pFV theory for the alkane-aromatic systems. Additionally, for consistent results with SXFIT, the less accurate RST+FH results will be reported as well.

3.6 Machine constant evaluations

The diluent activity for the standard data was calculated using the methods outline in the previous section, and the VPO equation was fit to the VPO signal for these solutions in order to obtain the machine constant, *k* for each experiment. The results are presented in Table 3.3 (page 70).

$$\Delta V = k(1 - a) \qquad 2.1$$

The numerical values of the machine constants are given for the assumption of an ideal solution, along with a one standard of deviation uncertainty expressed as

percent. The subsequent columns gives the percent decrease or increase from this ideal reference for each of the methods described in the previous section. The values using either pFV or FV1.1 with and without RST do not significantly alter the results for the *n*-alkane + *n*-alkane solutions since the change is within the error on the value for *k*. In contrast, the differences are outside the uncertainty for the aromatic compounds and cyclooctane. The FV1.1 method is reported to provide a poor fit for cycloalkanes,[71] underestimating the activity coefficients. In line with this observation, it yields a significantly smaller value of *k* than the pFV method yields. Using RST+FV1.1 also seems to underestimate the machine constant for the aromatic solutions. The FH method gives the lowest results in all but the cyclooctane system, and leading to artificially low machine constants. Low machine constant underestimate the diluent activity in the HDEHP solutions.

Thus, although the pFV and FV1.1 theories give similar results for the alkanes, the pFV will be used for the rest of the data analysis as it provides the best all around fit for these particular systems. For the standard corrections on toluene and o-xylene, the RST form of residual corrections is made as well. These 'best' *k* value are marked by bold font in Table 3.3. Although less accurate, results will also be reported using RST+FH for all data sets in order to be consistent with SXFIT.

Table 3.3: Summary of the VPO machine constant.
The sets in bold are used for the remaining analysis.

Experiment code	Diluent	VPO cell temp. (°C)	Standard code	Ideal solution machine constant	Percent change to the machine constant when non-ideality is modeled by						
				k/1000 ± uncert.	RST+pFV	pFV	RST+FV	FV	RST+FH	FH	RST
1	Heptane	21	H	52.1 ± 0.3%	0.3	**-0.1**	0.2	-0.1	-0.3	-0.7	0.4
2	Octane	35	H	41.4 ± 0.7%	0.2	**-0.1**	0.2	-0.1	-0.3	-0.6	0.3
3	Octane	45	T	5.72 ± 0.8%	0.1	**-0.5**	0.1	-0.6	-1.8	-2.5	0.7
4	Octane	45	T	54.5 ± 0.6%	0.1	**-0.4**	0.1	-0.5	-1.4	-2.0	0.5
5	Octane	65	T	95.2 ± 0.6%	0.3	**-0.5**	0.3	-0.5	-1.5	-2.3	0.8
6	Decane	80	T	37.3 ± 0.9%	0.1	**-0.2**	0.0	-0.3	-0.8	-1.1	0.3
7	Dodecane	80	T	3.33 ± 1.0%	0.0	**-0.1**	-0.2	-0.4	-1.0	-1.1	0.2
8	Dodecane	90	T	4.80 ± 0.3%	0.0	**-0.1**	-0.1	-0.3	-0.8	-0.9	0.1
9	Dodecane	90	T	12.9 ± 0.7%	0.0	**-0.1**	-0.1	-0.2	-0.6	-0.8	0.1
10	Dodecane	93	T	8.17 ± 0.5%	0.0	**-0.1**	-0.1	-0.3	-0.9	-1.0	0.2
11	Dodecane	95	T	15.1 ± 0.5%	0.0	**-0.1**	-0.1	-0.3	-0.8	-1.0	0.2
12	Dodecane	95	T	15.1 ± 0.8%	0.0	**-0.1**	-0.1	-0.2	-0.5	-0.7	0.1
13	Dodecane	100	T	13.4 ± 0.7%	0.1	**-0.1**	-0.1	-0.3	-0.8	-0.9	0.2
14	Dodecane	100	T	6.97 ± 2.4%	0.0	**0.0**	0.0	-0.1	-0.3	-0.3	0.1
15	Dodecane	110	T	9.66 ± 0.3%	0.1	**-0.1**	-0.1	-0.3	-0.9	-1.1	0.2
16	Dodecane	110	T	20.2 ± 0.8%	0.1	**-0.1**	0.0	-0.3	-0.8	-1.0	0.2
17	Cyclooctane	66	T	12.3 ± 0.6%	-0.5	**-1.4**	-6.1	-6.8	-3.3	-4.1	0.9
18	Toluene	30	T	22.4 ± 0.6%	**1.2**	-1.9	-0.3	-3.3	-2.6	-5.5	3.2
19	Toluene	40	T	6.63 ± 1.1%	**1.3**	-2.8	-0.8	-4.7	-4.2	-7.9	4.3
20	Toluene	45	T	9.14 ± 0.5%	**0.9**	-2.3	-0.7	-3.9	-3.7	-6.7	3.4
21	Toluene	45	T	4.93 ± 0.3%	**0.9**	-2.3	-0.7	-3.9	-3.7	-6.7	3.4
22	Toluene	65	T	133.8 ± 0.4%	**0.2**	-1.7	-0.8	-2.7	-3.3	-5.1	2.1
23	Xylene	45	H	39.2 ± 0.6%	**1.5**	-0.4	-0.1	-2.0	0.2	-1.7	2.0

3.7 Experimental HDEHP activity

The activity of the diluent in the HDEHP systems can now be calculated using the VPO equation with the non-ideality corrected machine constants. Using this data to integrate the Gibbs-Duhem yields the HDEHP dimer activity coefficient. The results are compared with HDEHP dimer activity coefficients reported for octane and dodecane in the literature at 25°C. All HDEHP used for these experiments was purified using the copper precipitation method as outlined by Partridge et al.[86]

If no assumptions are made as to the aggregation of HDEHP, the activity coefficient of the diluent increases for both the alkanes and the aromatics with increasing HDEHP, as shown in Fig. 3.6. The data is close for each of alkanes, but xylene and toluene show a trend different than the alkanes. However, HDEHP exists dominantly in dimer form, and it is common practice to use dimer concentration while ignoring residual monomer.[33–35] By Assuming that HDEHP exists exclusively in dimer form, the non-ideality shown in Fig. 3.6 is greatly reduced. Figure Fig. 3.7 gives the diluent activity when that assumption is made. o-Xylene shows an ideal solution of dimers, within error, and toluene shows a decreasing diluent activity coefficient. If monomer concentration were significant, contrary to the current assumption of negligible monomer concentration, the activity coefficient would initially start below one, and then increase with increasing HDEHP. It would not start at one and decrease with increasing HDEHP as is observed. Thus presence of monomer does not explain the decreasing trend for the diluent activity coefficient in toluene.

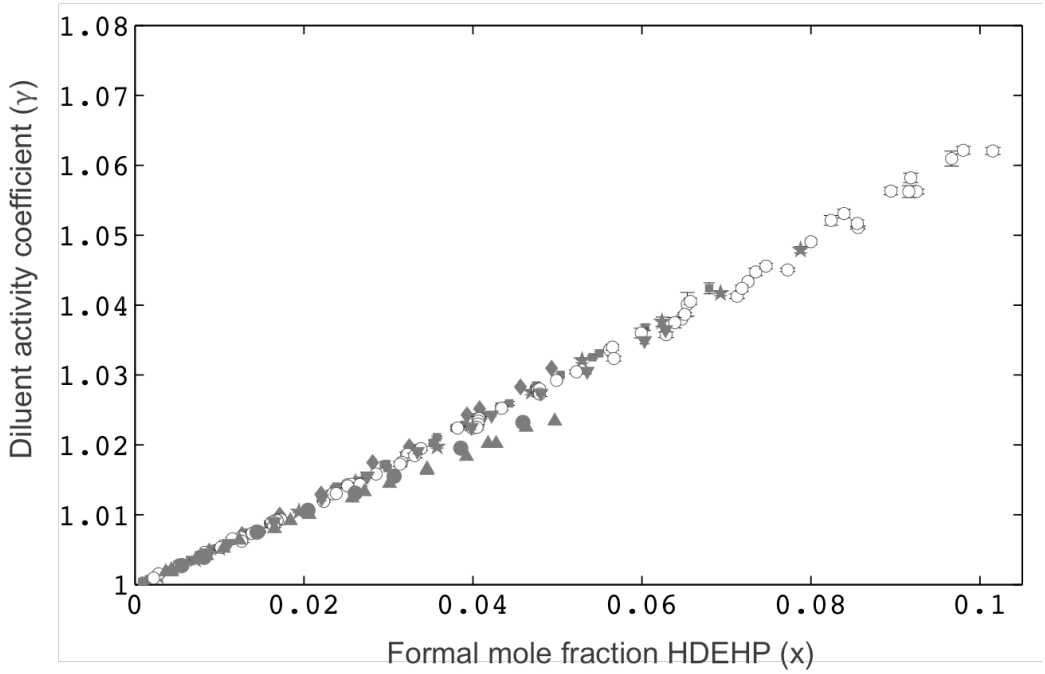

Fig. 3.6: Activity coefficient of the diluent when HDEHP is treated as a monomer
▲Toluene, ● o-xylene, ◆ *n*-heptane, ■ *n*-octane, ★ *n*-decane. ○ *n*-dodecane, ▼cyclooctane.

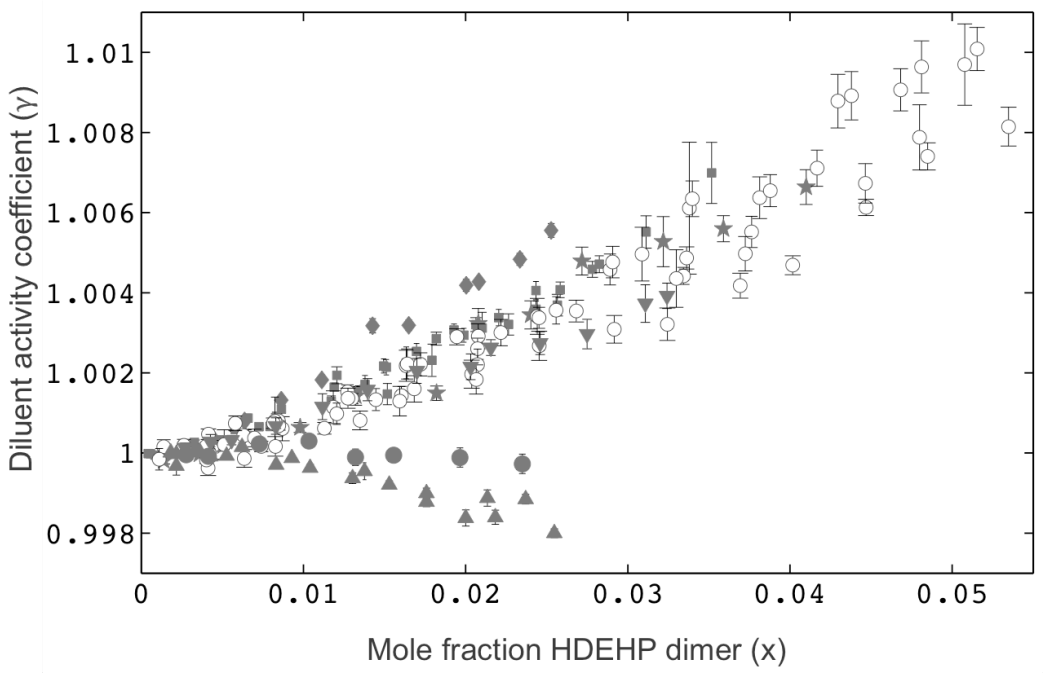

Fig. 3.7: Activity coefficient of the diluent when HDEHP is treated as a dimer
▲Toluene, ● o-xylene, ◆ *n*-heptane, ■ *n*-octane, ★ *n*-decane. ○ *n*-dodecane, ▼cyclooctane

Rather, the decreasing activity coefficient in toluene is due two factors. First, solutions with large size differences between molecules (e.g. solvents + polymers or the alkanes shown in Fig. 3.3 and Fig. 3.5) can show activity coefficients less than one due to entropic effects. The entropy of mixing is less favorable than in an ideal mixture. Second, the excess enthalpy of mixing for HDEHP with toluene shows an opposite trend than for HDEHP with the alkanes.[35] Mixtures of HDEHP in alkanes are endothermic, while mixtures of HDEHP in aromatics such as toluene are exothermic. Thus, these differing behaviors of the activity coefficients are reasonable.

For the alkane data, the most non-ideal system appears to be HDEHP in heptane, followed on average by octane, and then by dodecane. However, interpreting this difference requires further analysis since temperature of the experiment and size of the diluent changes simultaneously.

In order to obtain the activity coefficient of HDEHP dimer via the Gibbs-Duhem equation, the smoothing function, Eq. 3.11, was fit to the data.

$$ln\,\gamma_1 = \beta\, x^{1.5} \qquad 3.11$$

Example fits are given for HDEHP in toluene, heptane and dodecane in Fig. 3.8. Initially the exponent was fit as a second parameter, but using two parameters over fit the data. The two parameters were highly correlated, leading to high uncertainty in both values. Instead, the exponent was selected from the average for all data sets, leaving only the coefficient, β, as the fitting parameter. The parameter result for each data set is given in Table 3.4, where one standard of deviation uncertainties are also shown.

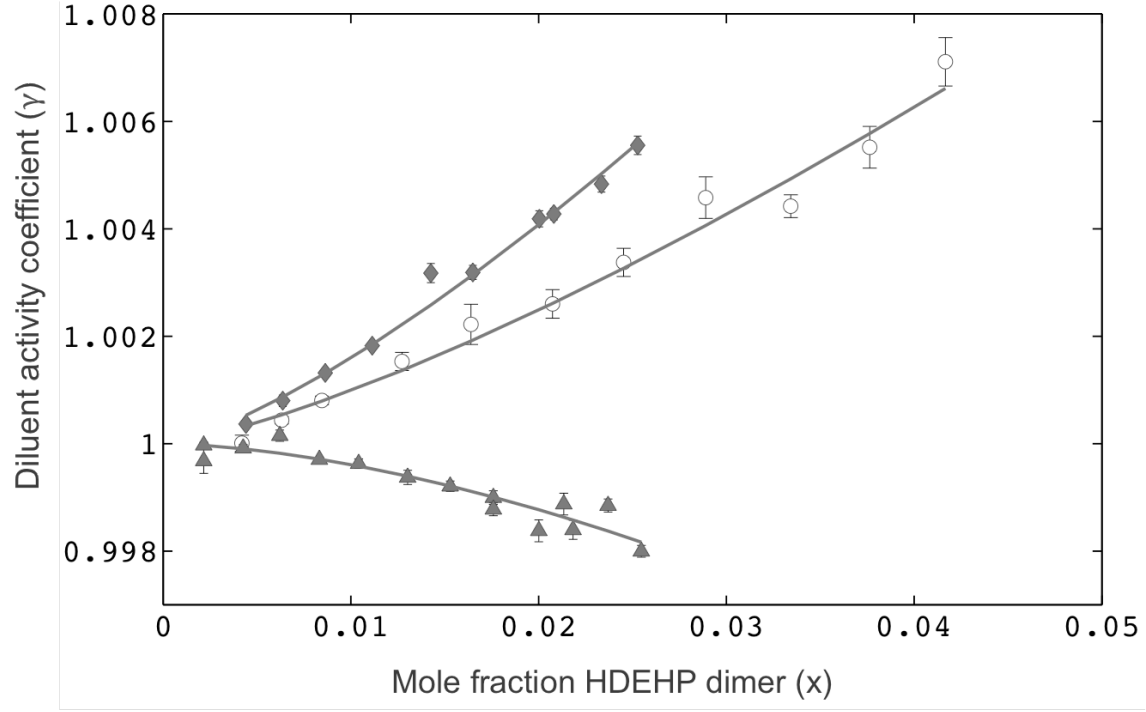

Fig. 3.8: Fit to the diluent activity data.
The lines show the fit for β. Data: ▲ Toluene 45°C, ◆ *n*-heptane 21°C ○ *n*-dodecane 92.7°C

Table 3.4: β parameter for each system for Eq. 3.11

Diluent	VPO cell temp. (°C)	Regressed Parameter β	Diluent	VPO cell temp. (°C)	Regressed Parameter β
Heptane	21	1.45 ± 0.04	Dodecane	95	0.80 ± 0.03
Octane	35	1.07 ± 0.05	Dodecane	100	0.87 ± 0.03
Octane	45	1.07 ± 0.03	Dodecane	110	0.64 ± 0.02
Octane	45	1.02 ± 0.03	Dodecane	110	0.70 ± 0.02
Octane	65	0.98 ± 0.02	Cyclooctane	66	0.72 ± 0.02
Decane	80	0.85 ± 0.04	Toluene	45	-0.44 ± 0.03
Dodecane	90	0.90 ± 0.02	Toluene	65	-0.20 ± 0.04
Dodecane	93	0.81 ± 0.03	Xylene	45	-0.012 ± 0.05
Dodecane	95	0.94 ± 0.02			

The activity coefficient of the diluent is related to the activity coefficient of HDEHP dimer via the Gibbs-Duhem equation for a binary solution, as shown in Eq. 3.12

$$\frac{d}{dx_2}(ln\,\gamma_2) = \frac{1-x_2}{x_2}\frac{d}{dx_2}(ln\,\gamma_2) \qquad 3.12$$

Integrating Eq. 3.12 and using an asymmetric activity coefficient reference yields the expression Eq. 3.13 for the activity coefficient of HDEHP dimer.

$$ln\,\gamma_2 = \beta(x^{1.5} - 3x^{0.5}) \qquad 3.13$$

The activity coefficients for HDEHP dimer are plotted in Fig. 3.9 for representative sets of the alkane diluents, and in Fig. 3.10 for toluene and xylene.

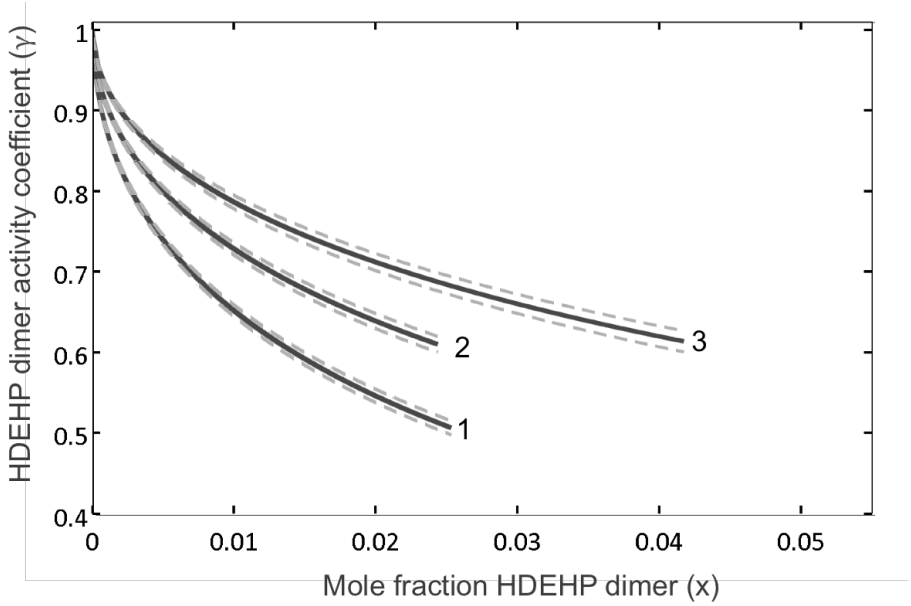

Fig. 3.9: Calculated HDEHP dimer activity for three alkane data sets.
1: for heptane at 21°C. 2: for octane at 45°C. 3: for dodecane at 92.7°C. Dashed lines represent propagated uncertainty.

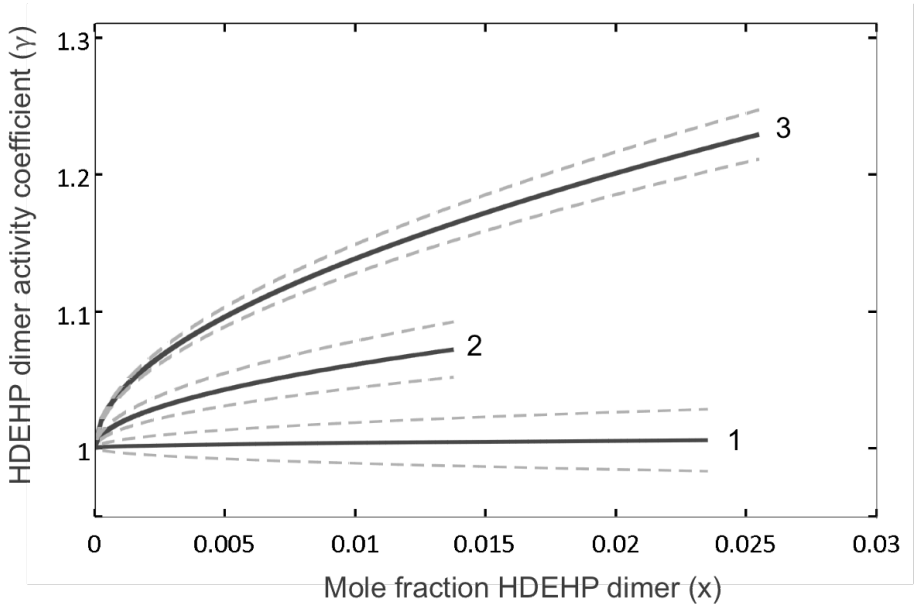

Fig. 3.10: Calculated HDEHP dimer activity for three aromatic data sets.
1: for o-xylene at 45°C. 2: for toluene at 65°C. 3: for toluene at 45°C. Dashed lines represent propagated uncertainty.

If the activity coefficients are converted[42] to molar activity coefficients, the difference between the values for octane, decane, and dodecane is greatly reduced, as shown in figure Fig. 3.11.

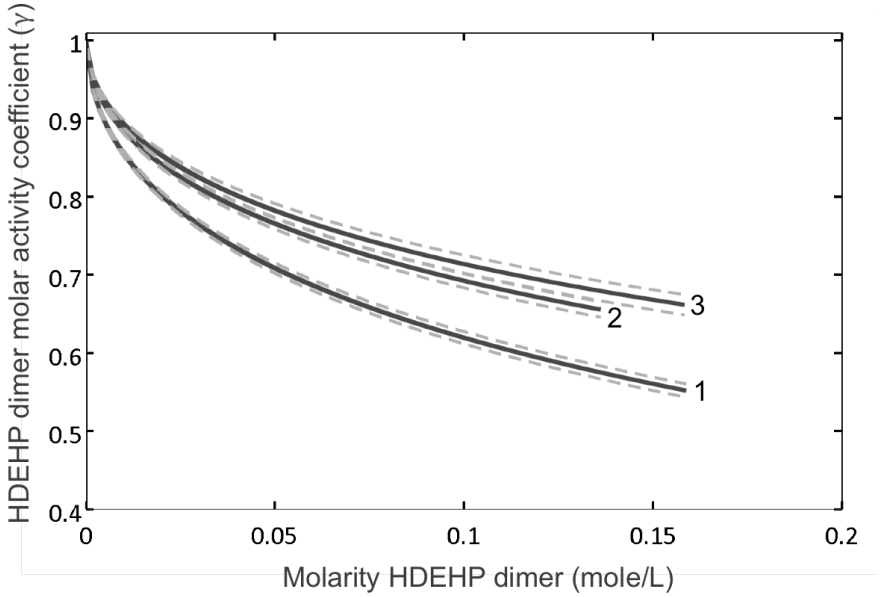

Fig. 3.11: Calculated HDEHP dimer molar activity for three alkane data sets.
1: for heptane at 21°C. 2: for octane at 45°C. 3: for dodecane at 92.7°C. The difference for the octane and dodecane results is reduced compared to the mole fraction results. Dashed lines represent propagated uncertainty.

The results for the fitting parameter, β, in Table 3.4 show weak temperature dependence based on the alkanes data. The temperature trend is shown in Fig. 3.12. The derivative of the natural log of HDEHP dimer activity coefficient with respect to temperature based on Eq. 3.13 is given by Eq. 3.14

$$\left(\frac{\partial ln\,\gamma_2}{\partial T}\right)_{P,x} = (x^{1.5} - 3x^{0.5})\left(\frac{\partial \beta}{\partial T}\right)_{P,x} \qquad 3.14$$

The temperature derivative of β was determined via a least squares fit yielding the dashed line in Fig. 3.12 using the *n*-alkane data for octane at 35°C to dodecane at 99.8°C. That slope is -0.0037±0.0006.

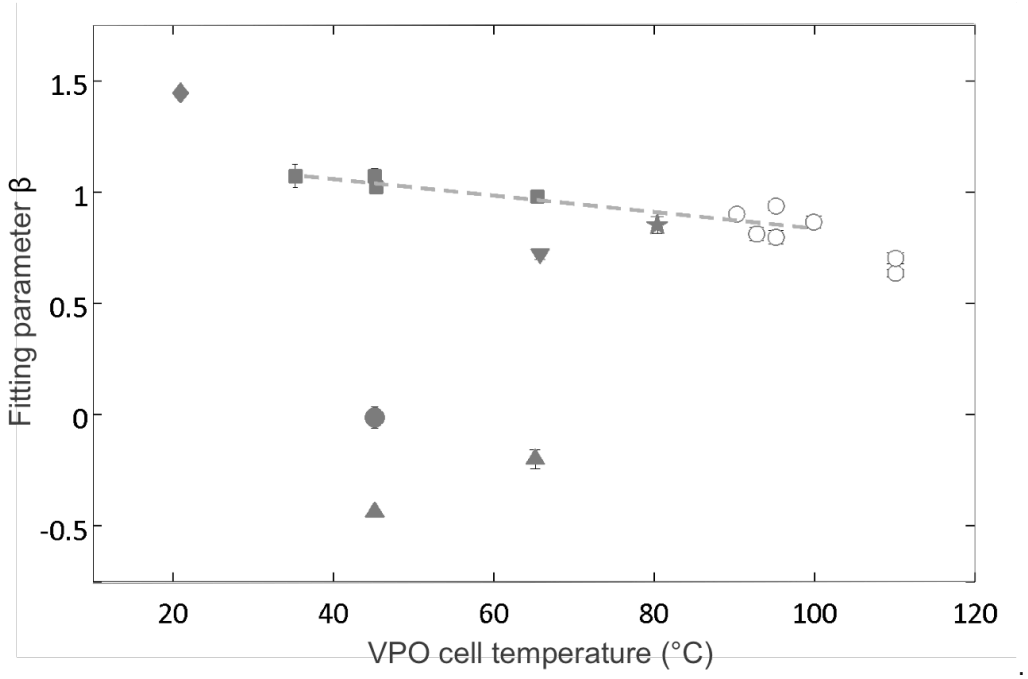

Fig. 3.12: Temperature dependence of β
Data: ▲ Toluene, ● o-xylene, ◆ *n*-heptane, ■ *n*-octane, ★ *n*-decane. ○ *n*-dodecane, ▼ cyclooctane. The dashed line is a linear fit to the *n*-alkane data. Note that cyclooctane is not part of that fit.

From thermodynamics we also have Eq. 3.15

$$\left(\frac{\partial ln\,\gamma_2}{\partial T}\right)_{P,x} = -\frac{\bar{h}_2^E}{RT^2} \qquad 3.15$$

Based on the correlation for heat of mixing given by Kolarik,[35] the infinite dilution referenced partial molar enthalpy at 25°C for HDEHP is given by Eq. 3.15

$$\bar{h}_2^E = x_{1,f}\left(A + 2Bx_{2,f} + 3Cx_{2,f}^2 + 4Dx_{2,f}^3\right) - A \qquad 3.16$$

Where the parameters *A, B, C*, and *D* are equal 3022, -7026, 11060, and -5732, respectively. The subscript '*f*' indicates this is the formal mole fraction, not the dimer mole fraction.

At an HDEHP dimer mole fraction of 0.03, Eq. 3.14 yields 0.0019±0.0003 K^{-1} , while Eq. 3.15 yields 0.0014 K^{-1} at 25°C. These values are surprisingly close considering the calculations based on the VPO data ignored that the diluent changed from octane, to decane and then dodecane. Plus, there is uncertainty in both the VPO data results and the calorimetric results of Kolarik. The heptane data set is an outlier to this trend, as it clearly does not follow the line fit to other *n*-alkane data. To a lesser degree the dodecane data sets at 110°C may be outliers, but the enthalpy of mixing was assumed to be constant with respect to temperature and that may not remain valid at that higher temperatures.

3.8 Comparison with slope analysis and isopiestic results

HDEHP dimer activity coefficents were determined experimentally in the past.[33,34] Danesi et al. reported that HDEHP dimer molar activity coefficients followed the trend given in Eq. 3.17

$$log_{10}\,\gamma_2 = -0.83\sqrt{c_{dimer}} \qquad 3.17$$

Where c_{dimer} is the concentration of HDEHP dimer on the molar scale.

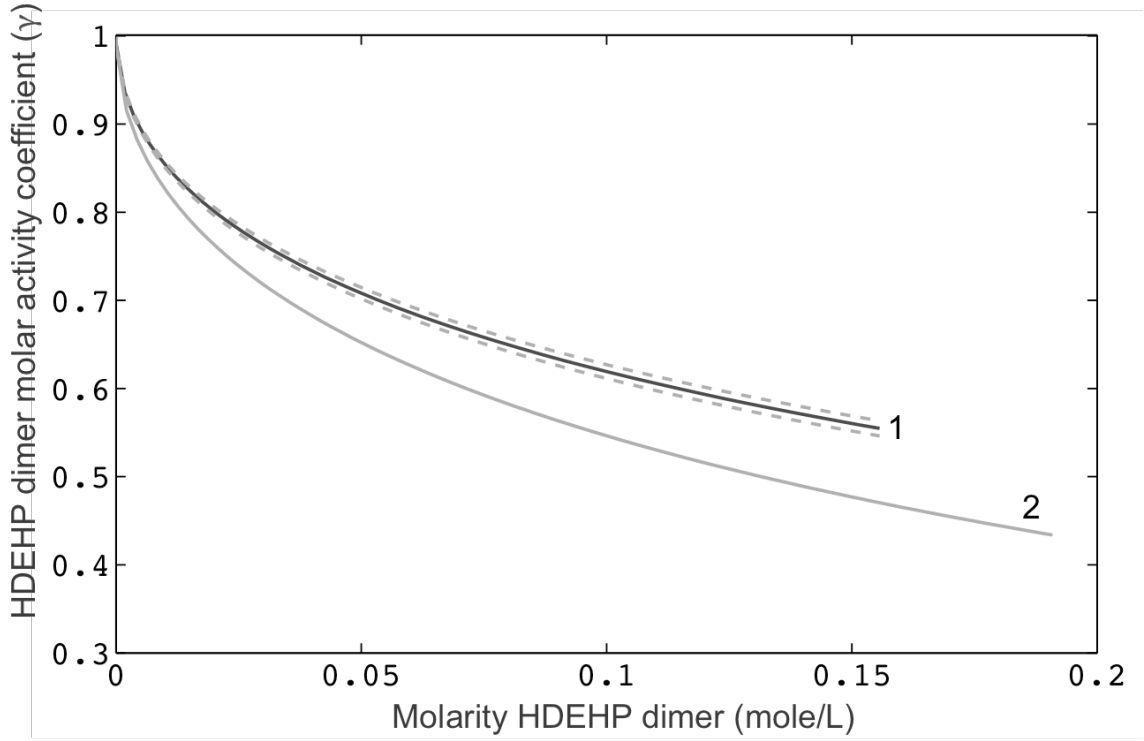

Fig. 3.13: Comparison of the activity coefficient from VPO and from Danesi et al.[34]
1: HDEHP dimer activity coefficient from heptane at 21°C. 2: Correlation fit to slope analysis data for dodecane, Eq. 3.17. Dashed lines represent propagated uncertainty.

This equation is an empirical fit to slope analysis data at 25°C, and it compares reasonably with the current data for HDEHP dimer in heptane at 21°C, as shown in Fig. 3.13. The VPO data shows that HDEHP dimer is slightly less non-ideal than the slope analysis data suggests. If the slope analysis experiment suffered from any phase contamination or model break down under the extreme distribution ratios seen in the experiments, the result would be an artificially low HDEHP dimer activity coefficient. If it turns out the heptane data is an outlier, and the true activity coefficient is nearer to the value obtained for octane at 35°C that is in line with the temperature trend from Kolarik, then the slope analysis is even more off. Unfortunately, Danesi et al. did not discuss uncertainties in the data and results in the paper.

The other data on HDEHP dimer activity coefficient is the work by Baes. Using both isopiestic techniques and slope analysis techniques, Baes determined molal activity coefficient of HDEHP dimer in octane at 25°C. That data is reproduced in Fig. 3.14 along with the current VPO result for HDEHP in heptane at 21°C.

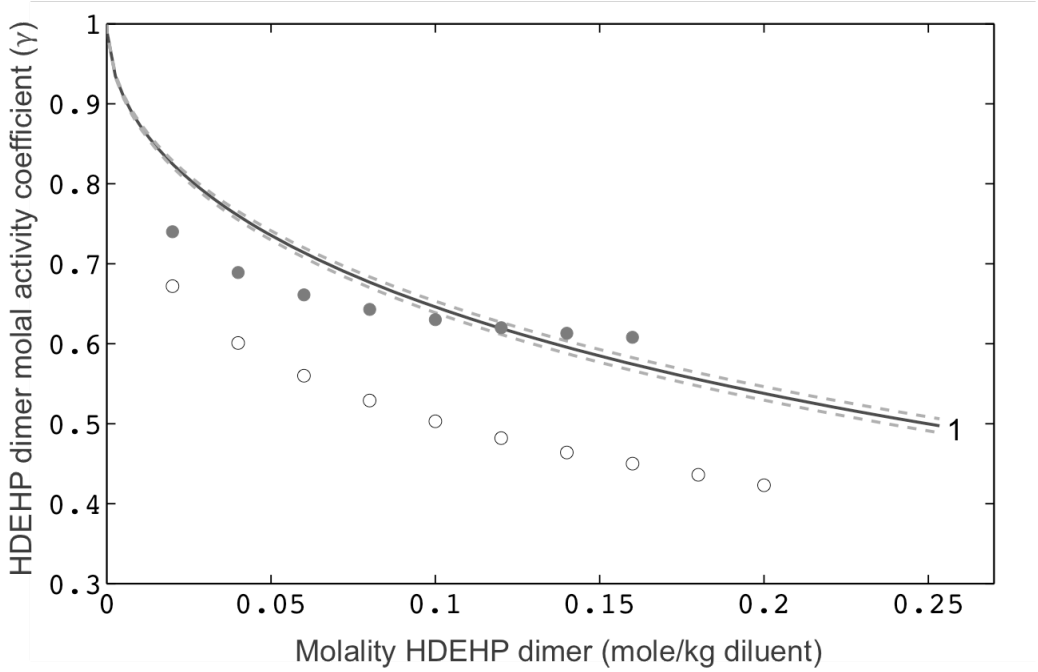

Fig. 3.14: Comparison of the activity coefficient from VPO and from Baes.[33]
1: HDEHP dimer activity coefficient from heptane at 21°C. ● Isopiestic data on HDEHP in octane at 25°C. ○ Slope analysis data on HDEHP in octane at 25°C. Dashed lines represent propagated uncertainty.

The data matches with the isopiestic data given by Baes, the closed points, but again is less non-ideal than the slope analysis data marked by the open points. The isopiestic experiment suffered from two issues leading Baes to write that the true activity coefficient lay somewhere in between the isopiestic results, and the slope analysis results. In fact, the current VPO data does fall with that range for concentrations over approximately 0.13 molal.

3.9 Solubility parameter results.

The discussion so far has focused on HDEHP dimer activity coefficient results determined by integrating the Gibbs-Duhem equation. However, a solubility parameter was also obtained for HDEHP dimer by fitting the RST-pFV equation, printed below.

$$ln(\gamma_i) = \frac{V_i}{RT}(\delta_i - \bar{\delta})^2 + ln\frac{\phi_i}{x_i} + 1 - \frac{\phi_i}{x_i} \quad 3.18$$

$$\phi_i = \frac{x_i S_i}{\sum x_i S_i}; \quad 3.8$$

$$S_i = (V_i - V_W)^p;\ p = 1 - V_{W,small}/V_{W,large} \quad 3.9$$

$$\bar{\delta} = \sum \phi_{V,i}\delta_i \quad 3.3$$

The solubility parameter of HDEHP dimer, δ_{dimer}, is obtained by fitting this series of equations to the diluent activity coefficient data. All parameters are known, except δ_i for δ_{dimer}. Examples of those fits are presented in Fig. 3.15 for the same data sets shown earlier for the β fit. Compared to the earlier function from Fig. 3.8, the RST-pFV does not map the shape of the alkane data well. However, the solubility parameter obtained from the HDEHP in heptane data is 18.7 $MPa^{1/2}$ which is close to the estimated value of 18.1 $MPa^{1/2}$ by Lumetta et al.[45]

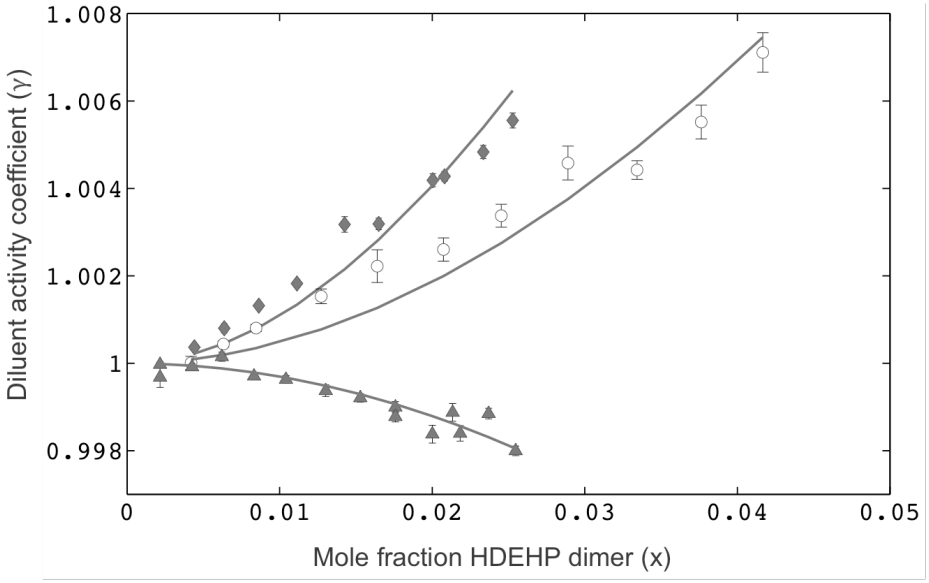

Fig. 3.15: RST-pFV solubility parameter fit to the diluent activity data.
The lines show the fit for the solubility parameter. Data: ▲ Toluene 45°C, ◆ *n*-heptane 21°C ○ *n*-dodecane 92.7°C. The curvature causes an undershooting of the data at the intermediate values.

Correspondingly, the HDEHP dimer activity calculated using the solubility parameter does not match the shape of the activity coefficient trend given by the earlier fit, or by the literature data. The data from Baes is used for the comparison in Fig. 3.16. The undershoot in the fit means that the activity coefficient of HDEHP remains closer to unity compared to the result given by the purely empirical fit performed earlier.

The calculated solubility parameters for each HDEHP data set are given in Table 3.5, and the trend with temperature is shown in Fig. 3.17. Based on the RST, the solubility parameter of HDEHP dimer should be a function of the temperature, but not of the other components in the system. However, the calculated solubility parameter does not stay constant in the three diluents at 45°C, and the three diluents at 65°C.

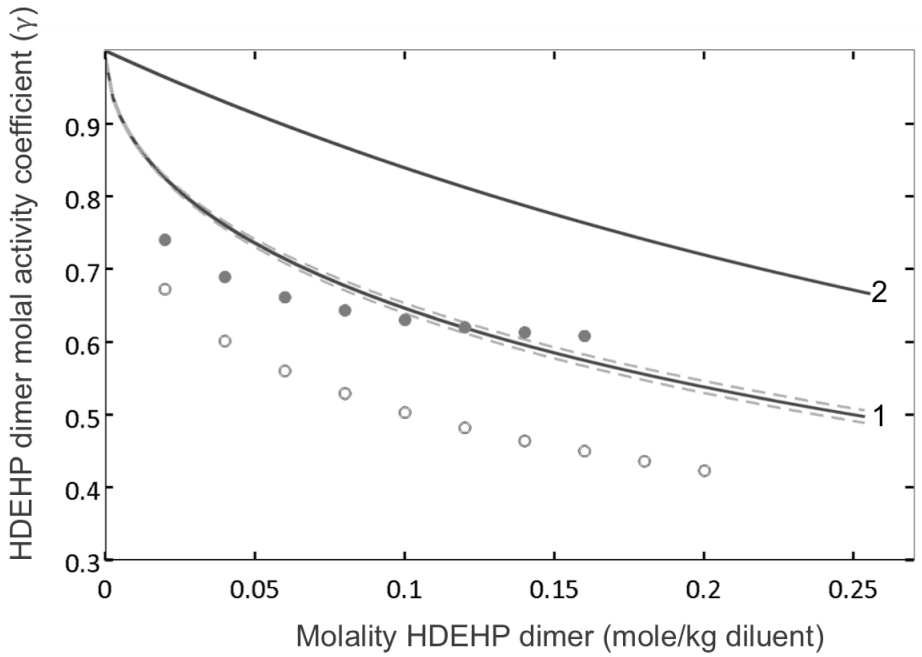

Fig. 3.16: RST-pFV solubility parameter comparison
1: Results based on the empirical fit and integration of the Gibbs-Duhem equation. 2: Result based on the solubility parameter. ● Isopiestic data[33] on HDEHP in octane at 25°C.○ Slope analysis data[33] on HDEHP in octane at 25°C. Dashed lines represent propagated uncertainty.

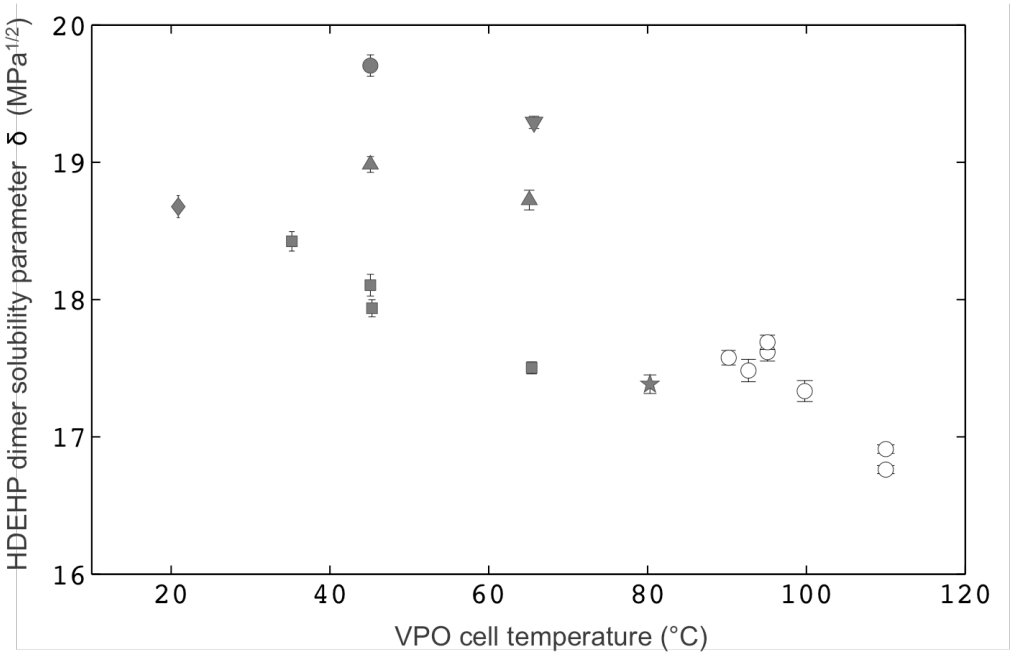

Fig. 3.17: Temperature trend of the fitted HDEHP dimer solubility parameters.
Data: ▲Toluene, ● o-xylene, ◆ *n*-heptane, ■ *n*-octane, ★ *n*-decane. ○ *n*-dodecane, ▼cyclooctane. The dashed line is a linear fit to the *n*-alkane data.

Table 3.5: HDEHP dimer solubility parameters fit for each system

Diluent	VPO cell temp. (°C)	HDEHP dimer solubility parameter δ	Diluent	VPO cell temp. (°C)	HDEHP dimer solubility parameter δ
Heptane	21	18.7 ± 0.1	Dodecane	95	17.7 ± 0.1
Octane	35	18.4 ± 0.1	Dodecane	100	17.3 ± 0.1
Octane	45	18.1 ± 0.1	Dodecane	110	16.8 ± 0.0
Octane	45	17.9 ± 0.1	Dodecane	110	16.9 ± 0.0
Octane	65	17.5 ± 0.0	Cyclooctane	66	19.3 ± 0.0
Decane	80	17.4 ± 0.1	Toluene	45	19.0 ± 0.1
Dodecane	90	17.6 ± 0.1	Toluene	65	18.7 ± 0.1
Dodecane	93	17.5 ± 0.1	Xylene	45	19.7 ± 0.1
Dodecane	95	17.6 ± 0.1			

This difference is not surprising. The RST theory is not meant for systems of polar, hydrogen bonding molecules. Empirically applied, it may give good qualitative results,[46] but not quantitative ones. And the entropic correction using pFV may not give the best results for HDEHP. That theory is accurate for the standards hexadecane and tetracosane in the diluents, but it may not work for HDEHP. An over-estimate of the entropic correction would push the fitted solubility parameter too high, and likewise an underestimate would push it artificially lower. That effect is seen in the results when the analysis is repeated using instead the SXFIT style RST+FH corrections for the standard and for the HDEHP fitting. As the FH entropic correction is an overestimated, the solubility parameter obtained via this method is higher.

While the HDEHP solubility parameters determined for n-alkanes do not follow a clear temperature trend, there is a clear linear correlation for the HDEHP dimer solubility parameter plotted against the diluent solubility parameter of the n-alkane diluent, as is evident in Fig. 3.18. Here, the HDEHP dimer solubility

parameter appears dependent on the solubility parameter of the diluent, with consistency among the n-alkanes. However, this appears to be mainly an artifact of the diluent solubility parameter temperature dependence along with the weakly increasing non-ideality of HDEHP in the alkanes with temperature. Plotting the difference between the HDEHP dimer solubility parameter and the diluent parameter shows this effect, Fig. 3.19.

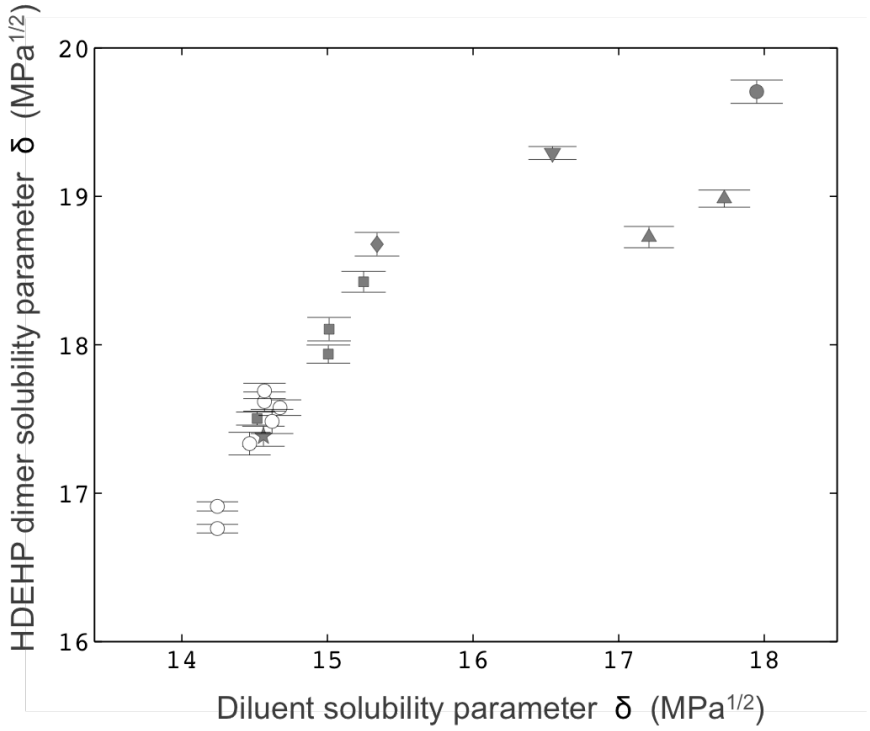

Fig. 3.18: HDEHP dimer solubility parameter versus diluent solubility parameter.
Data: ▲Toluene, ● o-xylene, ◆ *n*-heptane, ■ *n*-octane, ★ *n*-decane. ○ *n*-dodecane, ▼cyclooctane. The *n*-alkanes give a linear trend.

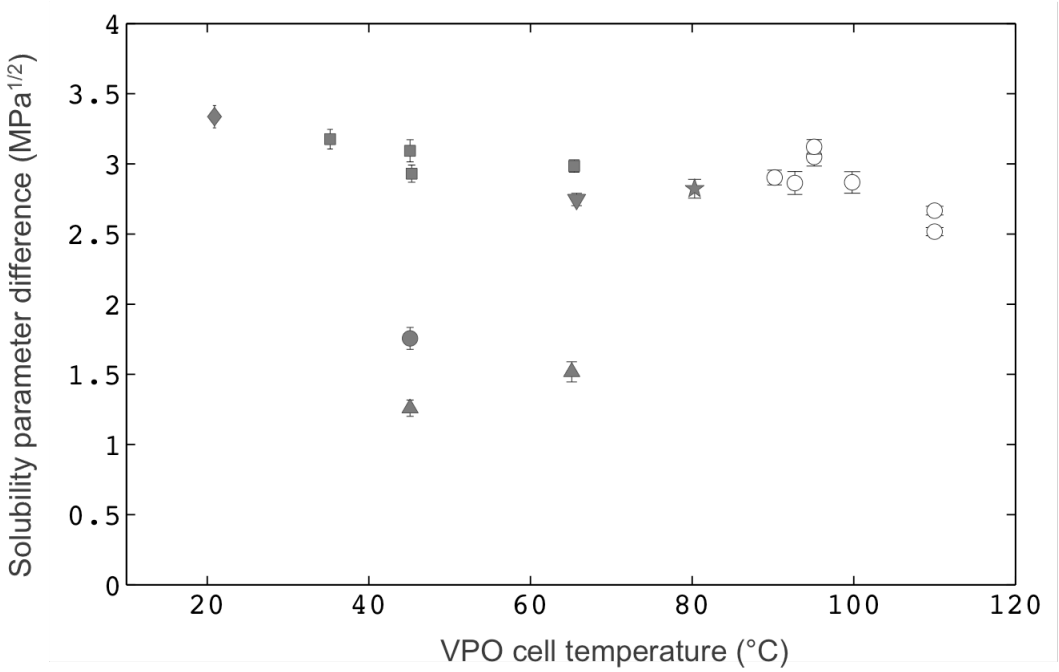

Fig. 3.19: HDEHP dimer solubility parameter minus the diluent solubility parameter.
Data: ▲ Toluene, ● o-xylene, ◆ *n*-heptane, ■ *n*-octane, ★ *n*-decane. ○ *n*-dodecane, ▼ cyclooctane.
The temperature effect is weak, and similar to Fig. 3.12

3.10 RST+FH based standard corrections and solubility parameter

The calculations were redone using the RST-FH corrections to compensate for the non-ideality of the standard, and to determine the solubility parameter for HDEHP dimer. As discussed earlier, this greatly over estimates the excess entropy and skews the results. However, the solubility parameter determined in this method will be consistent with the theory of SXFIT, so it would be more appropriate to use these values for that purpose.

For the n-alkanes there is not a major difference between the HDEHP dimer activity for the RST+FH and pFV based methods, except for the cyclooctane data. Table 3.6 gives the results where the non-ideality of the standard and of HDEHP is modeled using RST+FH for each data set. In the section evaluating the different

theories it was seen that the RST+FH can give similar results as the pFV when the overestimated entropic contribution by the FH terms balance against the over estimated enthalpic RST contributions for binary systems of *n*-alkanes. In general, though, the earlier assessment showed that the RST+FH is less accurate and using it to calculate the activity coefficient in cyclooctane gives inaccurately higher value, Fig. 3.20. The calculated values for the activity coefficient in toluene and o-xylene are significantly different between the methods, Fig. 3.21, as expected due to the poor match the RST+FH theory gave in the test cases earlier in the chapter with benzene.

The solubility parameter calculated for HDEHP dimer in each diluent is also higher than the ones obtained earlier. As the excess entropy is overestimated, the calculated solubility parameter for HDEHP dimer increases to compensate.

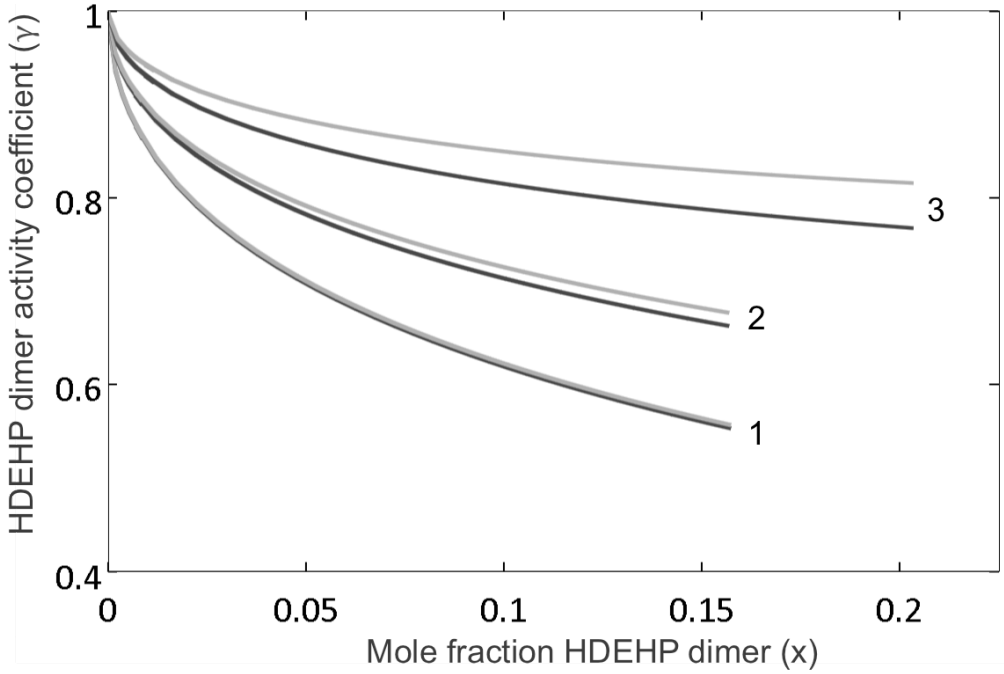

Fig. 3.20 Comparison of RST-FH (light gray) and pFV based analysis (dark gray)
1: heptane data at 21°C, 2: dodecane data 92.7°C, 3:cyclooctane data 65.7°C

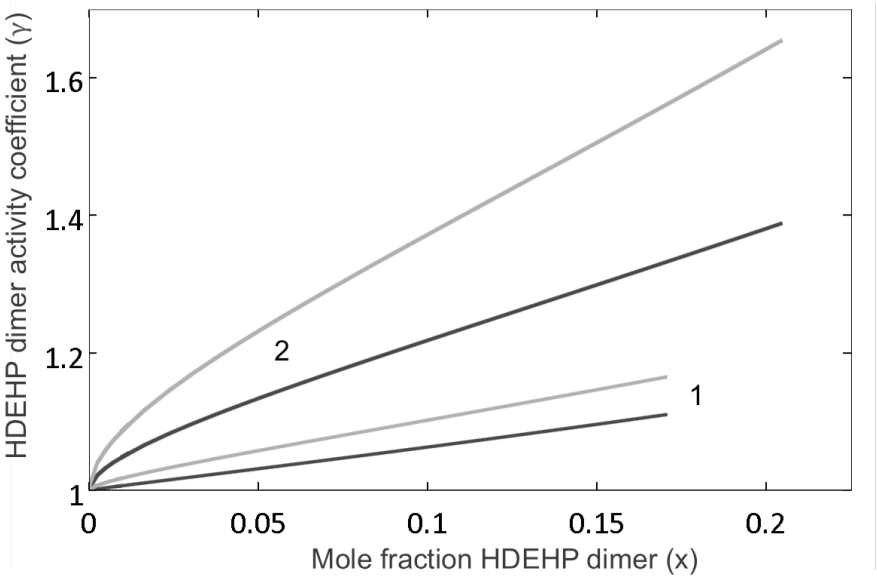

Fig. 3.21: Comparison of RST-FH (light gray) and pFV based analysis (dark gray)
1: o-xylene at 45°C, 2: Toluene at 45°C

Table 3.6: Parameter results using of RST-FH
RST-FH was used for standard corrections and solubility parameter fits

Diluent	VPO cell temp. (°C)	RST+FH HDEHP dimer solubility parameter δ	RST+FH Regressed Parameter β
Heptane	21	19.17 ± 0.1	1.43 ± 0.04
Octane	35	18.87 ± 0.1	1.05 ± 0.05
Octane	45	18.50 ± 0.1	0.99 ± 0.03
Octane	45	18.39 ± 0.0	0.96 ± 0.03
Octane	65	17.96 ± 0.0	0.92 ± 0.02
Decane	80	17.78 ± 0.1	0.82 ± 0.04
Dodecane	90	17.88 ± 0.0	0.88 ± 0.02
Dodecane	93	17.77 ± 0.1	0.78 ± 0.03
Dodecane	95	17.90 ± 0.1	0.90 ± 0.02
Dodecane	95	17.95 ± 0.0	0.77 ± 0.03
Dodecane	100	17.64 ± 0.1	0.84 ± 0.03
Dodecane	110	17.10 ± 0.0	0.60 ± 0.02
Dodecane	110	17.24 ± 0.0	0.67 ± 0.03
Cyclooctane	66	19.80 ± 0.0	0.61 ± 0.02
Toluene	45	19.92 ± 0.1	-0.81 ± 0.03
Toluene	65	19.43 ± 0.1	-0.59 ± 0.03
Xylene	45	20.552 ± 0.0	-0.12 ± 0.04

3.11 Chapter conclusions

Evaluating several potential theories to compensate for the non-ideality of the standard showed that both pFV and FH1.1 were accurate for *n*-alkane + *n*-alkane binary systems. pFV theory was used to calculate the non-ideality since it was reported to give more accurate results for cycloalkanes. In the alkane diluents pFV was used, and in the aromatic diluents RST+pFV was used to compensate for the non-ideality of the standard. Literature reports and the evaluation done here shows the RST+FH is inaccurate, but results were also reported based on this theory as they may be useful to some researchers in the solvent extraction community.

The most accurate treatment of the VPO data for the activity coefficient of HDEHP was by integrating the Gibbs-Duhem equation. This method yielded activity coefficient in agreement with activity coefficients calculated by Danesi et al., with only a slight offset. The solubility parameter results can give qualitative fits. If solubility parameters are used to predict activity coefficients in other diluents the values obtained using the pFV entropic corrections should be used rather than those with the FH entropic corrections.

Using the activity coefficients calculated for HDEHP dimer will permit the extraction equilibrium model to be used accurately over a wider range of concentrations.

4 VPO on ternary systems and activity coefficients by slope analysis

The activity coefficient of HDEHP dimer calculated in the prior chapter was one source of uncertainty in the extraction equilibrium represented by Eq. 1.4. Another

uncertainty is the activity coefficient of the metal complex, which has not been determined. This chapter presents VPO data collected on solutions containing an HDEHP metal complex, and discusses the analysis. Although an activity coefficient is not determined, a method to calculate an approximate value is proposed.

The second part of this chapter looks at the reasons why slope analysis data gives a slight offset compared to VPO determination of the HDEHP dimer activity coefficient. New metal extraction data was collected, but analysis shows that minor phase contamination led to artificially low activity coefficients. An improved slope analysis procedure is proposed where minor contamination will not affect the calculated activity coefficients.

4.1 VPO on HDEHP metal complexes

For conditions favorable to ion exchange in low polarity diluents HDEHP is known to form complex with three mono-deprotonated dimers at low metal loadings,[19,87,88] but precipitate as a polymer with three deprotonated HDEHP molecules at the highest metal loadings.[3,87,89] The interactions and species that form between these two extremes is less clear. Only a handful of papers provide data for the stoichiometry of the metal complexes at intermediate values as the metal to extractant ratio approaches the solubility limit.[29,89–91]

The lack of information motivated the use of VPO to examine solutions containing HDEHP-lanthanide metal complexes. However, it was found that only ternary systems with excess HDEHP in addition to the metal complexes and diluent could be measured, making the analysis of the VPO data challenging .

4.2 Complex behavior at high metal loading

There are various reports of where the HDEHP lanthanide solutions begins forming a precipitate or gel phase, but the quoted values differs. These values range between a ratio of 6 to a ratio of 8 extractant molecules to one metal ion. Under the typical conditions studied, the ligand to metal ratio in the organic phase is reported as the primary determinant of phase separation for this type of aggregate.

In one of the early investigations on HDEHP lanthanide extraction, Peppard[3] reported bringing the ratio below 6:1 formed a solid precipitate. Trivalent yttrium, which behaves similar to the lanthanides in solution, has been reported to precipitate at ratio of 6.9±0.2, forming the 3:1 ratio polymer.[87] Although the exact value was not given, precipitate has been reported to form somewhat below a ratio of 8:1 for neodymium in HDEHP.[89] Reports on the reverse reaction, the dissolution of the 3:1 coordinating polymer in HDEHP solutions, were not found in the literature. Some work has gone into characterizing other aspects of the solid. [92,93]

For high metal to ligand ratios, approaching the solubility limit, a complex with six HDEHP molecules and two neodymium atoms has been proposed by a few groups.[89,91] The 6:2 complex best explained neutron scattering data on HDEHP extraction at 9.0:1 and 8.2:1 overall ligand to metal ratios.[89] However, that analysis was based on only two data points, and was fit under the significant and arbitrary assumption that only one species of complex was present. A second group saw evidence of these 6:2 HDEHP neodymium complexes existing as a minor component at the vague concentration referred to as “not fully loaded” using electrospray ionization mass spectroscopy.[91] Not a single numerical concentration for any

component was reported in that paper, so it does not help evaluate the assumption that the 6:2 complex predominates at high loading. A third group[94] explained neodymium partitioning data between organic and aqueous phases under high metal to HDEHP ratios using an equilibrium between 6:1 and 3:1 complexes. Although that data is consistent with the formation of a 6:2 complex, the data is unreliable. The results were based on HDEHP that tested at only 93.9% pure, and included other uncertainties.

In contrast to the data on neodymium, an analysis with lanthanum showed that the 6:2 complex is not the predominant species at the total ligand to metal ratio of 11.5:1.[90] A possible reason for this difference is the lower bonding strength for lanthanum and HDEHP, making the results only approximately comparable. The listed electrospray ionization mass spectroscopy data does not show any peaks corresponding to the dual metal atom complex for lanthanum. All lanthanum complex peaks shown have at least two mono-deprotonated dimers attached.

4.3 Metal complex

Two series of HDEHP metal complex solutions were investigated in heptane at 21°C. In the first series, the HDEHP metal ratio was kept constant and the solution was progressively diluted with heptane. In the second series, the HDEHP to metal ratio started out at 8, and was successively increased by dilution with a constant HDEHP-heptane concentration. The inability to solubilize the 3:1 HDEHP-dysprosium polymer without adding excess HDHP limited the usefulness of the VPO data. The lowest overall HDEHP to metal ratio required to form a solution from the polymer was 7.9±0.1.

The VPO metal loaded organic solutions were prepared by dissolving a solid HDEHP-dysprosium coordination polymer in HDEHP diluent solutions. This route has several advantages over the method of carrying out an extraction for each VPO experiment to obtain a metal loaded organic phase. The process is streamlined since the composition analysis can be made once on the prepared coordination polymer. In contrast, composition analysis would need to be performed on each new extraction for each VPO experiment, wasting time and resources. Additionally the HDEHP concentration could change if a third phase appeared in those extraction experiments, making even the overall composition of the VPO solutions uncertain. The third phase can be clear, and would be possible to overlook.

The solid HDEHP-metal complexes were prepared by precipitation from a single ethanol/water phase following reported methods.[92,93] A 49.1mM dysprosium nitrate solution at pH 4 was prepared using $Dy(NO_3)_3$ hydrate 99.9% trace metals analysis (Aldrich). The concentration was determined using ICP-MS. 149.5ml of 49.1mM $Dy(NO_3)_3$ was diluted by 80% with ethanol, and 6.9117 grams of purified HDEHP diluted to 70ml in ethanol were added. A white precipitate immediately started forming. 20.0ml of 1.00M NaOH was added to drive the complexation. The total ratio of HDEHP to Dysprosium was 2.92, providing a slight excess of $Dy(NO_3)_3$. The solution was stirred for two hours, and then centrifuged. The supernatant was discarded, and the precipitate was re-suspended via sonication in a 50/50 v/v ethanol water mix. The centrifuge and re-suspension procedure was repeated three more times using ethanol to rinse the precipitate. The remaining ethanol and water was removed using rotary evaporator. The material was heated under vacuum at

85°C for one hour after reaching dryness. The total dysprosium content of the resulting powder was determined by comparative neutron activation analysis. Powder samples were dissolved in two different solutions with excess of HDEHP in dodecane for comparison against a sample of 1,005μg/mL ±2 dysprosium ICP-MS standard (Inorganic Ventures) by neutron activation. Neutron activation was used over ICP-MS because HDEHP solutions are not soluble in the dilute nitric acid typically used as the ICP-MS carrier solvent. Two samples of the dysprosium HDEHP samples were prepared, and activated in triplicate along with the standard. The HDEHP content was determined by mass balance on these results. The ratio of HDEHP to dysprosium in the solid was 3.04 ±0.08, confirming the formation of the 3:1 coordination polymer.

The polymer was insoluble in pure octane, toluene, acetone, butanol, ethanol, and water. However, it was soluble in solution of HDEHP, with full dissolution of the samples starting at an HDEHP to metal ratio of approximately 7.9. The solid appeared to swell but not dissolve in an HDEHP/octane solution at an overall 6:1 HDEHP to metal ratio. At a 7:1 overall ratio there is partial dissolution but significant white solid remains. At a 7.9:1 ratio the solution appears clear, without any visible solid.

The overall equilibrium between the 6:1 and the proposed 6:2 complex would be expected to be highly dependent on HDEHP concentration. Aggregation of two 6:1 metal complexes into a 6:2 metal complex give off three HDEHP dimers.

$$2[Dy(DEHP)_3(HDEHP)_3] \rightleftharpoons Dy_2(DEHP)_6 + 3(HDEHP)_2 \qquad 4.1$$

This would give a strong HDEHP concentration dependence for the dimer-monomer transition. However, the transition from 6:2 complex to solid coordination polymer would not explicitly depend on HDEHP concentration as shown in Eq. 4.2.

$$2[Dy(DEHP)_3]_{solid} \rightleftharpoons Dy_2(DEHP)_{6,org} \quad 4.2$$

Both the complex and the coordination polymer have the same 3:1 ratio. If the 6:2 complex predominates then explaining the solubility dependence on HDEHP is less straightforward since the equilibrium constant for Eq. 4.2 would depend only on the activity of the 6:2 complex.

For the traditional 6:1 complex, however, free HDEHP would directly feature as a component in the solid liquid equilibrium, Eq. 4.3, clearly highlighting the concentration dependence.

$$[Dy(DEHP)_3]_{solid} + 1.5(HDEHP)_{2,org} \rightleftharpoons Dy(DEHP)_3(HDEHP)_{3,org} \quad 4.3$$

4.4 VPO solution preparation

HDEHP-heptane-complex stock solutions were prepared gravimetrically at total HDEHP to metal ratios of at least 8.0. These solutions were then diluted with heptane, or with an HDEHP-heptane solution. Table 1.1 shows the mass fractions of solid metal complex dissolved, the additional HDEHP, and heptane, along with the overall HDEHP to metal molar ratios. Fig. 4.1 and Fig. 4.2 presents this data graphically using a ternary plot showing at region near pure heptane under two different aggregation assumptions. Fig. 4.1 was calculated assuming that the metal exists as the classic 6:1 complex, while Fig. 4.2 was calculated based on a 6:2 complex.

Table 4.1: Concentrations of the three components as prepared. The solid 3:1 metal coordination polymer dissolves to form a 6:1 metal complexe, but may include 6:2 complexes.

Mass fraction heptane	Mass fraction 3:1 metal complex	Mass fraction HDEHP	Overall HDEHP to metal molar ratio
0.8183	0.0741	0.1077	8.08
0.8518	0.0604	0.0878	8.08
0.9071	0.0379	0.0550	8.08
0.8726	0.0519	0.0755	8.08
0.9417	0.0238	0.0345	8.08
0.9694	0.0125	0.0181	8.08
0.9797	0.0083	0.0121	8.08
0.8174	0.0750	0.1075	8.01
0.8261	0.0629	0.1110	9.16
0.8352	0.0503	0.1145	10.95
0.8562	0.0210	0.1228	23.39
0.8623	0.0125	0.1252	38.13
0.8713	0.0000	0.1287	n/a

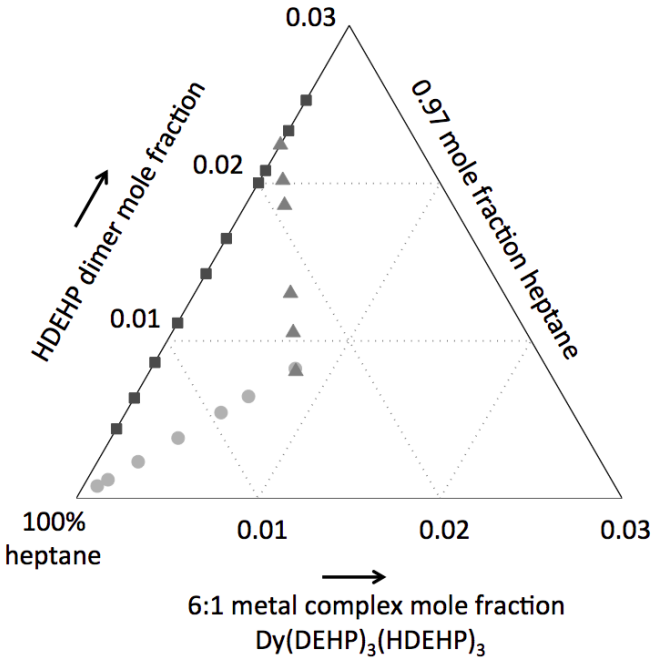

Fig. 4.1: Ternary plot for the mole fractions
Values calculated assuming that HDEHP forms a 6:1 metal complex with the dysprosium ion. ■ HDEHP ● Overall 8:1 HDEHP to metal ratio, ▲Varied overall HDEHP to metal ratio.

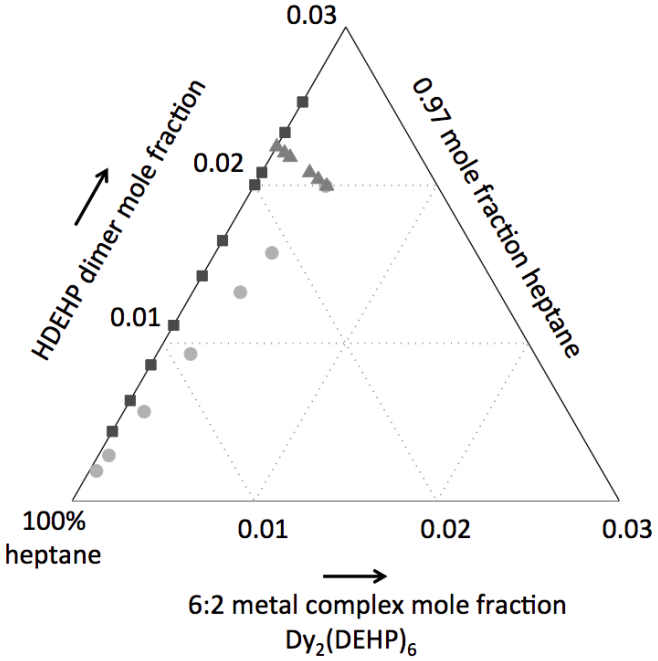

Fig. 4.2: Ternary plot for the mole fractions
Values calculated assuming that HDEHP forms a 6:2 metal complex with the dysprosium ion. ■ HDEHP ● Overall 8:1 HDEHP to metal ratio, ▲Varied overall HDEHP to metal ratio.

The VPO data run on heptane at 21°C included several measurement series. Results on the first two of these were reported in the prior chapter. The solution series for the standard hexadecane, and the solution series for HDEHP in heptane without any metal complex present were described and analyzed in the prior chapter. The machine constant and HDEHP activity result are used again here. The two measurement series on metal complexes were collected later in that same overall VPO experiment following the same measurement procedures.

Prior to the heptane experiment, two exploratory VPO runs were conducted on systems with HDEHP metal complexes in octane at 45°C. That data is also briefly reported.

4.5 VPO results and analysis

The VPO steady state signal averages at each of the concentrations listed in Table 4.1 is presented in Fig. 4.3. The x-axis gives the diluent mole fraction assuming that HDEHP is dimerized, and that the metal forms the classic 6:1 complex. Following this assumption, the VPO signal for the highest metal loadings diluted by heptane, indicated by gray circles, follows the same curve as the standard hexadecane, indicated by black circles. The solutions that were progressively diluted with a HDEHP heptane solution, shown by gray triangles, give a linear transition to the pure HDEHP values, shown by dark gray squares.

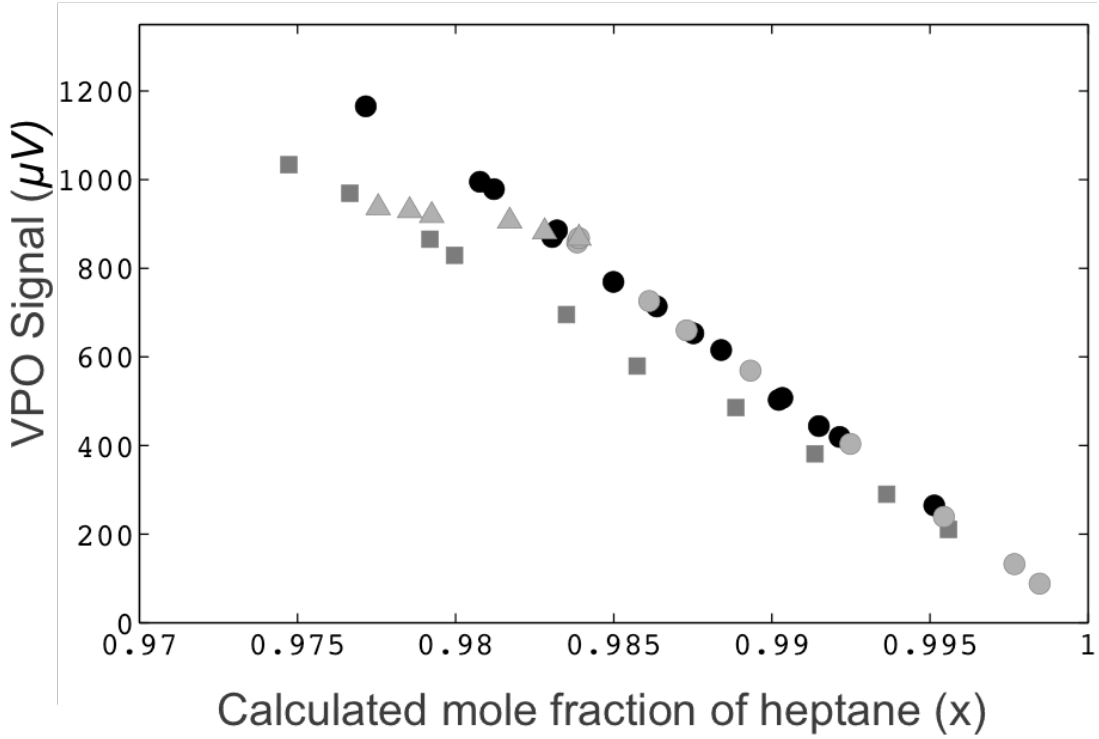

Fig. 4.3: Average VPO signals for in heptane at 21°C
● Hexadecane, ■ HDEHP ● Constant 8:1 HDEHP to metal ratio, ▲ Increasing HDEHP to metal ratios. The mole fraction of heptane was calculated assuming the classic 6:1 complex.

If, on the other hand, the true species was assumed to be a complex of 6:2 ratio, the calculated diluent mole fraction would shift. Yet if the 6:2 complex were assumed for the highest metal loadings in accordance with the analysis of Jensen et al.,[89] the equilibrium between the 6:1 and 6:2 complexes would need to be taken into account in analyzing the data with increasing HDEHP to metal ratios, indicated by the triangle markers.

Nonetheless, the diluent activity coefficient will be calculated for two limiting cases of either the 6:1 species or the 6:2 species existing as the sole significant component. Both of these cases are unlikely to be realistic.

First, the diluent mole fraction is calculated assuming the 6:1 aggregate is the only significant form of the complex and that HDEHP is fully dimerized. Then the

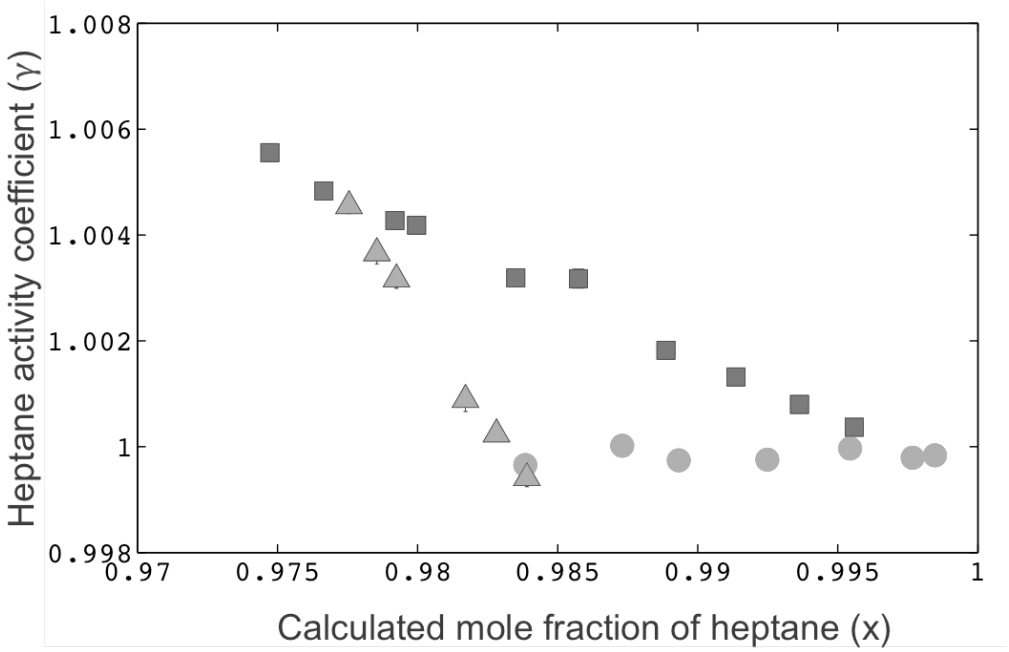

Fig. 4.4: Diluent activity assuming exclusively 6:1 complex
■ HDEHP only ● Constant 8:1 HDEHP to metal ratio, ▲ Increasing HDEHP to metal ratios.

VPO equation is used to calculate the diluent activity of the HDEHP complex solutions. The result is shown in Fig. 4.4.

The data marked by squares is the data for HDEHP dimer in heptane without metal, as was discussed in the prior chapter. For the series with an 8:1 total HDEHP to metal ratio, marked with circles, the diluent activity coefficient is equal to unity within error. However, it is unlikely that both the HDEHP and free dimer are ideal, but under these assumptions it seems that the effects cancel each other out in terms of diluent activity.

If the other assumption is made, the assumption that only 6:2 aggregates exist in significant amounts at these high loadings, then the diluent activity coefficient is given by the results in Fig. 4.5.

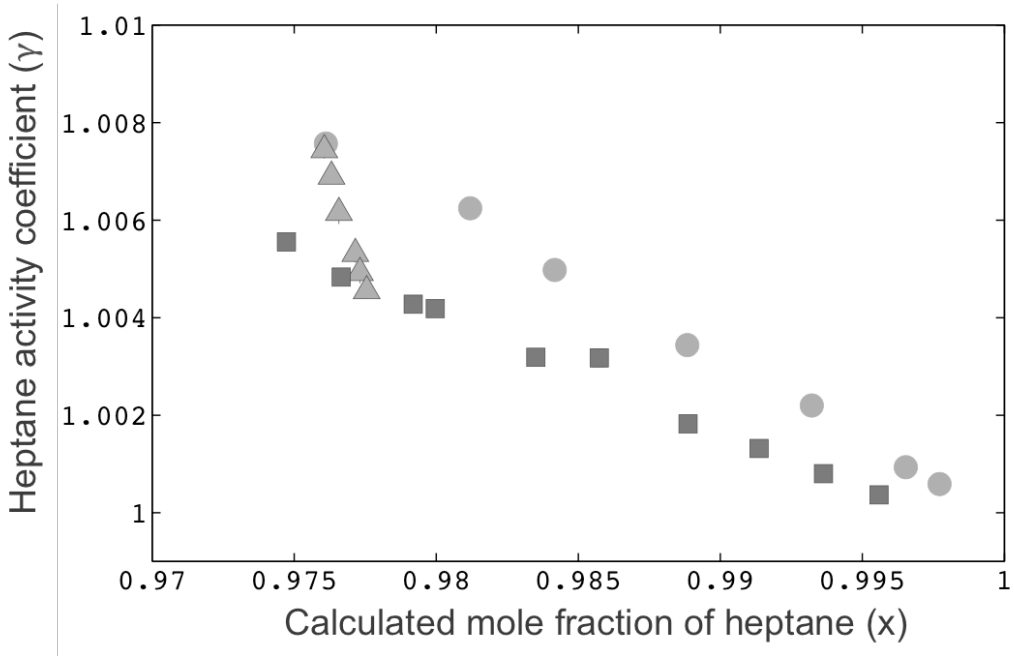

Fig. 4.5: Diluent activity assuming exclusively 6:2 complex
■ HDEHP only ● Constant 8:1 HDEHP to metal ratio, ▲ Increasing HDEHP to metal ratios.

Yet even if either of these simplifying assumptions were justified, data on the diluent activity coefficient does not lead to quantitative values of the activity coefficient of either HDEHP or the complex. For example, assuming that HDEHP is completely dimerized, and that only 6:1 complex forms, then there are three components present in the system. VPO provides the activity coefficient for one component, the diluent, but unlike in a binary system, the Gibbs-Duhem cannot be integrated to obtain the unknown activity coefficient without further information. Calculation of activity coefficients in ternary systems typically require binary parameters for each pair of constituents, and these not available for this system.[95] The activity coefficient calculated for HDEHP in the prior chapter is not applicable to this the highly loaded metal system. At a total metal to HDEHP dimer ratio of 8:1, there is an equal amount of free HDEHP dimer as there is metal complex and HDEHP readily interact with the metal complex. The HDEHP in the metal complex has been

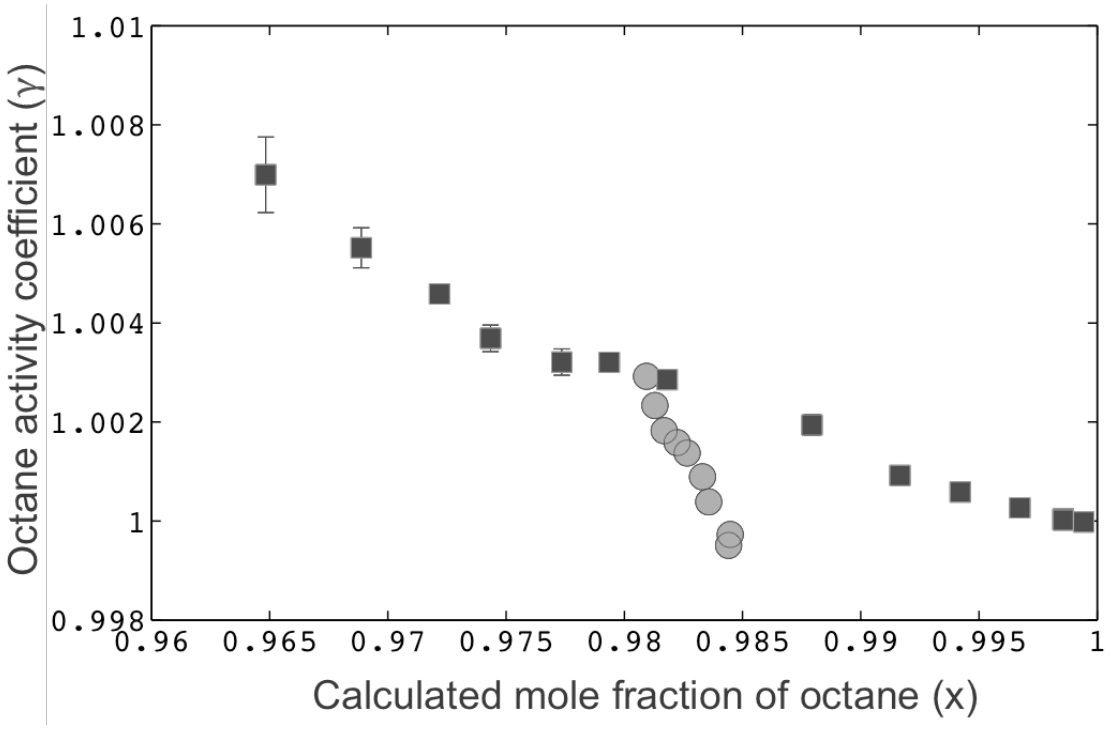

Fig. 4.6: *n*-Octane activity assuming exclusively 6:1 complex
● Increasing HDEHP to metal ratios. ■ HDEHP only. The activity coefficient for octane in binary solutions with HDEHP was taken from the results for from the prior chapter. The complex data was collected during a new experiment under the same conditions.

shown to rapidly exchanges with free HDEHP.[90] Thus the solution environment is quite different than in the binary system of HDEHP investigated in the prior chapter. If the non-ideality in a binary solution of HDEHP in heptane is due to further association, the high metal loading may limit the formation of the higher HDEHP associates.

It may be possible to obtain a qualitative value of the activity coefficient for the metal complex if two significant assumptions are made. If the metal complex is assumed to exist only as a 6:1 complex and the RST+pFV theory is assumed to provide a realistic fit to the data, then it may be possible to regress a solubility parameter for the metal complex. In order to do this, the molar volume of the complex and the free volume of the complex would also need to be determined.

For metal complexes in octane the solution behavior is similar to the behavior in heptane, as expected. Fig. 4.6 gives the activity coefficient of octane for the assumption that the 6:1 complex predominates. As with heptane, the diluent activity coefficient is approximately unity at the highest metal loading, and increases to the value for the binary solutions of HDEHP with octane as the metal loading decreases.

In summary, the diluent activity in solutions with both HDEHP and metal complexes was calculated based on VPO data, but the results do not yield a clearer picture on the aggregation of the complex. If several assumptions are made, it may be possible to obtain qualitative values.

4.6 Activity coefficients of HDEHP by slope analysis

Europium distribution data was collected to characterize HDEHP using slope analysis. Batch extractions were carried out using europium-152 tracer. Fourteen extractions with HDEHP concentrations ranging from $3.14 \bullet 10^{-4}$ M to 0.103 M in dodecane were carried out at using a constant aqueous phase. The aqueous phase was 3.9•10-3 M nitric acid in 1.0 M ammonium nitrate. These concentrations were selected based on a first set of extractions where aqueous phase was varied from $2.0*10^{-3}$ M to $5.0*10^{-2}$ M nitric acid with $1.48 \bullet 10^{-3}$ M HDEHP in dodecane as the organic phase. This work was conducted at Forschungszentrum Jülich in IEK-6.

Equal phase volumes were used for each extraction of 500µL or 700 µL. Each sample was contacted at 25°C using a vortex mixer for 15 minutes followed by 15 minutes in a centrifuge for phase disengagement. Then 200µl samples were then taken for spectroscopy using an HPGE detector. In order to minimize phase

contamination the organic phase was sampled first, and the remainder drawn off. Approximately three quarters of the aqueous phase was transferred to a new vial with care to avoid the small amount of organic remaining at the interface. The pipet actuator was slowly depressed as the tip entered the liquid to further reduce and chance of the organic phase contaminating the interior. The standard polypropylene pipet tips are not well suited for alkane systems, and the solution wets the tip more favorably than an aqueous solution does. After the 'clean' aqueous was transferred to the new vial it was centrifuged a second time. A tiny drop of organic phase was visible on the surface after centrifuge in some of those samples. This re-centrifuged aqueous phase was then sampled with the same pipetting technique. For the acid dependence experiment, the pH was measured after contact.

The results for europium extraction by HDEHP as a function of concentration are presented in Fig. 4.7. These results are represented by the distribution ratio, which is defined as the concentration of metal in the organic phase divided by the concentration of the metal in the aqueous phase after extraction. It is defined in Eq. 4.4 in terms of the Europium concentration, $[Eu^{3+}]$, in each phase.

$$D = \frac{[Eu^{3+}]_{org}}{[Eu^{3+}]_{aq}} \qquad 4.4$$

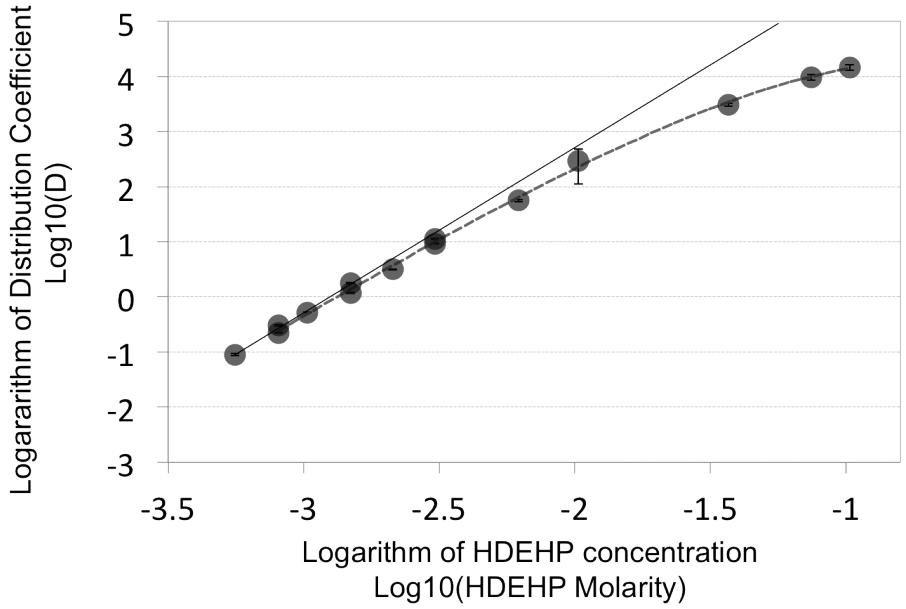

Fig. 4.7: Extraction results for europium-152 tracer by HDEHP.
Distribution ratio of europium-152 between 0.0039M nitric acid at 1.0M ionic strength and varying concentration of HDEHP in dodecane. The high distribution values show deviation from the line showing a slope of 3. Error bars show the uncertainty in the distribution coefficients due uncertainty in the counting statistics. Phase contamination likely affects the three highest distribution ratios.

The line indicates a slope of 3, which corresponds to the idealized extraction mechanism under low metal loading conditions where three dimers bind to one trivalent metal ion to bring it into the organic phase. Each point on the graph represents a single extraction. The error bars are based on the counting statistics and the area uncertainty in the peak area determination.

The curvature away from the line of slope of 3 could have a few causes. First, the activity coefficient of HDEHP is decreasing, and accounts for some of the curvature at the higher distribution ratios. Ideally, this effect would be the only one present, but there are two more to consider.

Another cause of the deviation would be a break down of the model, Eq. 4.5, for the extraction of Eu(III) by HDEHP at extremely high or low distributions ratios.. This expression is based on the reaction presented in chapter one by Eq. 1.2. Break down could be caused by impurities leading to an overlooked mechanism of extraction. However, as HDEHP was purified[86] using the copper extraction method, contaminants are unlikely to explain the current results.[96]

$$Log(D) = 3Log[(HDEHP)_2] + 3Log[\gamma_2] + C \qquad 4.5$$

In this equation the equilibrium constant, acid concentration and activity coefficients of the acid, the metal in the aqueous phase, and the metal in the organic phase are assumed to be constant and lumped into the constant *C*. The activity coefficient of the metal complex in the organic phase, however, may not be constant despite Danesi et al. making that assumption.[34]

Any interphase contamination during the preparation of the samples for counting would lead to distribution ratios shifting towards 1. At moderate distribution ratios the effect is minor, but even minor contamination creates a large shift for distribution ratios over 10^3. This contamination could be entrainment of the phases as a fine dispersion due to the vortex mixing. In the case of the aqueous phase measurement, the contamination could be due to left over organic phase at the surface of the aqueous solution that adheres to the pipet tip. Calculations show that the level of contamination that would fully explain the curvature away from a slope of three is miniscule. For example, at the distribution ratio of $10^{3.47}$ (the point at the $\log_{10}$(HDEHP) concentration of -1.43 in Fig. 4.7) the entire deviation away from the line of slope three can be explained by 290ppmv (part per million volume)

of organic in the aqueous phase. That concentration translates to only $57nL$ of organic contaminating the $200\mu L$ aqueous sample. The distribution ratios higher than this one require even less contamination to account for the deviation from a slope of three.

The impact of contamination in the aqueous phase was approximated using Eq. 4.6, which is accurate for small amounts of contamination when equal sized samples are counted for both phases.

$$\frac{V_{cont}}{V_{sample}} = \frac{D_{True} - D_{Observed}}{D_{True} D_{Observed}} \qquad 4.6$$

V_{cont} is the volume of the organic phase contamination in the aqueous sample being counted; V_{sample} is the total volume of the sample being counted; D_{True} is the distribution ratio if there were no contamination; and $D_{observed}$ is the distribution ratio measured when there is organic phase contamination of the aqueous sample. The equation is easily derived based on the definition of the distribution ratio given by Eq. 4.4.

The slope analysis by Danesi et al. is more reliable. Consistent results in three different extraction sets suggest the samples suffered less contamination. The publication, however, does not give a detailed description of the sampling procedure, so this effect cannot be excluded given the small amounts required to shift the highest distribution ratios.

The empirical function given in Eq. 4.7 was fit to the data in order to analyze the data on the extraction of Eu-152 tracer by HDEHP. The dashed line in Fig. 4.7 shows the result of this fit.

$$\log_{10} D = 3\log_{10}[(HDEHP)_2] + A[(HDEHP)_2]^B + C \quad 4.7$$

Where D is the distribution ratio of europium; [$(HDEHP)_2$] is the molar concentration of HDEHP dimer; and A, B, and C are fitting parameters. These were determined to be -8.19, 0.530, and 9.72, respectively. Based on comparison to Eq. 4.5 it can be seen that the activity coefficient is given by Eq. 4.8 using the parameters A and B determined above.

$$\log_{10} \gamma = \frac{A}{3}[HA]^B \quad 4.8$$

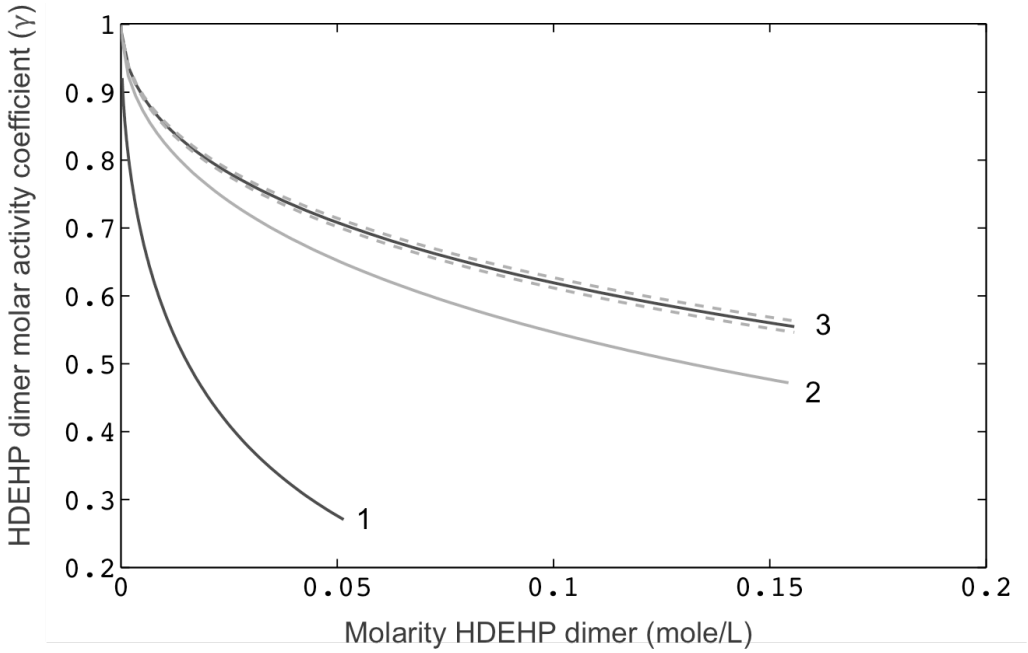

Fig. 4.8: Comparison of the activity coefficient of HDEHP dimer
1: New slope analysis results. 2: slope analysis by Danesi et al.[34] 3: VPO results presented in chapter 3. Dashed lines represent propagated uncertainty. The new slope analysis results are heavily skewed due to phase contamination potentially on the order of nanoliters.

The activity coefficient of HDEHP dimer is plotted in Fig. 4.8, but it is clearly skewed by phase contamination. The values are far lower than both the activity coefficient calculated using VPO (chapter 3) and the results by Danesi et al.. Although an extreme example, the current extraction results and discussion show that slope analysis is prone to underestimate the activity coefficient.

There are two ways to mitigate the phase contamination. First, multiple metal ions could be used as tracers. If these were selected so that there were always one ion with a distribution ratio between 10^{2} and10^{-2} then minor contamination would not be a problem. The different metals would provide windows of reliable data across the concentration range of HDEHP tested. Alternatively, high distribution ratios could be made more reliable in this experiment by separating and contacting the aqueous phase with pure dodecane after the extraction. The dodecane will not change the aqueous phase metal content unless there is dispersed HDEHP containing organic phase, in which case the contaminating organic phase would mix into the pure dodecane phase. Any remaining contamination of the aqueous phase would be orders of magnitude more dilute. The aqueous phase can be sampled and compared to a sample collected prior to this second contact to determine if phase contamination was affecting the distribution ratio.

Even if the phase contamination issue is resolved, there will be uncertainty in the slope analysis method results due to the assumption that the activity coefficient of the metal complex is constant with respect to varied concentration of HDEHP. If a method to calculate that value is determined, then that factor could also be compensated for. The VPO data for the metal complexes presented in the first part of the chapter is moving in that direction. If a solubility parameter is obtained for the metal complex, for example, the activity coefficient of the metal complex could be calculated on a qualitative level. Then the slope analysis could be repeated while

accounting for any variation in the activity coefficient of the metal complex rather than treating it as a constant.

5 Conclusions

The literature survey in chapter one established the need and value of reliable data for HDEHP activity coefficients. The past data often relied on unrealistic assumptions, including ideality of the standards used for vapor pressure osmometry. Thus, this work made careful correction for that non-ideality. For HDEHP in aromatic diluents, the impact of these corrections was significant.

The robustness of the VPO equation even under non-ideal conditions was demonstrated, and the osmometer performance was verified by comparing experimental water activity calculated for four different aqueous solutions against literature values.

The VPO data collected for solutions of HDEHP in various hydrocarbon diluents yielded activity coefficients for HDEHP dimer. While past work using VPO generally ignored the non-ideality of the standards, these new results account for those effects. The assessment of non-ideality models also showed that the theory used in SXFIT could be easily improved. An excess entropy correction more accurate than the Flory Huggins model should be used.

The results for the activity coefficient of HDEHP dimer matched literature data from slope analysis, with only a slight offset. This small offset may be due to the high distribution ratios used in the slope analysis, as they are shown to be highly sensitive to even minute amounts of contamination. The temperature trend of the

activity coefficients also matches the expected trend based on enthalpy of mixing data reported in literature.

At 21°C the solubility parameter of HDEHP dimer was calculated to be 18.7 $MPa^{1/2}$, close to the estimated value of 18.1 $MPa^{1/2}$ using group contribution methods. This is an empirically determined solubility parameter and should only be used in *n*-alkane diluents. Since solubility parameter theory is not strictly valid for HDEHP solutions, the experimental solubility parameter for HDEHP dimer in toluene and xylene is not identical to the value obtained for HDEHP dimer in *n*-octane at the same temperature. The solubility parameter can be used to qualitatively calculate the activity coefficient of HDEHP dimer in different *n*-alkanes, but the more accurate Gibbs-Duhem results should be used if the system is HDEHP in heptane near room temperature.

The final chapter examined HDEHP metal complexes. Adding a third component into the VPO system complicated the analysis, but qualitative activity coefficients for the metal complex may be achievable with a limited amount of additional data. That result will allow assessment of an assumption made in slope analysis determinations of the activity coefficient for HDEHP dimer.

Overall, it is evident that VPO provides a reliable method to calculate the activity coefficient of extraction agents such as HDEHP. Either the activity coefficients presented here or in the paper by Danesi et al. are recommended for modeling metal extraction equilbria.

6 References

1. Gouvea, L. R. & Morais, C. a. Development of a process for the separation of zinc and copper from sulfuric liquor obtained from the leaching of an industrial residue by solvent extraction. *Miner. Eng.* **23,** 492–497 (2010).

2. Grimm, R. & Kolařík, Z. Acidic organophosphorus extractants—XIX: Extraction of Cu(II), Ni(II), Zn(II) and Cd(II) by DI(2-ethylhexyl) phosphoric acid. *J. Inorg. Nucl. Chem.* **36,** 189–192 (1974).

3. Peppard, D. F., Mason, G. W., Maier, J. L. & Driscoll, W. J. Fractional extraction of the lanthanides as their di-alkyl orthophosphates. *J. Inorg. Nucl. Chem.* **4,** 334–343 (1957).

4. Kongolo, K., Mwema, M. D., Banza, a. N. & Gock, E. Cobalt and zinc recovery from copper sulphate solution by solvent extraction. *Miner. Eng.* **16,** 1371–1374 (2003).

5. Owusu, G. Selective extractions of Zn and Cd from Zn Cd Co Ni sulphate solution using di-2-ethylhexyl phosphoric acid extractant. *Hydrometallurgy* **47,** 205–215 (1998).

6. Zhang, P. *et al.* Hydrometallurgical process for recovery of metal values from spent nickel-metal hydride secondary batteries. *Hydrometallurgy* **50,** 61–75 (1998).

7. Mendiguchía, C., García-Vargas, M. & Moreno, C. Screening of dissolved heavy metals (Cu, Zn, Mn, Al, Cd, Ni, Pb) in seawater by a liquid-membrane-ICP-MS approach. *Anal. Bioanal. Chem.* **391,** 773–778 (2008).

8. BenkheddaPresent address: Health Ca, K., Larivière, D., Scott, S. & Evans, D. Hyphenation of flow injection on-line preconcentration and ICP-MS for the rapid determination of 226Ra in natural waters. *J. Anal. At. Spectrom.* **20,** 523 (2005).

9. Murakami, M. & Furuta, N. Novel preconcentration technique using bis(2-ethylhexyl) hydrogen phosphate (HDEHP) loaded porous polytetrafluoroethylene (PTFE) filter tube as a sorbent: Its application to determination of In(III) in seawater by ICP-MS with air segmented discrete sample. *Anal. Chim. Acta* **556,** 423–426 (2006).

10. Todd, T. Presentation slides for the Blue Ribbon Commission, Reactor Fuel Cycle Technologies Subcommittee. (2010).

11. Finck, P. *Presentation slides for the Advanced Fuel Cycle Initiative: Science Based Fuel Cycle Research*. (2009).

12. IAEAE. Nuclear Technology Review 2012. *Int. At. Energy Agency* (2012).

13. IEA. Key World Energy Statistics. *Int. Energy Agency* (2012). doi:10.1787/22202811

14. *Blue Ribbon Commission on America's Nuclear Future: Report to the secretary of Energy*. (2012).

15. *Report of American Nuclear Society President's Special Committee on Used Nuclear Fuel Management Options*. (2011).

16. Weaver, B. & Kappelmann, F. TALSPEAK: A new method of separating americium and curium from the lanthanides by extraction from an aqueous solution of an aminopolyacetic acid. (1964). doi:10.2172/4028257

17. Starý, J. TALANTA REVIEW. *Talanta* **13,** 421–437 (1966).

18. Vine, G. Abridged History of Reactor and Fuel Cycle Technologies Development: A White Paper for the Reactor and Fuel Cycle Technology Subcommittee of the Blue Ribbon Commission. (2011).

19. Nilsson, M. & Nash, K. L. Review Article: A Review of the Development and Operational Characteristics of the TALSPEAK Process. *Solvent Extr. Ion Exch.* **25,** 665–701 (2007).

20. Aneheim, E. Solvent Extraction and Ion Exchange A TBP / BTBP-based GANEX Separation Process — Part 2 : Ageing , Hydrolytic , and Radiolytic Stability. 157–175 (2011).

21. Magnusson, D. *et al.* Demonstration of a SANEX process in centrifugal contactors using the CYME4-BTBP molecule on a genuine fuel solution. *Solvent Extr. Ion Exch.* 37–41 (2009). doi:10.1080/07366290802672204

22. Pereira, C. *et al.* LAB-SCALE DEMONSTRATION OF THE UREX+1a PROCESS USING SPENT FUEL. *wm'07 Symp.* 1–10 (2007).

23. Todd, T. A. Fuel Cycle R & D Program Separations and Waste Form Research and Development. (2010).

24. Kolarik, Z. Review: Dissociation, Self-Association, and Partition of Monoacidic Organophosphorus Extractants. *Solvent Extr. Ion Exch.* **28,** 707–763 (2010).

25. Karraker, D. G. Coordination of trivalent lanthanide ions. *J. Chem. Educ.* **47,** 424 (1970).

26. Komasawa, I., Otake, T. & Ogawa, Y. THE EFFECT OF DILUENT IN THE LIQUID-LIQUID EXTRACTION OF COBALT AND NICKEL USING ACIDIC ORGANOPHOSPHORUS COMPOUNDS A typical example of category (a) is the extraction. *J. Chem. Eng. Japan* **17,** 410–416 (1984).

27. Nilsson, M. & Nash, K. L. Review Article: A Review of the Development and Operational Characteristics of the TALSPEAK Process. *Solvent Extr. Ion Exch.* **25,** 665–701 (2007).

28. Lee, M.-S., Ahn, J.-G. & Son, S.-H. Modeling of solvent extraction of zing from sulphate solutions with d2ehpa. *Mater. Trans.* **42,** 2548–2552 (2001).

29. Anticó, E. *et al.* Solvent extraction of yttrium from chloride media by di(2-ethylhexyl)phosphoric acid in kerosene. Speciation studies and gel formation. *Anal. Chim. Acta* **327,** 267–276 (1996).

30. Baes, C. F., Zingaro, R. a & Coleman, C. F. The Extraction of Uranium(VI) from Acid Perchlorate Solutions by Di-(2-ethyl-hexyl) -Phosphoric Acid in n-Hexane. *J. Phys. Chem.* **62,** 129–136 (1958).

31. Peppard, D. F., Ferraro, J. R. & Mason, G. W. HYDROGEN BONDING IN ORGANOPHOSPHORIC ACIDS. *J. Inorg. Nucl. Chem.* **7,** 231–244 (1958).

32. Mason, G. W., Lewey, S. & Peppard, D. F. Extraction of metallic cations by mono-acidic orthophosphate esters in a monomerizing diluent. *J. Inorg. Nucl. Chem.* **26,** 2271–2284 (1964).

33. Baes, C. F. Isopiestic investigation of di-(2-ethylhexyl)-phosphoric acid in n-octane. *J. Phys. Chem.* **66,** 1629–1634 (1962).

34. Danesi, P. R. & Vandegrift, G. F. Activity coefficients of bis(2-ethylhexyl) phosphoric acid in n-dodecane. *Inorg. Nucl. Chem. Lett.* **17,** 109–115 (1981).

35. Marcus, Y. & Kolarik, Z. The enthalpies of mixing of organophosphate esters with hydrocarbons. *J. Solution Chem.* **6,** 39–56 (1977).

36. Li, Y., Teng, Teng, Lu, J., Chen, G. & Li, J.-D. A study on Scatchard-Hildebrand solution theory for metal solvent extraction systems. *Fluid Phase Equilibria,* **30,** 297–306 (1986).

37. Miyake, Y. *et al.* Kinetics and mechanism of metal extraction with acidic organophosphorus extractants (I): Extraction rate limited by diffusion process. *Hydrometallurgy* **24,** 19–35 (1990).

38. J, K. V, Proyaev, V. & Dvorak, Z. methods for evaluating the association of some extractants in low polarity solvents. *J. Radioanal. Nucl. Chem. Artic.* **183,** 33–47 (1994).

39. Miralles, N., Sastre, A., Martinez, M. & Aguilar, M. On the Interaction of Metal Extractant Reagent. Part IV. The Aggregation of Organophosphorus Acid compounds in Toluene. *Anal. Sci.* **8,** 773–777 (1992).

40. Buch, a, Stambouli, M., Pareau, D., Durand, G. & Paris, C. Solvent Extraction of Nickel (II) By Mixture of 2-Ethylhexanal Oxime and Bis (2-Ethylhexyl) Phosphoric Acid. *Solvent Extr. Ion Exch.* **20,** 49–66 (2002).

41. Apelblat, A. Erratum to 'The concept of associated solutions in historical development: Part 1. The 1884-1984 period' [J. Mol. Liq. 128 (2006) 1-31] (DOI:10.1016/j.molliq.2006.02.005). *J. Mol. Liq.* **130,** 133–162 (2007).

42. Prausnitz, J. M., Azevedo, E. G. de & Lichtenthaler, R. N. *Molecular thermodynamics of fluid-phase equilibria.* (Pearson Education Taiwan, 2004).

43. Raal, J. D. & Mühlbauer, A. L. *Phase equilibria : measurement and computation*. (Taylor & Francis, 1998).

44. Biswas, R. K., Banu, R. a. & Islam, M. N. Some physico-chemical properties of D2EHPA Part 2. Distribution, dimerization and acid dissociation constants in n-hexane/1 M (Na+,H+)SO4 2- system, interfacial adsorption and excess properties. *Hydrometallurgy* **69,** 157–168 (2003).

45. Lumetta, G. J. *et al.* Lipophilic ternary complexes in liquid–liquid extraction of trivalent lanthanides. *J. Coord. Chem.* **65,** 741–753 (2012).

46. Barton, A. F. M. *CRC handbook of solubility parameters and other cohesion parameters*. (CRC Press, 1983).

47. Moyer, B. a., Baes, C. F., Case, F. I. & Driver, J. L. Liquid–Liquid Equilibrium Analysis in Perspective Ii. Complete Model of Water, Nitric Acid, and Uranyl Nitrate Extraction By Di-2-Ethylhexyl Sulfoxide in Dodecane. *Solvent Extr. Ion Exch.* **19,** 757–790 (2001).

48. Klocker, H., Bart, H., Marr, R. & Muller, H. Mass Transfer Based on Chemical Potential Theory: ZnSO4,/H2S04/D2EHPA. *AICHE J.* **43,** 2479–2487 (1997).

49. Baes, C. F. Modeling Solvent Extraction Systems With Sxfit. *Solvent Extr. Ion Exch.* **19,** 192–213 (2001).

50. De Oliveira, W. a. & Lima, J. M. B. Behavior and use of benzil as an ebulliometric standard. *J. Chem. Thermodyn.* **12,** 1065–1068 (1980).

51. Roddy, J. W., Ridge, O. & Laboratoryt, N. REFERENCE SOLUTES FOR ISOPIESTIC AND DYNAMIC VAPOR PRESSURE OSMOMETRY IN ORGANIC SOLVENTS : TRIPHENYLMETHANE , AZOBENZENE , AND BENZIL IN DRY BENZENE. *J. Inorg. Nucl. Chem.* **32,** 3891–3898 (1970).

52. Rossotti, F. J. C. & Hazel, R. Graphical Methods of Determining Self-Association Constants. I. Systems Containing Few Species. *J. Phys. Chem* **63,** 926–930 (1961).

53. Roddy, J. W. & Coleman, C. F. Reference solutes for isopiestic and dynamic vapor pressure osmometry in organic solvents: tri-n-octylamine in n-hexane and benzophenone in carbon tetrachloride. *J. Inorg. Nucl. Chem.* **35,** 4317–4319 (1973).

54. Bonner, O. D., Gilkerson, W. R., Paljk, S. & Klofutar, C. Practical osmotic coefficients and excess Gibbs free energies of benzene solutions of tri-n-octylamine and tri-n-octylammonium bromide at 298.15 K. *J. Chem. Eng. Data* **32,** 458–459 (1987).

55. Solie, T. N. Vapor pressure osmometry. *Methods Enzymol.* **26 PtC,** 50–74 (1972).

56. Design Institute for Physical Properties, S. by Aic. *DIPPR Project 801 - Full Version*. *Design Institute for Physical Property Research/AIChE* (Design Institute for Physical Property Research/AIChE, 2005).

57. Yaws, C. L. Yaws' Thermophysical Properties of Chemicals and Hydrocarbons (Electronic Edition).

58. Hefter, G., May, P. M., Marshall, S. L., Cornish, J. & Kron, I. Improved apparatus and procedures for isopiestic studies at elevated temperatures. *Rev. Sci. Instrum.* **68,** 2558 (1997).

59. Gillespie, D. Vapor-Liquid Equilibrium Still for Miscible Liquids. *Ind. Eng. Chem.* **18,** 575–577 (1946).

60. Baes, C. F. *AN ISOPIESTIC INVESTIGATION OF AND TRi-n-OCTYLPHOSPHINE OXIDE IN n-OCTANE*. (1959). doi:ornl-2737

61. Meridiano, Y. *et al.* Aggregation in Organic Solutions of Malonamides: Consequences for Water Extraction. *Solvent Extr. Ion Exch.* **27,** 607–637 (2009).

62. Yu, Z.-J., Ibrahim, T. H. & Neuman, R. D. AGGREGATION BEHAVIOR OF COBALT(II), NICKEL(II), AND COPPER(II) BIS(2-ETHYLHEXYL) PHOSPHATE COMPLEXES IN n - HEPTANE. *Solvent Extr. Ion Exch.* **16,** 1437–1463 (1998).

63. Otu, E. & Chiarizia, R. Temperature Effects in the Extraction of Metal Ions by Dialkyl-Substituted Diphosphonic Acids. I. The Am(Iii) Case. *Solvent Extr. Ion Exch.* **19,** 885–904 (2001).

64. Sugamiya, K., Kamide, K. & Nakayama, C. Theory of vapor pressure osmometry when ambient solvent vapor is unsaturated. *Die Makromol. chemie* **133,** 101–109 (1970).

65. Lobo, V. M. M. & Quaresma, J. L. *Handbook of electrolyte solutions*. (Elsevier, 1989).

66. Starzak, M. & Peacock, S. D. Water activity coefficient in aqueous solutions of sucrose. A comprehensive data analysis. *Zuckerindustrie (Berlin)* **122,** 380–387 (1997).

67. Kamide, K. On the evaluation of the second virial coefficient and activity in dilute solutions by vapor pressure osmometry. *kobunshi kagaku* **25,** 648–656 (1968).

68. Kamide, K., Terakawa, T. & Uchiki, H. Molecular Weight Determination of Macromolecules by Vapor Pressure Osmometry. **1464,** 1447–1464 (1976).

69. Kamide, K. Theory of Vapor Pressure Osmometry on Ternary Mixture. **147,** 261–269 (1971).

70. Serth, R. W. & Lestina, T. G. Process heat transfer principles, applications and rules of thumb. (2014).

71. Kontogeorgis, G. M., Coutsikos, P., Tassios, D. & Fredenslund, A. Improved models for the prediction of activity coefficients in nearly athermal mixtures. *Fluid Phase Equilib.* **92,** 35–66 (1994).

72. *Vapor pressure osmometer model 833 instruction manual (Version 1.00)*. (UIC Inc).

73. Koekemoer, L. R., Badenhorst, M. J. G. & Everson, R. C. Determination of viscosity and density of di-(2-ethylhexyl) phosphoric acid + aliphatic kerosene. *J. chem. eng. data* **50,** 587–590 (2005).

74. ChemAxon. MarvinSketch.

75. Bondi, A. van der Waals Volumes and Radii. *J. Phys. Chem.* **68,** 441–451 (1964).

76. Zhao, Y. H., Abraham, M. H. & Zissimos, A. M. Fast calculation of van der Waals volume as a sum of atomic and bond contributions and its application to drug compounds. *J. Org. Chem.* **68,** 7368–7373 (2003).

77. Buch, A., Pareau, D., Stambouli, M. & Durand, G. SOLVENT EXTRACTION OF NICKEL(II) BY 2-ETHYLHEXANAL OXIME FROM VARIOUS AQUEOUS SOLUTIONS. *Solvent Extr. Ion Exch.* **19,** 277–299 (2001).

78. Berthon, L., Martinet, L., Testard, F., Madic, C. & Zemb, T. Solvent Penetration and Sterical Stabilization of Reverse Aggregates based on the DIAMEX Process Extracting Molecules: Consequences for the Third Phase Formation. *Solvent Extr. Ion Exch.* **25,** 545–576 (2007).

79. Gray, M. F., Zalupski, P. & Nilsson, M. Determination of Activity Coefficients of di-(2-ethylhexyl) Phosphoric Acid Dimer in Select Organic Solvents Using Vapor Phase Osmometry. *Solvent Extr. Ion Exch.* **31,** 550–563 (2013).

80. Polyzou, E. N., Vlamos, P. M., Dimakos, G. M., Yakoumis, I. V & Kontogeorgis, G. M. Assessment of Activity Coefficient Models for Predicting Solid-Liquid Equilibria of Asymmetric Binary Alkane Systems. *Ind. Eng. Chem. Res.* **38,** 316–323 (1999).

81. Stenby, E. H. Evaluation of activity coefficient models in prediction of alkane solid-liquid equilibria. *Fluid Phase Equilib.* **103,** 23–39 (1995).

82. Weiguo, S., Mcelroy, P. J., Williamson, A. G. & Qin, A. X. Vapor liquid equlibria of n-hexane+n-hexadecane, n-hexane+n-octane, and n-octane+n-hexadecane. *J. chem. Thermodyn.* **22,** 905–914 (1990).

83. Smith, V. C. & Robinson, R. L. Benzene hexane data. **15,** 391–395 (1970).

84. Elshayal, B. I. M. & Lu, B. C. ISOTHERMAL VAPOUR-LIQUID EQUILIBRIA FOR THE BINARY SYSTEM BENZENE-n-OCTANE. *J. appl. Chem.* **18,** 277–280 (1968).

85. Ott, J. B., Stokes, R. H. & Marsh, K. N. Excess enthalpies, excess volumes, and excess Gibbs free energies for n-hexane + n-dodecane at 298.15 and 308.15K. *J.Chem.Thermodyn.* **13,** 371 (1981).

86. Partridge, J. a & Jensen, R. C. PURIFICATION OF DI- (2-ETHYLHEXYL) PHOSPHORIC ACID BY PRECIPITATION OF COPPER (II) di- (2-ethylhexyl) phosphate. *J. Inorg. Nucl. Chem.* **31,** 2587–2589 (1969).

87. Harada, T. & Smutz, M. Extraction of yttrium in the system YCl3□HCl□H2O di(2-ethylhexyl) phosphoric acid. *J. Inorg. Nucl. Chem.* **32,** 649–662 (1970).

88. Sato, T. & Ueda, M. The extraction of yttrium (III) and lanthanum (III) from hydrochloric acid solutions by di-(2-ethylhexyl) phosphoric acid. *J. Inorg. Nucl. Chem.* **35,** 1003–1010 (1973).

89. Jensen, M. P., Chiarizia, R. & Urban, V. Investigation of the Aggregation of the Neodymium Complexes of Dialkylphosphoric , -Oxothiophosphinic , and -Dithiophosphinic Acids in Toluene. *Solvent Extr. Ion Exch.* **19,** 865–884 (2001).

90. Marie, C., Hiscox, B. & Nash, K. L. Characterization of HDEHP-lanthanide complexes formed in a non-polar organic phase using 31P NMR and ESI-MS. *Dalt. Trans.* **41,** 1054 (2012).

91. Scharf, C. *et al.* Investigation of the structure of neodymium-di-(2-ethylhexyl) phosphoric acid combinations using electrospray ionization and matrix-assisted laser desorption ionization mass spectrometry and nuclear magnetic resonance spectroscopy. *Metall. Mater. Trans. B* **36,** 429–436 (2005).

92. Tasaki-Handa, Y., Abe, Y., Ooi, K., Tanaka, M. & Wakisaka, A. Central metal ion exchange in a coordination polymer based on lanthanide ions and di(2-ethylhexyl)phosphoric acid: Exchange rate and tunable affinity. *J. Colloid Interface Sci.* **413,** 65–70 (2014).

93. Tasaki-Handa, Y., Ooi, K., Tanaka, M. & Wakisaka, A. Tunable selectivity of lanthanide ion exchange within a coordination polymer. *Anal. Sci.* **29,** 685–687 (2013).

94. Sanchez, J. M., Hidalgo, M., Salvadó, V. & Valiente, M. Extraction of Neodymium(Iii) At Trace Level With Di(2-Ethyl-Hexyl)Phosphoric Acid in Hexane. *Solvent Extr. Ion Exch.* **17,** 455–474 (1999).

95. Ali Mansoori, G. CLASSICAL THERMODYNAMIC BASIS OF ACTIVITY COEFFICIENTS: PREDICTIVE AND CONSISTENCY RULES FOR BINARY AND TERNARY MIXTURES BASED ON THE RELATION BETWEEN EXCESS GIBBS FREE ENERGIES OF (c)- AND (c - l)-COMPONENT MIXTURES G. *Fluid Phase Equilib.* **4,** 197–209 (1980).

96. McDowell, W. J., Perdue, P. T. & Case, G. N. Purification of di(2-ethylhexyl)phosphoric acid. *J. Inorg. Nucl. Chem.* **38,** 2127–2129 (1976).

Appendix A. List of Symbols and Abbreviations

Listed by chapter in approximate order of appearance

Chapter 1

HDEHP	Di(2-ethyl hexyl) phosphoric acid
DEHP	Deprotonated di(2-ethyl hexyl) phosphoric acid
VPO	Vapor pressure osmometry
UNF	Used nuclear fuel
MA	Minor Actinide e.g. Americium and Curium
DOE	Department of Energy
TALSPEAK	(Trivalent Actinide-Lanthanide Separations by Phosphorous reagent Extraction from Aqueous Komplexes)
M^{x+}	Generic metal ion of charge +x
x	Charge number
Aq	Aqueous phase
Org	Organic phase
n	Number of non-deprotonated HDEHP molecules in the complex
K	Equilibrium constant of the metal extraction
γ	Activity coefficient. Subscript MA_3HA_3 refers to the HDEHP metal complex Subscript HA2 refers to HDEHP dimer Subscript M refers to aqueous metal ion Subscript H refers to the hydrogen ion
$(HDEHP)_2$	Dimer of HDEHP
SXFIT	Solvent extraction modeling program developed at Oak ridge National Laboratory
K_2	Dimerization constant
K_i	Overall association constant for an aggregate of size *i*
IAS	Ideal associating solution

Chapter 2

ΔV	Osmometer signal, the voltage change in the thermistor ciruit
k	VPO machine constant
a	Chemical activity of the diluent
ΔH	Enthalpy of vaporization of the diluent
$\frac{dQ}{dt}$	Rate of heat increase
n	Moles of diluent in the drop
k_1	Heat transfer coefficient at the drop/vapor interface
k_2	Heat transfer coefficient from drop to thermistor
k_3	Mass transfer coefficient for the diluent vapor at the drop Surface
A_1	Surface area of drop
A_2	Surface area in contact between drop and thermistor

ΔT	Temperature difference between the thermistors
T	Temperature
T_0	Temperature of the vpo cell
Subscript 'c'	Refers to VPO cell
Subscript 'r'	Refers to reference diluent drop, the drop of pure diluent
Subscript 's'	Refers to solution drop
m	Mass of solution in drop
C_p	Heat capacity of the drop
P(T)	Partial pressure of the diluent in the solution drop at Temperature T
$P_o(T)$	Saturation pressure of the diluent at temperature T
R	Universal gas consant
β_1	Denominator of Eq. 2.17, approximated as a constant
β_2	Proprionality between the ΔT and ΔV
β_3	Constant defined in Eq. 2.29

Chapter 3

RST	Regular solution theory, Eq. 3.2
FH	Flory Huggins entropic correction Eq. 3.6
pFV	Modified free volume entropic corrections given by Eq. 3.10
FV1.1	Modified free volume entropic corrections given by Eq. 3.9
γ_i	Mole fraction activity coefficient unless specified otherwise
$\gamma_i^{Comb,FV}$	Combinatorial - free volume contribution to the activity coefficent
γ_i^{res}	Residual contribution to the activity coefficient
δ_i	Solubility parameter of component i
$\bar{\delta}$	Volume averaged solubility parameter
$\phi_{V,i}$	Volume fraction of component i
V_i	Molar volume of component i
x_i	Mole fraction of component i
ϕ_i	Volume fraction, Free volume fraction for component i
S_i	free volume term for component i
$V_{w,i}$	Van der Waals volume of component i
$V_{w,large}$	Van der Waals volume of the larger component
$V_{w,small}$	Van der Waals volume of the smaller component
c	Exponent in the FV S_i term
p	Exponent in the pFV S_i term
β	Fitting constant in *Eq.* 3.11
$\bar{h}_2^E$	Partial molar excess enthalpy
subscript 'f'	Formal concentration units. The concentration calculated if there was no aggregation
c_{dimer}	Molar concentration of HDEHP dimer

Chapter 4

6:1 Complex	$Dy(DEHP)_3(HDEHP)_3$
6:2 complex	$Dy_2(DEHP)_6$
D	Distribution ratio
A,*B*, and *C*	Constants
V_{cont}	Volume of organic phase that is contaminating the aqueous sample measured for tracer concentration
V_{sample}	Volume of aqueous sample measured for tracer concentration
D_{True}	Distribution ratio in a system with no contamination of the counted samples
$D_{observed}$	Distribution ratio in a system with contamination of the counted samples

Appendix B. Osmometer Quality Control

The VPO could not be operated at the temperatures ideal for dodecane despite what the provided manual and specifications state. Additionally, the osmometer suffered several instances of leaking. These were at first attributed to cracking of the glass thermistors. The unit was sent to the company for evaluation and the thermistors were replaced. Although it is possible they were fractured, later evidence suggests that improper installation may have been the real source of the leak. Issues with the thermistor quality and large delays in replacing them motivated the development of a less fragile version at UCI.

The vapor pressure osmometer manual specifications state that the upper operating temperature is 130°C, and in a table of example diluent/temperature combinations shows o-dichlorobenzene gives good data at 130°C. This temperature would be optimum for measuring HDEHP in dodecane based on the vapor pressure.

When the VPO was set to 130°C, and the syringe heater set to 90°C, the plastic insulating cover on the VPO cell began to degrade. A patch of the surface plastic under the syringe heater started changing color, and became brittle. This surface easy scraped off. When the cell was opened for cleaning it was discovered the paper wick used to maintain the nearly saturated conditions had turned from white to light beige, indicating oxidation of the paper or diluents.

On consulting the manufacturer, the spokesman claimed the manual was incorrect, and that the unit could not be operated at those temperatures. However,

the company website as of June 23, 2015 (http://www.uicinc.com/model-833/) claims the temperature range is up to 130°C.

The wick was observed to turn an off white color after approximately a week for the 110°C runs, indicating that some oxidation was taking place. However, the measurements were concluded within four days to prevent interference due to volatile oxidized products. In an effort to further prevent this, several new wick materials were tested to replace the paper. A stainless steel cloth was tested, but after the VPO was equilibrated overnight and solution removed through the drain port a pale yellow was observed. Ions from the metal may have been released due to galvanic corrosion, but at any rate the stainless steel cloth was an unsuitable substitute. Fiberglass and silica fiber fabrics were also tested. The fiberglass similarly browned in dodecane at 90°C. The silica fiber did not wick as well as the other materials or paper. Thus no replacement for the paper wick was identified. Also, the chemicals may have been reacting along with or instead of the paper, so replacing the wick may not improve the issue. Operating in an oxygen free environment may mitigate the issue, but it not realistic for this instrument design.

The thermistors were originally believed to be fractured due to diluent found leaking out the bottom of the cell where the thermistors are located. Fluid had also entered the hollow glass riser portion of the thermistors. The company said the leak could be due to broken thermistors or due to loose fittings holding them in. When it was sent in, they replaced the thermistors. Since the thermistors had appeared to have internal fracture/stress planes where the glass riser was attached to the glass thermistor, it seemed reasonable that the stress fracture had reached the surface.

However, the replaced thermistors did not resolve an issue where the unit would seemingly at random show high random noise. The unit was sent back under warranty to evaluate. The company claimed they were unable to reproduce the behavior, but anyway replaced the thermistors under warranty and sent it back. Only after the unit was shipped did they say that they had installed thermistors more suited for higher temperature operations. This change had not been discussed prior to that, and was not authorized. However, the project had been delayed a long time so the thermistors were accepted. They function welled, but provided lower signal sensitivity.

After several data sets using the less sensitive thermistors were collected, a set of the standard thermistors were ordered for install at UCI rather than by the company. The new set was not manufactured properly and was fractured prior to arrival, as shown in Fig. B.2 . However, it could not be proven the break did not occur at UCI because the break was not noticed until a few weeks after the package arrived, when they were to be installed. After taking months to repair them, the company sent them back. However, by repairing them they meant sealing the fraction and they did not test the resistance. Melting the glass to seal the fracture altered the resistance. The thermistor were no longer a matched pair and useless for VPO. The resistance only had to be quickly measured with a multimeter to check this. It is unclear why the company did not do that check. Furthermore, the company was out of stock of replacement thermistors, and took several months to produce more. During this time the less sensitive thermistors that still functioned well were used for VPO experiments.

After the company finally produced new thermistors, the unit was sent in for them to install the thermistors so there would be no risk of receiving a broken set. These appeared to function well, and did not appear to leak initially. Soon, though, a leak developed. As before, the thermistors had visible liquid in the glass riser, and liquid was observed on the bottom outside surface of the cell. An internal stress plane was clearly evident at the join between the glass riser and the thermistors bead, so it was assumed to have reached the surface to form a slow leak. The thermistors are temperature cycled from 25°C to 90°C so it appeared reasonable that fracture may grow.

It turned out, however, that they were not fractured, but had been installed improperly by the company, as shown in Fig. B.1. Due to the prior delays and problems with thermistors, a pair of matched thermistors with Teflon risers rather than the glass risers had been manufactured at UCI. When the old thermistors were being removed to install these new ones it was discovered that two steps of the factory installation were not correct. The thermistors had not been tightened down, and the o-rings, washers, and o-ring spacers were installed in the improper order. Without proper tightening of the assembly, the o-rings likely did not form a good seal. Additionally, though, the improper order meant the second o-ring did not get compressed against the thermistor in the correct manner. The thermistors were not broken, and the leak was not observed after correctly installing the fittings and properly tightening them. Thus the leak had been around the seals, and not through broken thermistors. The liquid was inside the thermistor riser due to capillary action.

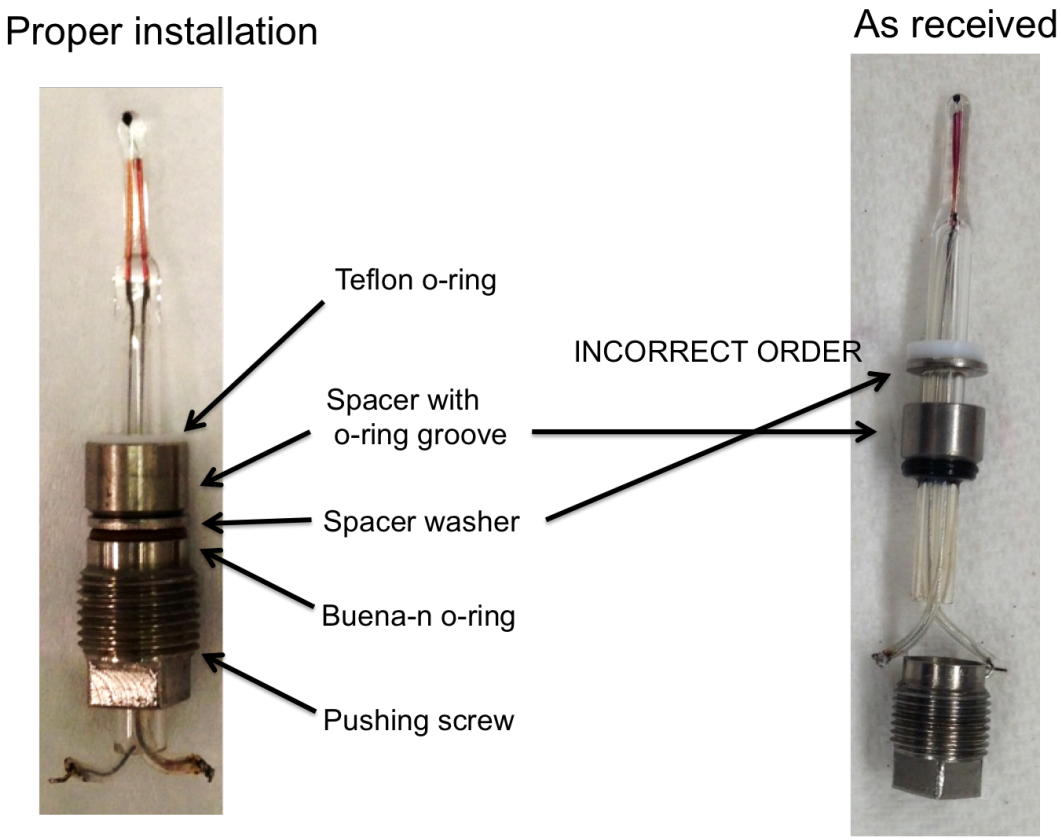

Fig. B.1: Correct and incorrect thermistor installation.
The thermistor on the left is is correctly installed into the fittings according to the to the provided design schematics. Both o-rings seat into grooves that compress them against the glass thermistor riser when the pushing screw is tightening. The thermistor on the right leaked, and when the unit was disassembled it was found with the order switched as indicated, and the pushing screw was not tightened sufficiently. The Teflon o-ring was not set in the groove due to the intervening washer, so it could not be compressed against the glass riser to form a seal even if the unit had been properly tightened.

Unfortunately, checking the fittings requires desoldering the thermistors, so that was not done earlier. However, the thermistors are less delicate than the company claims. This pair was removed, inspected, and reinstalled with no problem, and the pair of less sensitive thermistors was removed and reinstalled multiple times.

Based on these findings, it was no longer clear that the original thermistors were broken when the unit was sent in for repair for the earlier instance of leakage.

The prior leak had presented in the exact same manner as the leak due to the improper installation of the thermistors.

Both ordering thermistors to install at UCI and having the company install thermistors is risky. If the ~$800 thermistors arrive broken or break shortly after due to the manufacturing problems, they are a loss. If the thermistors are installed by them, it takes a few weeks and costs ~$1400 with shipping and may need re-installed anyway, risking breakage.

The possibility of making thermistors for the VPO at UCI was also investigated during the delays.

Comparison showed that the thermistors were 1/2" Glass encapsulated Honeywell 100KOhm thermistors part 121-104KAH-Q01 with a 300°C max operating temperature. That bead is Fig. B.2 part A. Matched thermistors in small quantities were not available at the distributor contacted.

The company uses two of these beads with resistances that match to within 1% at three distinct temperatures over the range of VPO operating temperatures, and then contract a glass blower to attach a glass riser onto the thermistors. Fig. B.2 part B and C show examples of the thermistors as received from UIC inc with the addition of the glass riser. This extended form is installed in the VPO. Eight of the original unmatched Honeywell thermistors were ordered from a distributor. These thermistors were 100Kohm ±20%, so there was a significant variance in the resistance between each of these thermistors. However, the goal of buying these unmatched thermistors was to explore ways to install them in the VPO

without a glass riser. A matched set without glass riser could be ordered from the company.

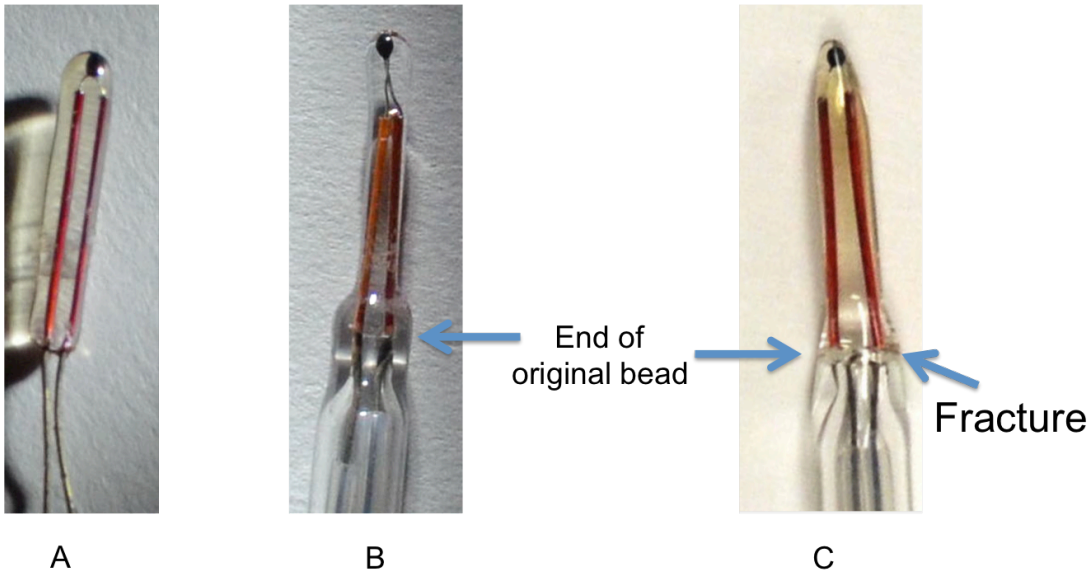

Fig. B.2: Three different thermistors
A: A thermistor bead without the glass riser attached. The wires are an orange red color inside the bead. B: A 'good' thermistor with the glass riser attached. The join forms a blunt edge and the thermistor bead ends significantly inside the larger diameter riser portion based on where the wire color changes. C: The thermistor which arrived fractured. The join is tapered with only a tiny amount of riser material on the original bead; the bead was not inserted in the riser. The thermistors typically show the weaker tapered form factor.

An alternative to the glass riser was needed. Joining the glass bead to a glass riser leads to a high chance of failure. First, the thermistor bead is irreversibly altered if subjected to excessive temperatures, including those needed to melt glass. At high temperature, the doping that gives the characteristic resistance curve migrates and the resistance is irreversibly altered. Second, without exact matching of the thermal expansion coefficients for the thermistor bead and the attached riser, the join will stress and fracture as it cools.

Teflon tubing of the same outside dimension as the glass riser was used instead, as shown in Fig. B.3. Initially Teflon heat shrink tubing was evaluated in

order to give a compression fitting on the bead. The heat shrink added no benefit over melting the Teflon tubing around the end of bead using the heat gun. When immersed in either dodecane or toluene at room temperature for one week there was no observed liquid intrusion. If the seal does break, the part can be reheated. The heat gun did not alter the resistance of the thermistors even after direct application to the actual bead at the tip for 5 minutes, longer than needed to form the Teflon around the end.



Fig. B.3: Thermistor with Teflon riser